

POLITECNICO DI TORINO

Master Degree in Biomedical Engineering

Human Tubulin Conformational Dynamics and Global Correlations Driven by Colchicine Binding



Thesis Supervisor

Prof. Marco Agostino Deriu

Co-supervisors

Prof. Jacek Adam Tuszynski

Prof. Umberto Morbiducci

Candidate

Lorenzo Pallante

ACADEMIC YEAR 2018-2019

Contents

ABSTRACT	1
1 INTRODUCTION	2
2 MATERIALS AND METHODS	4
2.1 Molecular modelling	4
2.2 Molecular Mechanics	4
2.2.1 Potential Energy Function	4
2.2.2 Bonded interactions	5
2.2.3 Non-bonded interactions	6
2.2.4 Periodic boundary conditions	8
2.2.5 Potential energy minimization	8
2.3 Molecular Dynamics	9
2.3.1 Statistical ensemble	9
2.3.2 Molecular Dynamics implementation scheme	11
2.4 Dimensionality Reduction Techniques	12
2.4.1 Principal Component Analysis	13
2.4.2 Functional mode analysis	14
2.5 Binding free energy prediction	15
3 BIOLOGICAL BACKGROUND	19
3.1 Introduction	19
3.2 Functions of microtubules	19
3.3 Tubulin dimers	20
3.3.1 Tubulin domains	20
3.4 Microtubule architecture	22
3.5 Microtubule polymerization	25
3.5.1 Allosteric and lattice model	26
3.6 Microtubule targeting agents	27
3.6.1 Colchicine and colchicine derivatives	28

3.7	Tubulin structures	28
3.8	Tubulin isotypes	28
3.9	Molecular modeling of microtubule	31
4	HUMAN TUBULIN CONFORMATIONAL DYNAMICS AND GLOBAL CORRELATIONS DRIVEN BY COLCHICINE BINDING	33
4.1	Abstract	33
4.2	Introduction	33
4.3	Materials and methods	35
4.3.1	Homology modeling of tubulin isotypes	36
4.3.2	System set up	36
4.3.3	Functional mode analysis	38
4.3.4	Structural analysis	38
4.4	Results	40
4.4.1	Model Validation	40
4.4.2	Local effects induced by the presence of colchicine	41
4.4.3	Global effects induced by the presence of colchicine	44
4.4.4	Functional mode analysis	49
4.5	Discussion	52
4.6	Conclusions	53
4.7	Supporting information	55
4.7.1	Homology modelling	55
4.7.2	RMSD of simulated structures	58
4.7.3	Binding energy prediction	58
4.7.4	RMSD of internal beta sheets	59
4.7.5	RMSF of alpha tubulin	59
4.7.6	Functional Mode Analysis	61
5	ACKNOWLEDGMENTS	66
6	REFERENCES	67

ABSTRACT

In the past years, microtubules have been widely studied as interesting target for anti-cancerous treatments. Microtubules are cytoskeletal structures, formed by α - β heterodimers, and play important roles in several essential cellular processes, especially during mitosis; their functionality is linked to a complex polymerization dynamic, influenced by conformational changes of tubulin dimers. Microtubule polymerization/depolymerization equilibrium alterations may strongly affect the cell homeostasis. Antimitotic drugs, such as colchicine, influence the above mentioned equilibrium, leading to mitotic arrest and eventually to cell death. The expression of several tubulin isotypes in normal and cancerous cells suggests employing drugs with increased specificity for only those isotypes principally expressed in cancerous cells and minimizing damages to the healthy ones. In the present work, several human tubulin isotypes were built and simulated using molecular dynamics approach to elucidate the effect of colchicine on tubulin dynamic. Computational methods underline structural modifications of tubulin dimer, such as the intradimer bending and twisting angles, related to variations in local fluctuations due to the presence of the drug. Thanks also to dimensionality reduction techniques, this research highlights the correlation between the motion of the β tubulin M loop and the conformational changes of the tubulin dimer, revealing that the action of colchicine is mediated by alterations in the fluctuations of this loop. Future studies may be important to highlight the destabilizing action of other colchicine binding site inhibitors with lower toxicity than colchicine and high activity on isotypes over expressed in cancer cells and implicated in drug resistance.

1 Introduction

The present chapter deals with a general introduction of this master thesis work, summarizing the biological background, the aims of the research and the organization of the dissertation.

Microtubules are cytoskeletal structures involved in several cell functions, including cell shape maintenance, cell signaling and cell division; in particular, during mitosis, they form the mitotic spindle, which is fundamental to divide the chromosomes. They are composed by α and β heterodimers, aligned in head-to-tail fashion, forming linear protofilaments, that bound laterally to form a hollow cylindrical polymer. Microtubule functionality is linked to the complex process of polymerization and depolymerization, called *dynamic instability*, which is characterized by switching between phases of slow growth and rapid disassembly. The molecular mechanism which drives the polymerization process is still unclear and different models were proposed in the past years: according to the *allosteric model*, tubulins in GTP state are straighter than those bound to GDP and are more compatible for microtubule integration, while, for the *lattice model*, tubulin dimers adopt curved conformations regardless of the nucleotide state and, after integration in the lattice, they are forced to straight conformation due to lateral contacts. The debate between these two models is still open and there are evidences for both, but anyway conformational state of tubulin is strongly related to microtubule dynamic. The polymerization process is fundamental in many cellular functions and the inhibition of microtubule dynamic can eventually leads to the arrest of the mitotic process and cellular death. In this context, many antimitotic drugs, such as colchicine, have been developed in the past years, especially for anti-cancerous therapies. The action of these drugs is highly influenced by the expression of different tubulin isotypes, which differ for punctual or restricted structural variations: this is a great opportunity to design novel drugs based on specific isotype differences, to improve the efficacy of the pharmacological treatment and to reduce the side effects.

Nowadays, the computational studies have exponentially grown thanks to tremendous improvements in computer hardware and software, making it possible to simulate biological systems consisting of huge number of molecules. Computational Molecular Modeling provides tools, as Molecular Dynamic (MD) or Functional Mode Analysis (FMA), for analyzing the physical properties of molecular systems with atomic resolution.

The aim of the present work is to elucidate the action of colchicine on several human tubulin isotypes through molecular dynamics simulations, focusing on the relation between local structural rearrangements and conformational changes of tubulin dimer, which influence the microtubule stability.

The thesis is divided in the following sections.

Chapter 1 is the present introduction.

Chapter 2 is an overview of the methods used in this work. Molecular mechanics and molecular dynamics are firstly described in general, focusing on physical and theoretical aspects; follows a description of dimensionality reduction techniques, including Principal Component Analysis (PCA) and Functional Mode Analysis (FMA) finally, binding free energy calculation methods are presented.

Chapter 3 is dedicated to the biological background of microtubule, describing the molecular structure, the polymerization dynamic, the role in anti-cancerous therapies and the isotype expression in humans.

Chapter 4 is devoted to investigating the conformational changes induced by the presence of colchicine in tubulin isotypes $\alpha\beta\text{IIa}$, $\alpha\beta\text{III}$ and $\alpha\beta\text{IVa}$. Molecular dynamics simulation on free tubulin dimers are analyzed, focusing on local structural rearrangements and conformational modifications, such as intradimer bending and twisting angles. Moreover, Functional Mode Analysis (FMA) is performed to identify collective motions related to the variations on residue fluctuations.

2 Materials and methods

The present chapter provides a general overview of Molecular Modelling, including the theoretical and physical bases behind the computational methods employed in the present Master Thesis. In a greater detail, Molecular Mechanics and Molecular Dynamics are described together with dimensionality reduction techniques, such as the Functional Mode Analysis (FMA), and methods for binding free energy prediction.

2.1 Molecular modelling

Molecular modelling includes all theoretical and computational techniques used to investigate the behavior and properties of chemical complexes and more specifically subcellular constituents such as proteins, membranes, nucleic acids, polymers.

The complexity and the high number of atoms of the interested systems make impossible an analytic resolution of the problem and numerical methods are necessary. The most accurate description of a molecular system includes an explicit modelling of the electrons of each atom, quantum mechanics or *ab initio* calculation, that implies solving the electronic Schrödinger equation; however, the calculations are computational expensive due to the large number of particles considered and this method can be applied only for small systems. Molecular Mechanics (MM) approach, instead, is based on force field methods, that ignore the electronic motion and calculate the energy of a system as a function of the nuclear positions only¹. MM cannot identify properties influenced by the electronic distribution, but can describe systems of many thousands of atoms, predicting macroscopic properties.

2.2 Molecular Mechanics

Molecular Mechanics method solves the Newton equation of motion for a system of atoms, using a *potential energy function* V to model atom interactions. The potential energy is defined by a set of equation and parameters, named *force field* (FF).

2.2.1 Potential Energy Function

The potential energy function is calculated as the sum of two energy contributions, one correlated to the bonded interactions between atoms linked by covalent bonds and one to the non-bonded interactions (electrostatic and Van der Waals forces):

$$V = V_{bonded} + V_{non-bonded} \quad (1)$$

These components are described by the following equations:

$$V_{bonded} = V_{bond} + V_{angle} + V_{dihedral} \quad (2)$$

$$V_{non-bonded} = V_{VDW} + V_{Coulomb} \quad (3)$$

The potential energy is a function of the positions (\mathbf{r}) of the N particles in the systems:

$$V = V(\mathbf{r}^N) \quad (4)$$

There are several implementations of the potential energy depending on the force field choice and each term can be modelled in different ways according to the specific applications.

2.2.2 Bonded interactions

The bonded terms refer to energy variations due to changes in internal coordinates, such as bond lengths, bond angles and rotation of bonds¹.

The energy variation due to changes in bond length is typically modelled as a harmonic potential:

$$V_{bond} = \sum_{bonds} \frac{1}{2} K_{ij} (r_{ij} - r_{0,ij})^2 \quad (5)$$

where r_{ij} is the bond length between atoms i and j , K_{ij} is the bond stiffness and $r_{0,ij}$ is the bond length at the equilibrium and depends on the atom types; the summary operator includes all the bonds in the studied systems and all the pairs of atoms connected by covalent bonds are considered.

The variation of the bond angle includes three atoms and it is also modelled with a harmonic potential:

$$V_{angle} = \sum_{angles} \frac{1}{2} \xi_{ijk} (\theta_{ijk} - \theta_{0,ijk})^2 \quad (6)$$

where θ_{ijk} is the bond angle between atoms i , j , and k , ξ_{ijk} is the angle stiffness and $\theta_{0,ijk}$ is the bond angle at the equilibrium.

Bond rotation, instead, affects four atoms linked by covalent bonds and it is modelled by the dihedral term:

$$V_{dihedral} = \sum_{dihedrals} \psi_{ijkl} [1 + \cos(n\phi_{ijkl} - \phi_{0,ijkl})] \quad (7)$$

where ϕ_{ijkl} is the dihedral angle between atoms i , j , k and l , ψ_{ijkl} is the dihedral stiffness and $\phi_{0,ijkl}$ is the dihedral angle at the equilibrium.

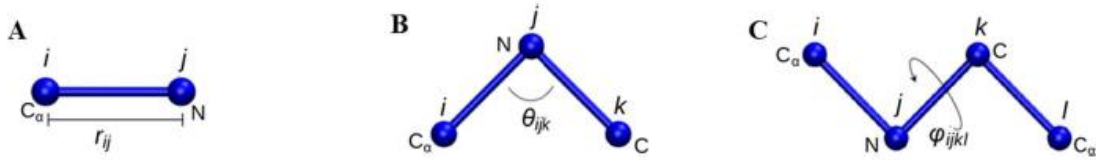


Figure 2.1 – Schematic representation of three types of bond interaction: A) bond between i -carbon and j -nitrogen atoms with bond length of r_{ij} B) angle θ_{ijk} between i -carbon, j -nitrogen and k -carbon atoms C) dihedral angle ϕ_{ijkl} between vectors defined by atoms i, j and k, l .

2.2.3 Non-bonded interactions

The non-bonded interactions consider the forces between atoms not linked by covalent bond and they are divided into long-range interactions, or rather the Coulomb energies, and short-range ones, such as the Van der Waals.

For two particles i and j with charges q_i and q_j the electrostatic energy is described by the Coulomb law:

$$V_{Coulomb} = \frac{q_i q_j}{4\pi\epsilon_0\epsilon_r r_{ij}} \quad (8)$$

where ϵ_0 is the vacuum permittivity, ϵ_r the relative permittivity and r_{ij} the distance between the atoms i and j . This equation describes a long-range interaction because the electrostatic potential decrease when the interatomic distance increases.

Short-range interactions, constituted by the Van der Waals forces, are often described by the Lennard-Jones 12-6 equation, that consider both the repulsive and attractive effects:

$$V_{VdW} = 4\epsilon_{ij} \left[\left(\frac{\sigma_{ij}}{r_{ij}} \right)^{12} - \left(\frac{\sigma_{ij}}{r_{ij}} \right)^6 \right] \quad (9)$$

r_{ij} is again the distance between the atoms i and j , σ_{ij} is the collision diameter, that is the interatomic distance where the Van der Waals potential is equal to zero, and ϵ_{ij} is the well depth, such as the minimum of the Van der Waals forces. The first term models the repulsive effect due to the overlapping of the electron orbitals, while the second one considers the attractive long-range forces.

The non-bonded interactions are very expensive in term of computational cost, because their number increases as the square of the number of atoms in the system, and many methods were proposed to reduce the computational effort. The *cut-off distance*, for example, allows to calculate non-bonded interactions only for the atoms closer than the cut-off distance; this method could generate artifact, especially in the count of the long-range interactions, and more accurate methods are normally used, such as shift or switched cut-off, Particle Mesh Ewalds² and Multiple Cells³.

Merging together the bonded and the non-bonded terms, a complete definition of the potential energy function is obtained:

$$V = \sum_{bonds} \frac{1}{2} K_{ij} (r_{ij} - r_{0,ij})^2 + \sum_{angles} \frac{1}{2} \xi_{ijk} (\theta_{ijk} - \theta_{0,ijk})^2 + \sum_{dihedrals} \psi_{ijkl} [1 + \cos(n\phi_{ijkl} - \phi_{0,ijkl})] + \sum_{i=1}^N \sum_{j=i+1}^N \left\{ \frac{q_i q_j}{4\pi\epsilon_0 \epsilon_r r_{ij}} + 4\epsilon_{ij} \left[\left(\frac{\sigma_{ij}}{r_{ij}} \right)^{12} - \left(\frac{\sigma_{ij}}{r_{ij}} \right)^6 \right] \right\} \quad (10)$$

2.2.4 Periodic boundary conditions

All the atoms in the simulated systems are put in a space-filling box of different geometry and normally filled with water or other solvents; in order to reduce the edge effects of the walls of the box, the *periodic boundary conditions* (PBCs) are usually applied and the box will be surrounded by copies of itself. Dimensions has to be settled respecting the *minimum image convention*: each particle interacts with the closest image of the remaining particles of the system but not with itself. The presence of Periodic Boundary Conditions causes imprecisions, but still less severe than the error resulting from artificial boundary with vacuum.

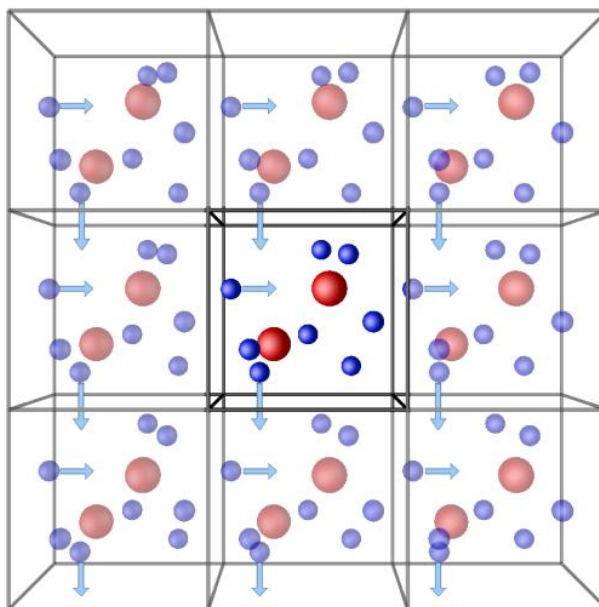


Figure 2.2 – Representation of Periodic Boundary Condition (PBC): the central box is replicated in copies of itself. SOURCE: <http://isaacs.sourceforge.net/phys/psc.html>

2.2.5 Potential energy minimization

The potential energy function can be represented by a multidimensional surface called Potential Energy Surface (PES) and each variation of the internal coordinates of the systems causes a variation of the potential energy function and a change in the location of the system in the PES. The PES is characterized by various stable states and any movement from these configurations corresponds to higher energy state: these points are called *local minima* and the lowest energy point is the *global minimum*. An energy minimization (EM) can reduce the potential energy of the system and to lead it in a stable state; EM is usually fundamental, especially for complex system, before starting the simulation to avoid possible collapses. There are two different approaches to perform energy minimization: *derivative methods* and *non-derivative methods*. The first ones are divided into *first order methods*, such as Steepest Descent and Conjugate

Gradient, that use the direction of the first derivate of the potential energy, the gradient, to reach the minimum, and *second order methods*, such as Newton-Raphson and LBFGS, that use the second derivate to find where the energy function change direction. Second order methods have a high computational cost, but they are often more accurate than the first order ones.

2.3 Molecular Dynamics

Molecular Dynamics (MD) is a computational method able to describe the dynamic evolution of complex chemical and biological systems: the trajectories of the interacting particles are calculated during the simulation period and the average properties of the system can be derived by numerically solving the Newton's equation of motion.

2.3.1 Statistical ensemble

A statistical ensemble defines all the accessible physical states of a molecular system at a specific temperature: it is a collection of system configurations which have different microstates but identical macroscopic or thermodynamic state. Each microstate is represented by a single point in the *phase space*, that is the space in which all possible physical states of a system are represented. Each point in the phase space for a system of N atoms is defined by 6N values (three coordinates of position and three components of momentum) and represents a specific state of the system. Different points in the phase space can have the same thermodynamic state and they form a statistical ensemble.

The definition of the ensemble is necessary to determine the macroscopic properties of the system and different ensembles are usually used:

- The Micro-Canonical Ensemble (NVE) corresponds to an isolated system and it is characterized by a fixed volume, energy and number of atoms;
- The Canonical Ensemble (NVT) corresponds to a closed system and it is characterized by a fixed volume, temperature and number of atoms;
- The Grand Canonical Ensemble (μ VT) corresponds to an open system and it is characterized by a fixed volume, temperature and chemical potential;
- The Isobaric-Ensemble (NPT) is characterized by a fixed pressure, temperature and number of atoms.

The aim of the MD is sampling the phase space and calculating the ensemble average of the macroscopic properties of interest. The ensemble average of property A is determined by integrating over all possible configurations of the system:

$$\langle A \rangle = \iint A(p^N, r^N) \rho(p^N, r^N) dp^N dr^N \quad (11)$$

where $A(p^N, r^N)$ is the observable of interest, r is the atomic positions, and p the momenta. The probability density function $\rho(p^N, r^N)$ of the ensemble is given by:

$$\rho(p^N, r^N) = \frac{1}{Q} \exp \left[-\frac{H(p^N, r^N)}{K_b T} \right] \quad (12)$$

where K_b is the Boltzmann constant, T the temperature, H the Hamiltonian and Q the partition function, expressed by the following equation.

$$Q = \iint \exp \left[-\frac{H(p^N, r^N)}{K_b T} \right] dp^N dr^N \quad (13)$$

The partition function is the sum of Boltzmann factors over all microstates and expresses the accessible states of the system: it relates microscopic thermodynamic variables to macroscopic properties. However, the previous equation is not analytically solvable, because the integration is extended to all possible states of the system and to overcome this problem the *ergodic hypothesis* is used: over a long period of time the ensemble average is equal to the time average.

$$\langle A \rangle_{ensemble} = \langle A \rangle_{time} \quad (14)$$

where the time-average of the property A is expressed by the equation:

$$\langle A \rangle_{time} = \lim_{\tau \rightarrow \infty} \frac{1}{\tau} \int_{t=0}^{\tau} A(p^N(t), r^N(t)) dt \approx \frac{1}{M} \sum_{i=1}^M A(p^N, r^N) \quad (15)$$

where t is the time, M is the number of steps in the simulation and $A(p^N, r^N)$ is the instantaneous values of the property of interest.

According to the ergodic hypothesis it is possible to compute an ensemble-average property of the system with a sufficiently long simulation (high number of steps), which can exhaustively sample the microstates of a specific ensemble.

2.3.2 Molecular Dynamics implementation scheme

The purpose of molecular dynamics simulations is to solve the Newton's equation of motion and to obtain atom trajectories (positions and velocities): the acceleration a_i of each particle i is the derivate of the potential energy V respect to particle position r .

$$a = -\frac{1}{m} \frac{dV}{dr} \quad (16)$$

Due to the complexity of the potential energy function, the previous equation cannot be analytically solved, and a numerical integration scheme is required. The choice of the integration methods and the integration parameters, especially the integration time-step, is crucial to avoid instability and correctly sample the phase space. A good time step should be less than 1/10 of the period of the fastest harmonic oscillation and there are different integration algorithms, for example the Verlet, Leap-frog and Velocity Verlet.

Figure 2.3 illustrates a generic MD flowchart. Starting atomic positions are known from the starting structure (e.g. from the Protein Data Bank), while the starting velocities are chosen randomly from the Maxwell-Boltzmann distribution at a given temperature. The potential energy is defined according to the chosen force field. At each step the accelerations of particles are calculated deriving the potential with respect to the actual atomic positions and new positions and velocities are consequently calculated. Positions and velocities as function of time form the atomic trajectories. The system reaches an equilibrium state after initial changes and this state is a statistical ensemble, that permits to determine macroscopic properties of the systems as time averages, for example temperature, pressure, energy, using the ergodic hypothesis. After reaching the equilibrium the simulation can be stopped.

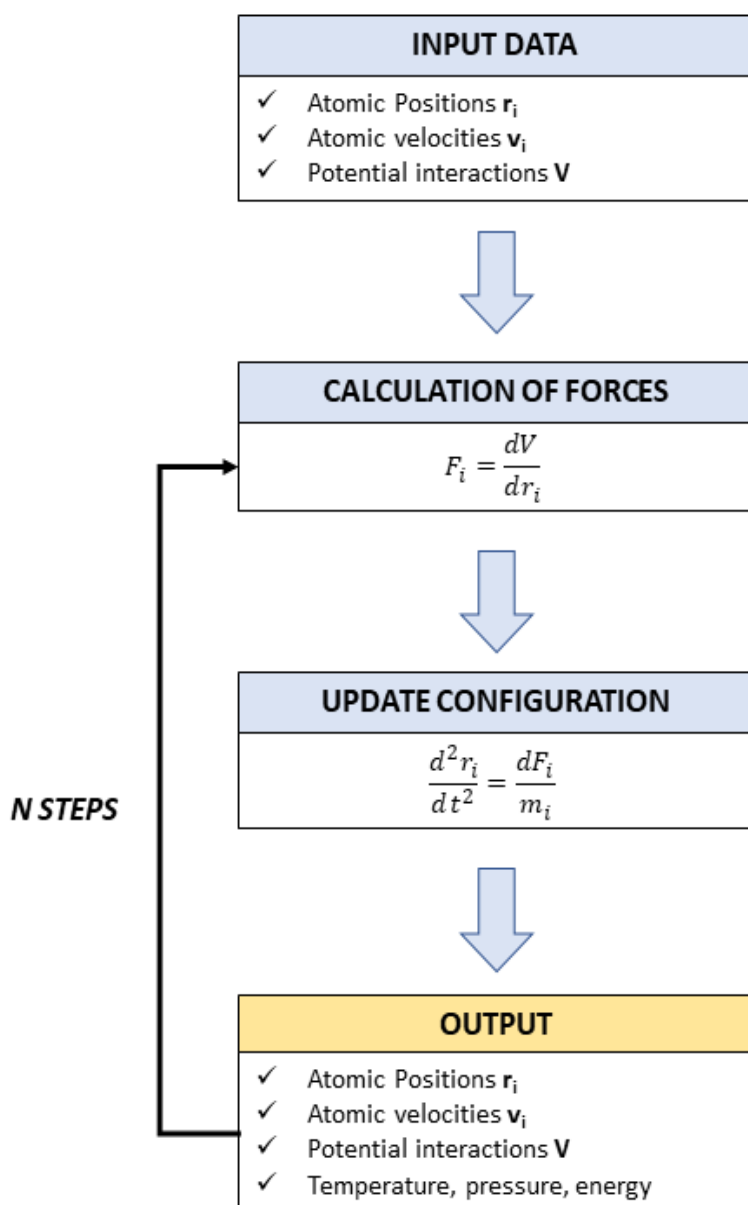


Figure 2.3 – Molecular Dynamics algorithm scheme. Initial atomic positions and velocities are the input data; the atomic force F_i for each atom is calculated deriving the potential energy V , which models the atomic interactions; then the acceleration for each atom is calculated using Newton's equation and atomic positions and velocities are update. The cycle is repeated for N steps until the convergence is reached and the system is in an equilibrated state.

MD is a deterministic method: the system configuration can be predicted at any time after assigning for the first-time atomic positions and velocities. There are also non-deterministic methods, like the Monte Carlo, in which the system configuration at each step is stochastic.

2.4 Dimensionality Reduction Techniques

Conformational structure of biological systems, especially for proteins, is usually correlated to their function and for this reason is fundamental to underline the most probable and stable

configurations in a molecular dynamics simulation. However, the complexity of the molecular systems often produces dynamics with very large dimensionality and a reduction of degrees of freedom is usually necessary to analyze simulation data: Principal Component Analysis (PCA)⁴⁻⁷ and Functional Mode Analysis (FMA)^{8,9} are two techniques commonly used for reducing the dimensionality of a data set.

2.4.1 Principal Component Analysis

Principal Component Analysis (PCA) is a statistical procedure that can be used to reduce a large set of variables into a small set of linearly uncorrelated variables, called principal components (PCs); therefore, this technique determines collective motions with the largest contribution to the variance of the atomic fluctuations.

PCA starts with the definition of the covariance matrix of the atomic positions, that is for a system of $3N$ coordinates $x_i(t)$ ($i=1,2,\dots,3N$)

$$C_{ij} = \langle (x_i - \langle x_i \rangle) (x_j - \langle x_j \rangle) \rangle \quad (17)$$

After diagonalizing the covariance matrix, a set of $3N$ orthonormal eigenvectors (e_j) with corresponding eigenvalues (σ_j^2) is obtained; the eigenvectors are then ordered according to descending eigenvalues and referred to as PCA vectors. Eigenvectors with highest amplitude correspond to motions with largest contribution to the atomic fluctuations; the projections $p_j(t)$ of the protein positions along the PCA vectors j are therefore calculated in order to highlight the mode along the considered vector.

$$p_j(t) = [x(t) - \langle x \rangle] \cdot e_j \quad (18)$$

The motion of the protein quantified as Mean Square Fluctuations (MSF) is the sum of $3N$ contributions from different PCs:

$$\langle (x(t) - \langle x \rangle)^2 \rangle = \sum_{j=1}^{3N} \text{var}(p_j) = \sum_{i=1}^{3N} \sigma_i^2 \quad (19)$$

In general, the first PCs represents a large fraction (80-90%) of the atomic MSF. Hence, usually the first few PCs are reasonable basis set to analyze the biomolecular simulation. However, a functionally relevant mode is in most cases not identical to a specific PCA mode but may be distributed over several PCA modes. To overcome this problem, the Functional Mode Analysis (FMA) is often used.

2.4.2 Functional mode analysis

The aim of FMA is to elucidate collective motions directly related to a specific protein function: starting from a set of protein conformations, together with a ‘functional quantity’ $f(t)$ that quantifies the protein function of interest (e.g. distance between residues, solvent accessible surface), the technique seeks the collective protein motion that is maximally related to the functional quantity. Defining a collective vector of protein atoms, \mathbf{a} , the motion along \mathbf{a} maximally correlated to the change in the functional quantity $f(t)$ is called ‘maximally correlated motion’ (MCM) ⁸. The MCM as a function of time t is given by the projection:

$$p_a(t) = [x(t) - \langle x \rangle] * a \quad (20)$$

where $\langle \dots \rangle$ denotes the average over all simulation time and $x(t)$ the $3N$ coordinates for a system of N atoms.

Two measures are used to determine the correlation between $f(t)$ and p_a : the Pearson’s correlation coefficient, that identifies only linear correlation, and the mutual information (MI). The Pearson’s correlation coefficient is defined as

$$R = \frac{cov(f, p_a)}{\sigma_f \sigma_a} \quad (21)$$

where $cov(f, p_a)$ denotes the covariance between $f(t)$ and $p_a(t)$, and σ_f and σ_a denote the standard deviations of $f(t)$ and $p_a(t)$, respectively. MCM can be determined maximizing the Pearson’s coefficient, but a reduction of the dimensionality of the data set using PCA is necessary; vector \mathbf{a} can be therefore expressed as a linear combination of the first few PCA vectors, d .

$$\mathbf{a} = \sum_{i=1}^d \alpha_i \mathbf{e}_i \quad (22)$$

where coefficients α_i denote the coordinates of \mathbf{a} with respect to the eigenvector \mathbf{e}_i . Numerically solving the coupled linear set of equations, it is possible to maximize the Pearson's coefficient:

$$\sum_{i=1}^d \alpha_i \text{cov}(p_j, p_k) = \text{cov}(f, p_k) \quad (23)$$

with $k = 1, \dots, d$.

If non-linear correlations between the arbitrary function and protein motions occur, the maximization of the MI is necessary to obtain the MCM; anyway, the maximization of R or MI can lead to overfitting if too many free parameters α_i are used in the optimization. To avoid this problem, it is convenient to divide the simulation data into frames for model building and for cross-validation: the maximization of R or MI is performed on the model building set only, obtaining a value of R_m , while the derived model is validating by predicting $f(t)$ using the cross-validation set only, yielding a correlation R_c . Using this approach, overfitting is indicated by a substantially smaller R_c as compared to R_m .

2.5 Binding free energy prediction

In biochemical systems, macromolecules normally interact with each other; molecular modelling techniques provide several computational methods to estimate the binding energy between two molecules, providing a measure of their affinity.

The standard binding free energy in a non-covalent ligand-protein complex is related to the association constant K_i by the equation:

$$\Delta G^0 = \Delta H^0 - T\Delta S^0 = -RT \ln K_i \quad (24)$$

where H is the enthalpy, S is the entropy, T is the absolute temperature, R is the gas constant and the superscript "0" means that the binding free energy is evaluated at standard conditions.

Therefore, to correctly evaluate the binding energy, both enthalpic and entropic effects must be considered. The enthalpic contributions consider standard terms from the Molecular Mechanics theory, such as the electrostatic and the Van der Waals interactions, and the contribution to the solvation free energy, while the entropic contributions accounts somehow for the flexibility of the molecules¹⁰.

The calculation of the binding free energy is computational demanding and approximated methods are normally used to define the binding energy with a good compromise between computational time and accuracy. Molecular Mechanics Generalized Born/(Poisson Boltzmann) Surface Area (MMGB/(PB)SA) are two of the most used methods for binding free energy calculations of complexes formed by small ligands bounded to biological macromolecules¹¹.

The binding energy is calculated as the difference between the energy of the complex (PL) and the energy of unbounded receptor (P) and free ligand (L) alone.

$$\Delta G_{bind} = \langle G_{PL} \rangle - \langle G_P \rangle - \langle G_L \rangle \quad (25)$$

Normally, only the complex is simulated, and the ensemble averages of the free receptor and ligand are calculated removing the uninterested atoms from the entire structure, obtaining:

$$\Delta G_{bind} = \langle G_{PL} - G_P - G_L \rangle_{PL} \quad (26)$$

The energy in each state, P, L and PL, is calculate according to the equation:

$$G = E_{bond} + E_{el} + E_{vdW} + G_{pol} + G_{np} - TS \quad (27)$$

The first terms are standards terms from molecular mechanics theory, such as bounded (bond, angle, dihedral), electrostatic and Van der Waals interactions. G_{pol} and G_{np} are polar and non polar contributions to the solvation free energy. The inclusion of solvent effects is very important, because it affects, also the ligand-protein binding. Currently the inclusion of explicit water molecules in the system leads to increase the computational time for the free energy binding evaluation. Consequently a smart way is to consider water implicitly. Polar contribute

represents the energy stored in the continuum dielectric in response to the presence of the solute's charge distribution and it is calculated using a finite-difference solution equation, in the MM-PBSA method, or a Generalized Born (GB) pairwise approximation, in the MM-GBSA approach, of the Poisson-Boltzmann equation (PBE)¹², which is defined by the equation:

$$\nabla \cdot \epsilon(\mathbf{r}) \nabla \phi(\mathbf{r}) = -4\pi \rho^f(\mathbf{r}) \quad (28)$$

where $\epsilon(\mathbf{r})$ is a predefined dielectric distribution function for the solvated molecular system, $\phi(\mathbf{r})$ is the potential distribution function, and $\rho^f(\mathbf{r})$ is the fixed atomic charge density. For example, in the generalized Born equation the electrostatic contribution¹ is given by:

$$\Delta G_{polar} = -\frac{1}{2} \sum_{i,j} \frac{q_i q_j}{f(r_{ij} a_{ij})} \left(1 - \frac{1}{\epsilon}\right) \quad (29)$$

where $f(r_{ij} a_{ij})$ depends upon the inter-particle distances and the Born radii and ϵ is the solvent dielectric constant¹³.

The non-polar term, instead, is calculated using a linear relation to the solvent accessible surface area (SASA).

$$G_{np} = \gamma SASA \quad (30)$$

where γ is the microscopic surface free energy for formation of a cavity in water (surface tension).

The sum of polar and non-polar terms gives the solvation energy:

$$G_{solv} = G_{pol} + G_{np} \quad (31)$$

Finally, the last term in equation (27) is the product of the absolute temperature (T) and the entropy (S)¹¹. The entropy term can be evaluated by either performing a normal mode analysis¹⁴ or a quasi-harmonic analysis¹⁵. However the entropy estimate is computationally demanding,

thus in order to speed up the calculation it is possible to use low quality empirical evaluations, or in particular cases, such as docking approach with a common target, the entropy can be neglected¹⁶.

3 Biological Background

This chapter provides a description of microtubules, explaining their structure, functions and the central role in chemotherapeutic treatments. Then, an overview of Microtubules Targeting Agents (MTA) is provided, followed by a description of different human tubulin isotypes and an introduction on microtubule modeling.

3.1 Introduction

Microtubules play important roles in several cellular processes. They are cylindrical protein filaments assembled from $\alpha\beta$ -tubulin heterodimers that align in a head-to-tail fashion¹⁷. Any factor altering tubulin polymerization/depolymerization dynamics may strongly affect the cell homeostasis and leads to mitotic arrest, eventually resulting in cell death¹⁸. In past years, microtubules became targets in cancer therapy for a wide range of molecules, including taxanes, vinca alkaloids, macrolides and peptides, able to interfere with the microtubule dynamics¹⁹. In this context, colchicine and colchicine derivatives have been largely studied as chemotherapeutic drugs against cancer.

3.2 Functions of microtubules

Microtubules (MTs) with actin microfilaments (MFs) and intermediate filaments (IFs) form the cytoskeleton, that is a complex network extended from the cellular nucleus. MTs are involved in many cellular processes and three main functions may be identified. First, they act as structural elements, supporting cells to maintain their shape: microtubule disruption may lead cells to lose their elongated shape or form blebs, caused by the cell membrane extending from the cell body in a bulb shape manner²⁰. Secondly, MTs play a role as transportation tracks for motor proteins, such as kinesins and dyneins, to perform directed transport inside the cell. Finally, MTs assist the cell to position and separate the chromosomes during cell division forming the mitotic spindle²¹. This function is closely related to microtubule *dynamic instability*: MT structure is very instable going through continuous cycling phases of growth and rapid shrinkage, called catastrophes^{18,22}. This feature leads to a rapid turnover of microtubules and a constant remodeling of the cytoskeleton, which is fundamental for MT functionality.

The central role of microtubules in cell life make them key targets for pharmacological treatments: stabilizing microtubules or enhancing their depolymerization, it is possible to lead the cell to apoptosis or block the mitotic process²³. In the last years, many studies have therefore selected microtubules as target for anti-tumoral drugs, such as colchicine and colchicine derivatives, in order to block the rapid and uncontrolled cell division of cancer cells¹⁹.

3.3 Tubulin dimers

Microtubules are long and hollow biopolymers, with cylindrical shape consisting of $\alpha\beta$ -tubulin dimers, which are composed by two globular proteins, α and β tubulins. Structurally, α and β tubulin are known to be similar from the primary to the tertiary structure level, indistinguishable at a resolution of 6 Å²⁴. Each tubulin monomer has a weight of about 50 kDa and can be divided into three distinct domains: the amino terminal domain, or Rossmann fold, (composed of residues 1–205), an intermediate domain (residues 206–381) and a carboxy terminal domain, which contains the flexible C-terminal tail (residues 382–444)²⁵. In solution, each tubulin dimer is bound to two GTP molecules, one on each monomer. The nucleotide bound to α -tubulin is at the interface between the two monomers, and is nonexchangeable; GTP bound to β -tubulin, instead, is exposed to the surface and is exchangeable and can hydrolyze to GDP^{25,26}.

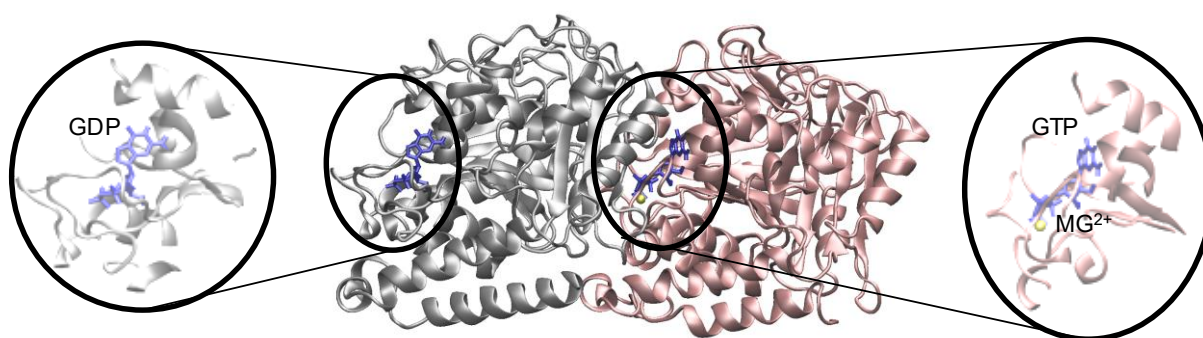


Figure 3.1 - The $\alpha\beta$ -tubulin hetero dimer with α -tubulin (right) and β -tubulin (left) together with guanosine-5'-triphosphate, guanosine-5'-diphosphate. The dimer is shown in a side view such that the top part of the monomers would constitute the inner interface of the MT while the bottom would be the MT outer surface. In the circles, zoomed GTP (α -tubulin) and GDP (β -tubulin) kept in the correspondent nucleotide sites are reported.

3.3.1 Tubulin domains

The N-terminal region (Figure 3.2a) consists of six parallel beta strands (S1-S6) alternating with five alpha helices (H1-H5). Between each strand and the following helix, there is a loop (T1-T5) which interacts with the nucleotide. Other secondary structures, such as turns and loops, exist in the region but have not been given specific name. The intermediate region

(Figure 3.2b) contains a mixed beta sheet (B7-B10) surrounded by alpha helices (H6-H10). Several loops are present in this region; loop T6 found between B6 and H6, loop T7, between H7 and H8, and finally the so-called M-loop, which lies between B7 and H9. Just like for the N-terminal region, other loops (e.g., the H6-H7 loop and the B9-B10 loop) also exist in the region but have not been named. The C-terminal (Figure 3.2c) is made up by two anti-parallel alpha helices (H11 and H12), which lie on the monomer surface in the direction of the protofilament. The last 10-20 residues of the C-terminal are known to be highly variable among the monomer isotypes and structurally disordered²⁷. As a result, these C-terminal residues have not been clearly identified yet from crystal structures and are missing in all available atomic resolution structure models. Despite of the extreme part of C-terminal is poorly defined, the region also features two alpha helices, which are very peculiar of tubulin monomers. The whole C-terminal region is known to be very important for the MT functions, since it regulates the interaction with other proteins, such as microtubule associated proteins (MAPs) and motor proteins such as kinesin and dynein²⁸.

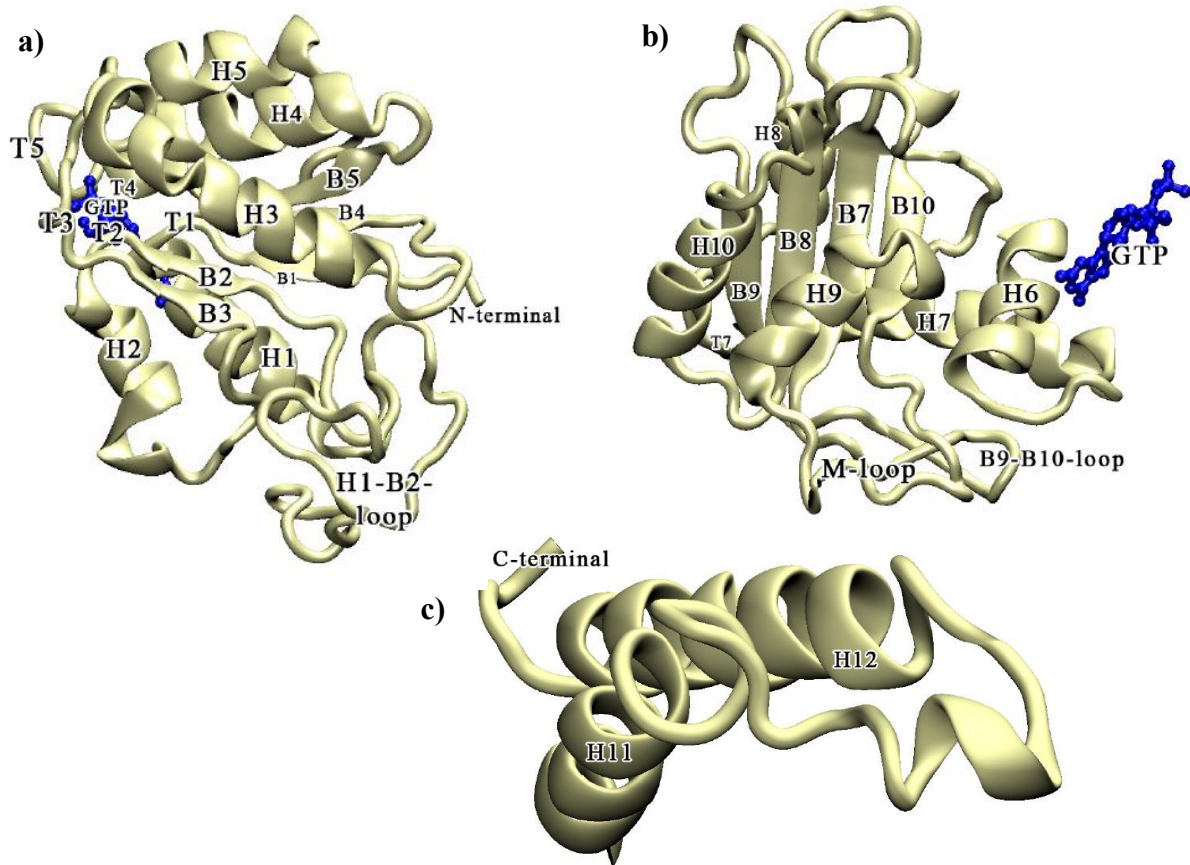


Figure 3.2 - a) The N-terminal region of α -tubulin together with GTP shown in side view with the top closest to the MT outside surface and the bottom pointing into the MT lumen. The central core is composed of parallel beta sheets S6 (hidden in the picture), S5, S4, S1, S2, and S3 surrounded by alpha helices. Three of these helices (H5, H4, and H3) are positioned above and two (H1 and H2) below the beta core. The loops between each strand and the following helix are all close to the nucleotide. b) Intermediate region (α -tubulin) in side view. The central core is composed of parallel beta sheets S7, S8, S9, S10 surrounded by alpha helices H6, H7, H8, H10. On the bottom the M-loop and the S9-S10 loop are shown. c) C-terminal region (α -tubulin) with the distinctive alpha helices (H11 and H12) on the MT surface.

In summary, the tubulin monomers have a structure characterized by a rigid core with rather flexible superficial loops which manage the longitudinal and lateral interactions. For example, lateral interactions are largely governed by the M-loop on one side and on the other side by the loops H1-B2 and helix H3. The M-loop protrudes from the dimer structure and is quite free to move and wiggle. It has been suggested that it acts as a hinge allowing the protofilaments to stay closer or further apart into the MT wall depending on the number of protofilaments building the MT lattice²⁴.

3.4 Microtubule architecture

Bound together in a head to tail fashion tubulin dimers make long protofilaments, which are arranged side-by-side in parallel with a relative angle so that the result is a highly regular cylindrical lattice structure, in which each dimer is in close contact with four surrounding

dimers: two in the same protofilament and the other two in the adjacent protofilaments. Different types of MTs exist with several protofilaments ranging between nine and eighteen²². In the MT lattice each protofilament is staggered with respect to the next one. Such shift or rise means that a chain of monomers circumferentially bound together form a helix rather than a ring. The result is a slightly skewed lattice, in which dimers connect indirectly to dimers further ahead on the same protofilament. The distance between such two dimers on the same protofilament is called pitch, P .

MTs are usually defined indicating how many protofilaments they consist of and the pitch number (e.g., 13:3 indicates a MT with 13 protofilaments and pitch of 3 monomers). Combinations of the number of protofilaments and pitch number, which have been theoretically predicted to be particularly favorable, are the MTs 10:2, 11:3, 12:3, 13:3, 14:3, 15:3, 16:4, and 17:4²⁹. Usually adjacent monomers are of the same type, i.e., α -tubulin monomers bind laterally to α -tubulin monomers and β -tubulins bind to β -tubulins. The exception, however, is when the pitch is equal to an odd number of monomers. In this case, adjacent protofilaments will be characterized everywhere by $\alpha\alpha$ - and $\beta\beta$ -interfaces, but at the seam, where two adjacent protofilaments bind together, they will be characterized by a $\alpha\beta$ -interface (Figure 3.3a).

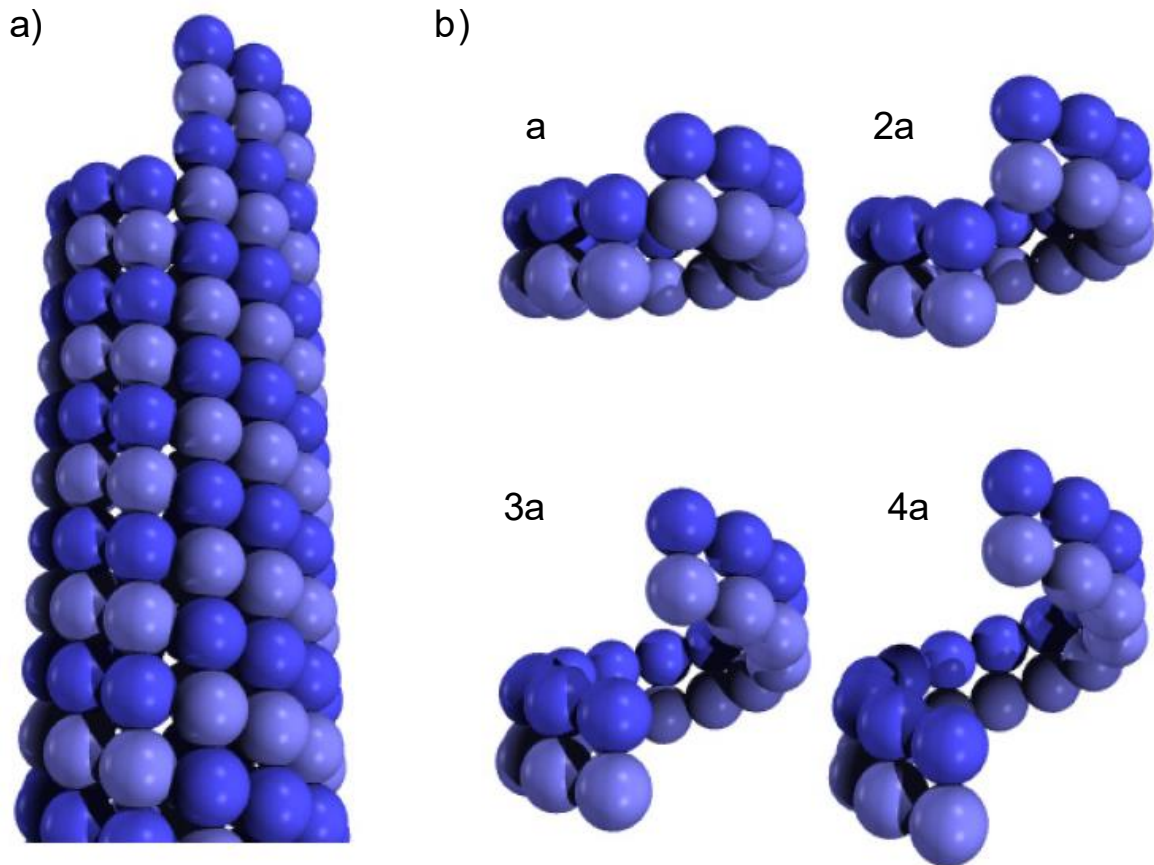


Figure 3.3 - a) MT with seam between the two protofilaments closest to the viewer. b) Four schematic illustrations of how dimers in lateral contact form different helices depending on the pitch. From left to right and from top to bottom the pitches are a, 2a, 3a, and 4a, where a is the size of the single monomer (~4 nm). For a pitch determined by an odd number of monomers, the result is the formation of a so-called seam along which α -tubulins (dark blue spheres) bind laterally to β -tubulins (light blue spheres) and vice versa. Such a mismatch among the lateral contacts occurs only at the seam, and thus only in MTs with an odd pitch.

Because of the pitch, a number of protofilaments higher or lower than 13 would imply a distortion of the MT lattice where the protofilaments are not straight anymore. However, it has been demonstrated that, due to the occurrence of isoforms with specific changes in the amino acid sequences of the monomer, 15:3 MTs can still show straight protofilaments as observed in the nematode *Caenorhabditis elegans*³⁰.

MTs vary in size in accordance to their number of protofilaments. For a 13:3 MT the typical inner and outer diameters are about 17 nm and 25 nm, respectively. Lengths range from 1-10 μm in eukaryotic cells up to 50-100 μm in axons.

3.5 Microtubule polymerization

Binding together on the plus end of the microtubule, α and β monomers start the polymerization: the β -tubulin subunit is exposed on the plus end of the microtubule while the α -tubulin subunit is exposed on the minus end. Before the integration in the microtubule wall, tubulin binds a GTP molecule that eventually hydrolyzes into GDP after the polymerization; only the tubulin dimers at the end of the microtubule stay in the GTP state, forming the GTP-cap. The GTP or GDP states influence the stability of the microtubule: tubulin bound to GTP tends to assemble into microtubule, while dimers bound to GDP tend to fall apart. For this reason, the loss of the GTP-cap leads to the opening of one end of the microtubule and to its depolymerization: once the GTP cap is lost, the lateral interactions in the GDP-bound tubulin weaken allowing the protofilaments to curl apart, leading to disassembly³¹.

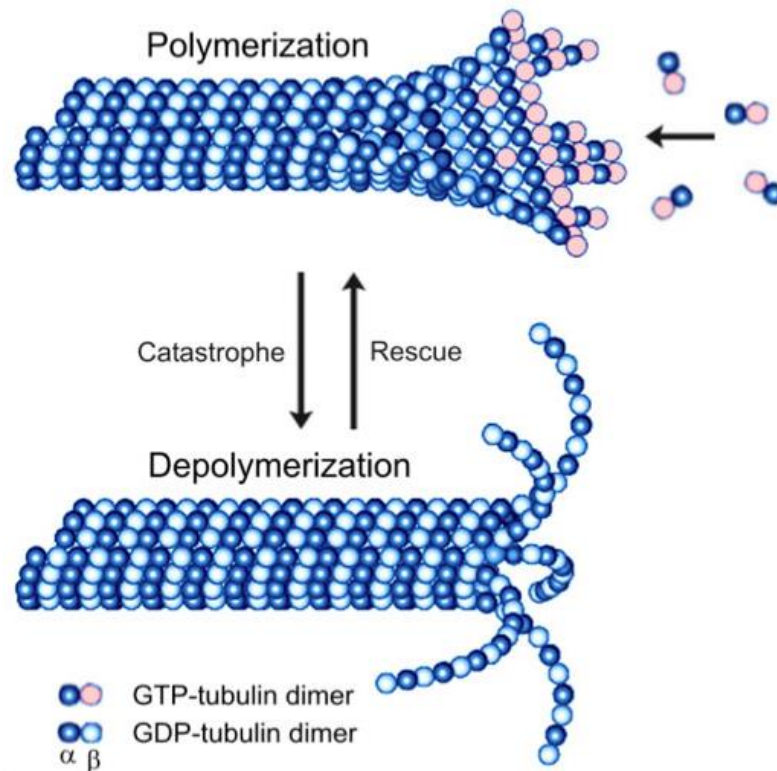


Figure 3.4 – Polymerization and depolymerization of microtubule: the construction and the disruption of the microtubule depend on the nucleotide state of tubulin dimers.

SOURCE: <https://www.embrn.eu/resources/wiki/microtubules-and-mast-cell-signaling.html>

Microtubules are therefore polar molecules like actin filaments, with a fast-growing plus end and a slow-growing minus end. The minus ends of microtubules are typically anchored at the centrosome and grow at slow rates; the highly dynamic plus ends, instead, are free to explore

the cytoplasmic space by stochastically switching between periods of growing and shortening; this switching behavior is termed *dynamic instability*³².

3.5.1 Allosteric and lattice model

MT polymerization is associated with a structural modification of tubulin dimers from curved to straight conformations; what is not already clear is if the conformation of tubulin is determined by the nucleotide state of β subunit. *Allosteric model* provides that the binding of GTP to free tubulin before assembly leads to a kinked-to-straight conformation switch, making the tubulin dimer sterically compatible for microtubule integration; *lattice model*, instead, postulates that free tubulin dimers adopt curved conformations both in GTP and in GDP state, and, after the integration in the microtubule wall, dimers are forced to assume the straight conformations due to lateral contacts^{33,34}. In the second model the binding to GTP does not cause a conformational change.

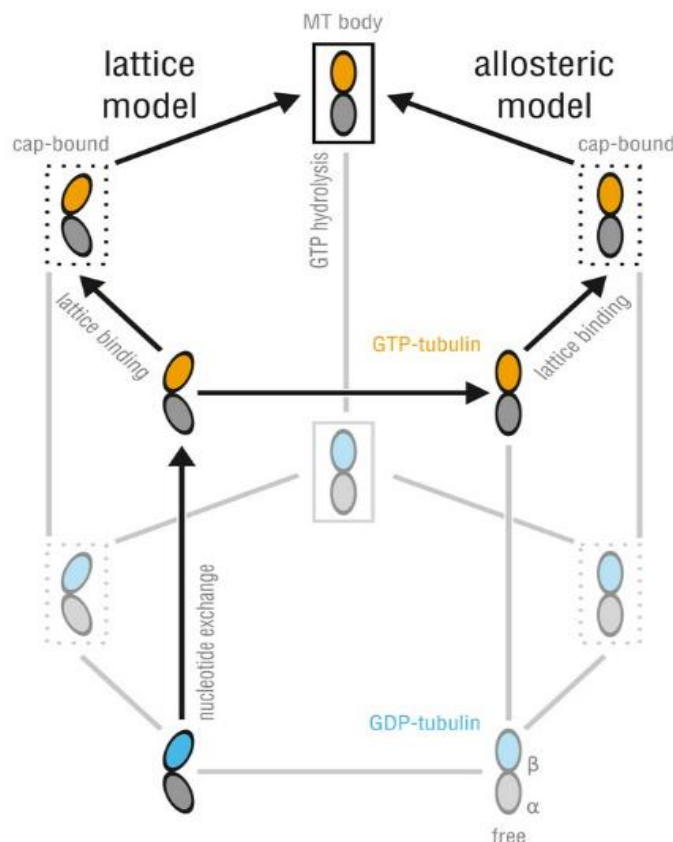


Figure 3.5 - Allosteric and lattice models of MT. GTP- (orange) and GDP-dimers (blue) can be free (no box), MT-cap-bound (dotted box), or integrated into the MT body (solid box). The dimmed states denote energetically unfavored states. DOI: <https://doi.org/10.7554/eLife.34353.002>

The debate between these two models is still open and there are evidences for both.

In 2009 Bennett et al. proposed a blended model of assembly³⁵: the different nucleotide state of tubulin leads to a different intradimer flexibility and therefore the assembly properties of the free dimer are better described based on flexibility. In this model free-dimer allosteric effects retain importance, but assembly process is dominated by lattice-induced effects.

3.6 Microtubule targeting agents

Microtubules are widely used as target for cancer chemotherapy and drugs normally employed are called *microtubule targeting agents* (MTAs). MTAs can be divided into two classes that either stabilize or destabilize microtubules³⁶. These agents bind tubulin in at least four binding sites: the laulimalide, taxane/epothilone, vinca alkaloid, and colchicine sites.

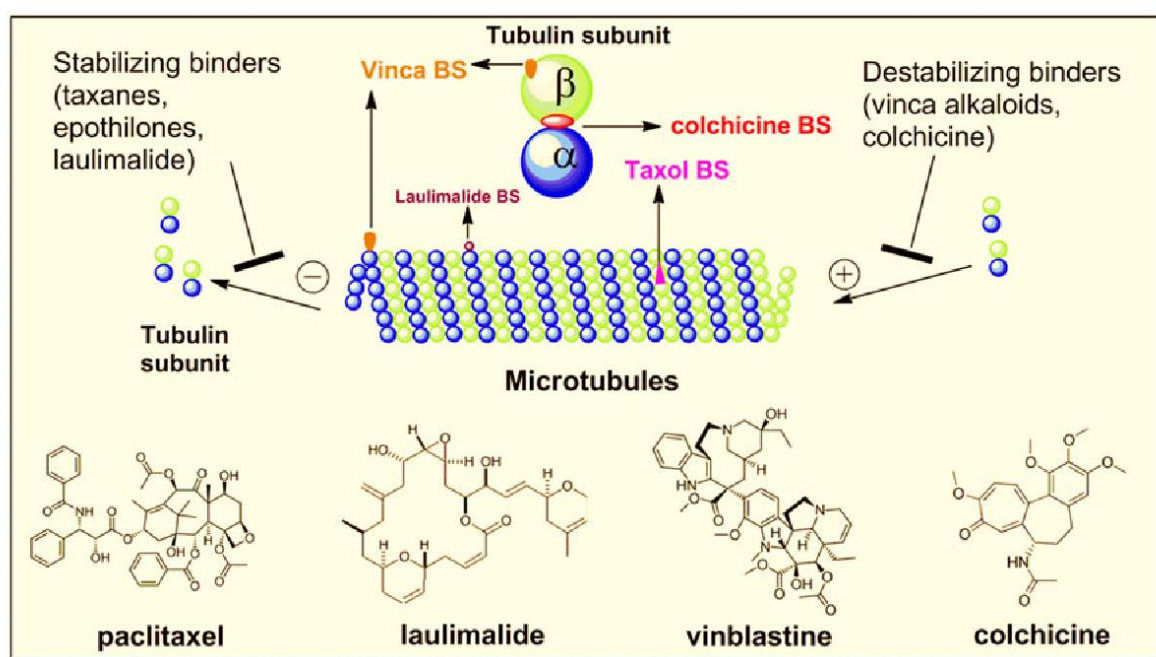


Figure 3.6 – Principal microtubule targeting agents and their binding site on tubulin and microtubule.
DOI: 10.1007/s11095-012-0828-z

Taxanes, including paclitaxel and docetaxel, promote tubulin stabilization, interfering with tubulin dynamics; similarly, laulimalide can promote the tubulin-microtubule assembly. On the other hand, vinca alkaloids, including vinblastine, vincristine, and vinorelbine, promote depolymerization of microtubules. Also colchicine and its derivatives can promote the microtubule depolymerization: the binding of colchicine to β tubulin prevents tubulin to adopt a straight conformation, inhibiting microtubule assembly³⁷. The colchicine binding site is one of the most important pockets for potential tubulin inhibitors for the development of apoptotic-inducing chemotherapeutic agents³⁸.

3.6.1 Colchicine and colchicine derivatives

Colchicine is derived from the seeds and corms of *Colchicum autumnale*. Extracts of this plant were introduced for the treatment of acute gout in the sixth century and have been in continuous use for this purpose for more than 200 years. In the last years, colchicine was again studied for its antimetabolic activity: cancer cells are more susceptible to colchicine poisoning than normal ones, because they undergo mitosis at higher rate. The crucial problem in the colchicine application is its toxicity, that is largely gastrointestinal in customary doses. Larger doses in addition produce disseminated intravascular coagulation, marrow failure, hepatocellular failure, and late central-nervous-system dysfunction, among other effects³⁹. Anyway, it is clear the importance of the colchicine binding site in microtubule dynamics: many colchicine binding site inhibitors (CBSI) have been proposed in the past years and multiple efforts have been made to outline new colchicine derivatives with lower toxicity^{37,40-44}.

3.7 Tubulin structures

In the last twenty years, several crystallographic structures of tubulin have been released and are now available from the RSCB Protein Data Bank (PDB). The first tubulin structure, 1TUB, was crystallized as a flat Zn^{2+} induced sheet of antiparallel protofilament-like end-to-end α/β dimer repeats, using docetaxel as a stabilizing agent²⁵. In 2000 a new structure, 1FFX, was derived from the 1TUB using a stathmin-like domain⁴⁵. Due to difficulties in fitting electron density, these structure contains misalignments and were superseded by 1JFF, in which paclitaxel was utilized as a stabilizing agent²⁶. Then the 1TVK was produced using epothilone A, which binds at the taxane binding site and stabilizes the MTs⁴⁶. In 2004 Ravelli et al. discover the colchicine binding site, producing the structures 1SA0 and 1SA1, both using a stathmin-like domain⁴⁷. Then the 1Z2B was obtained: in this structure both the colchicine and vinblastine binding sites are observed^{48,49}. Finally, in 2014 two high resolution structures were build, the 3J6E⁵⁰ and the 4O2B¹⁷. The first one contains nine α/β dimers arranged to form a portion of the microtubule wall, while the second one contains two dimers, a Stathmin-4 and a tubulin-tyrosine ligase.

3.8 Tubulin isotypes

Even in the same organism there are several genomic copies of α or β tubulin, that differ for punctual or restricted structural variations; tubulins characterized by the same mutations form

an isoform, if they are common through different species, or an isotype, if they are confined in the same organism. Variations of tubulin structure, in particular in the beta chain, highly affect microtubule dynamics⁵¹; this means that the organism produces specific isotypes of tubulin according to the external stimuli to correctly maintain the MT assembly/disassembly equilibrium⁴⁹.

Several isotypes of α and β tubulin in humans were identified in the last years. Anyway, in this work only β tubulin isotypes were considered, because most available data in literature deal with this subunit as a target for drugs and the colchicine binding site is located there. In 2006, Huzil et al. characterized ten different beta tubulin isotypes β I, β IIa/b, β III, β IVa/b, β V, β VI, β VII and β VIII⁵².

Different cells express different tubulin isotypes⁵³. Isotype β I is the most commonly expressed in humans and it is also the most common in cancer cells⁵⁴; in nontumoral tissues β I, β IVb, and β V were ubiquitous, β VI was hematopoietic cell-specific, and β IIa, β IIb, β III, and β IVa had high expression in brain, while in tumoral tissues isotypes β II and β III was usually over expressed. Isotypes β II and β III look therefore as potential targets for cancer therapies. Anyway, isotype β II is very abundant in the nervous system and a few other tissues, hence many side effects may occur; isotype β III, instead, is much less widespread than β II⁵⁵, it is expressed in metastatic and aggressive tumors⁵⁶, it is found only in neurons and not in glial cells⁵⁷ and it is often correlated with drug resistance⁴³. β III is therefore an excellent target for anti-tumoral therapies^{58,59}. In the following figure the isotype expression of the eight major isotopes in several tissues is represented.

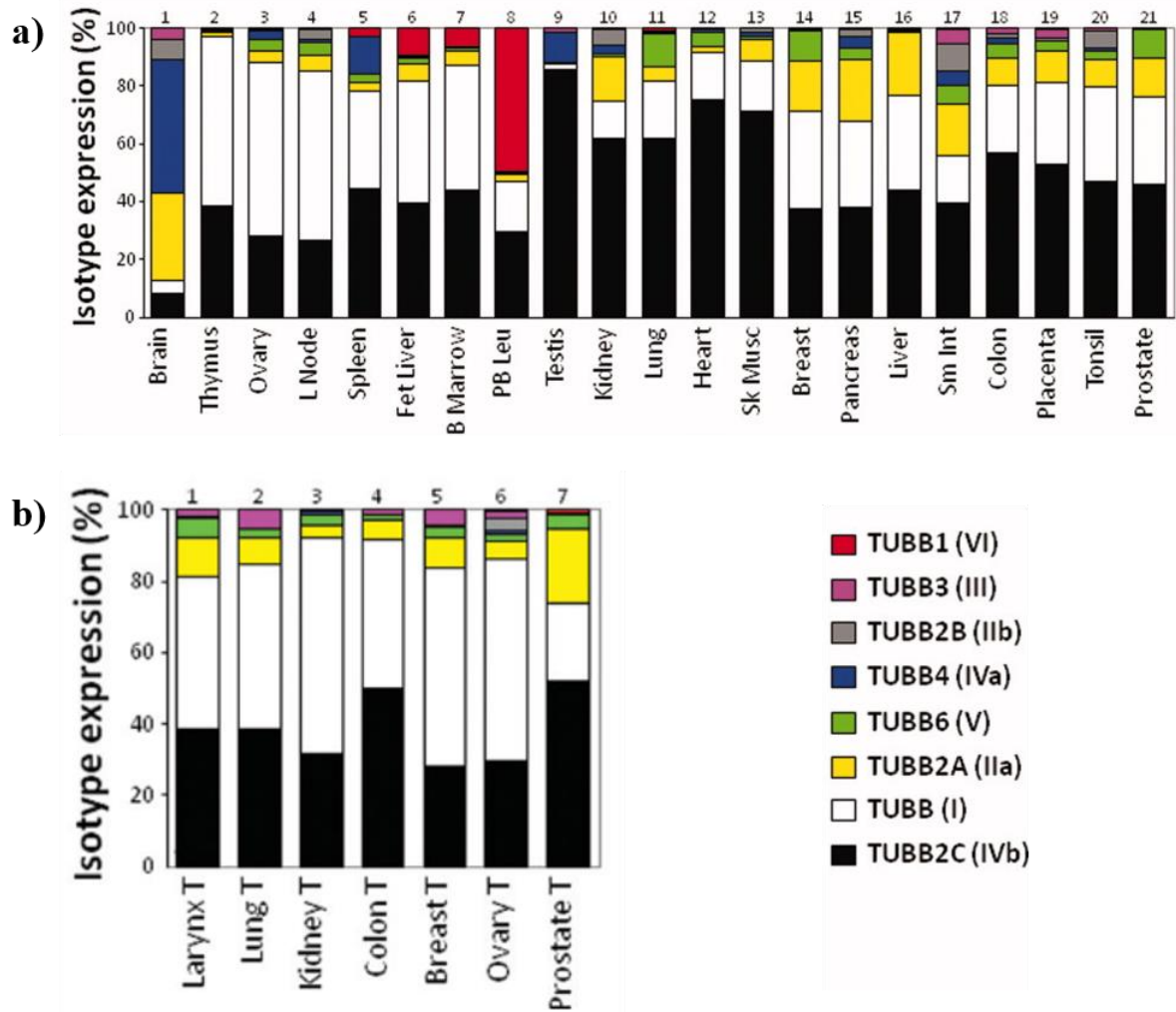


Figure 3.7 – Expression of the eight major tubulin isotypes in normal (a) and cancer (b) tissues.
DOI: 10.1002/cm.20436

Based on structural similarity, it is possible to divide some isotypes in different classes and, for example, Johnson et al. identify three types⁴⁰:

- Type I = $\{\alpha\beta\text{I}, \alpha\beta\text{IVa}, \alpha\beta\text{IVb}\}$
- Type II = $\{\alpha\beta\text{IIa}, \alpha\beta\text{IIb}\}$
- Type III = $\{\alpha\beta\text{III}, \alpha\beta\text{V}\}$

The different expression of tubulin isotypes is a great opportunity to design novel drugs based on isotype specific differences and to improve the efficacy of the pharmacological treatment. The expression of several β -tubulin isotypes, in fact, permits to develop drugs with increased specificity for only those isotypes expressed principally in cancerous cells^{59–61}. Moreover, a chemotherapy drug selected to target a tubulin isotype expressed preferentially in cancer cells could potentially minimize damage to non-cancerous cells⁶².

The presence of several tubulin isotypes is also correlated with drug resistance to anti-tubulin agents, which is one of the major problem in chemotherapeutic therapies⁴⁹; several studies have highlighted the link between the isotype expression and drug resistance^{63–66}. In this context, isotype $\alpha\beta$ III seems to be implicated, especially in the resistance to paclitaxel, through a mechanism which reduces the microtubule stability: this isotype suppresses the drug's ability to affect MT dynamics directly⁶⁷. Anyway, the real molecular mechanism which correlate isotype expression and drug resistance is not well understood and the only evidence is that the over-expression of isotype $\alpha\beta$ III, such in case of cancer cells, lead to more dynamic microtubules⁶⁸.

3.9 Molecular modeling of microtubule

Cellular mechanics depends on the mechanical and physical properties of MTs, actin microfilaments (MFs) and intermediate filaments (IFs), which build the cytoskeleton.

Several theoretical models have been developed in order to justify some experimental evidences demonstrating that the mechanical behavior of the MT could be better described by using the elasticity theory for transversely anisotropic structures^{69–71}. Generally, in these theoretical models the mechanical properties of the tubulin dimers are assigned based on the experimental results on the whole MT, thus following an up-to-bottom approach. The main limitation in this approach is that no direct information about the mechanic properties of the single building blocks are assumed a priori. On the other hand, a precise information about the spatial compliance of the MT is needed, because the reasons lying at the basis of the mechanical MT behavior can be investigated only at the atomic level.

Then, another way to study MT properties is to inspect its mechanical characteristics starting from the atomic level by using a bottom-up approach. This means that a direct characterization of tubulin dimers and their interactions is needed. Computational Molecular Modeling provides tools, as Molecular Dynamics (MD) or Functional Mode Analysis (FMA), for analyzing the physical properties of molecular systems with atomic resolution. In the latest years several advances on protein mechanics has been obtained by using computational atomistic simulations^{72–79}. Since that none specific experimental investigation has been done in order to access the mechanical properties of the tubulin dimer, computational studies on single monomers cannot be directly related to experimental data. On the other hand, these data could be integrated in a hierarchical multi-scale approach aimed at building an entire MT. Then the

whole MT model could be simulated mimicking experimental set-ups gaining both the possibility to directly compare simulation results with experimental data and the great advantage to have a comprehensive understanding about the reasons of the results obtained at the atomic scale.

4 Human Tubulin Conformational Dynamics and Global Correlations Driven by Colchicine Binding

4.1 Abstract

Microtubules play important roles in several essential cellular processes, especially in cell division, and their functionality is influenced by complex polymerization dynamic, which is driven by conformational changes of tubulin. The presence of antimitotic drugs, such as colchicine, stabilizes curved conformation of tubulin, preventing the integration in microtubule lattice and leading to the arrest of polymerization process and eventually to cell death. In this study, the effect of colchicine on three different isotypes, $\alpha\beta$ IIa, $\alpha\beta$ III and $\alpha\beta$ IVa, was evaluated through molecular dynamics simulations with focus on the relation between local structural rearrangements and global conformational changes. The presence of colchicine increases the fluctuations of the β tubulin M loop for isotypes $\alpha\beta$ III and $\alpha\beta$ IVa, but not for isotype $\alpha\beta$ IIa; according to these variations, structural modifications, including intradimer bending and twisting angle variations, occur, suggesting a correlation between the M loop motions and conformational changes of tubulin dimer. Thus, computational methods provide an insight into the action of colchicine on conformational changes of tubulin dimer, which alter the microtubule polymerization process, and underline the effect of isotype expression on drug activity.

4.2 Introduction

Microtubules (MTs) with actin microfilaments (MFs) and intermediate filaments (IFs) form the cytoskeleton, that is a complex network extended from the cellular nucleus. They are involved in several biological process, for example supporting cell to maintain its shape, driving motor proteins such as kinesins and dyneins, and forming mitotic spindle during cell division. Their central role in the mitotic process make them great targets for anticancer therapies since cancerous cells proliferate by unregulated cell divisions⁸⁰: stabilizing microtubules or enhancing their depolymerization, it is possible to block the mitotic process and eventually lead cells to apoptosis²³.

Microtubules are hollow cylindrical polymers formed from the self-association of two monomers, α and β tubulin, into linear protofilaments; many protofilaments joining together laterally form the final microtubule⁷⁸. Structurally, α and β tubulin are known to be similar from

the primary to the tertiary structure level, indistinguishable at a resolution of 6 Å²⁴. Each tubulin monomer has a weight of about 50 kDa and can be divided into three distinct domains: the amino terminal domain, or Rossmann fold, (composed of residues 1–205), the intermediate domain (residues 206–381) and the carboxy terminal domain, which contains the flexible C-terminal tail (residues 382–444)²⁵. Tubulin dimer binds two molecules of GTP, one for each monomer, but only the nucleotide bound to β tubulin is exchangeable and can hydrolyze in GDP state^{25,26}. In the polymerization process, free tubulin dimers are integrated in the microtubule lattice: tubulin bound to GTP tends to assemble into microtubule and then to hydrolyze, while dimers bound to GDP tend to fall apart. The MT lattice, consisting of GTP-tubulin, is more stable in terms of depolymerization than a lattice of GDP-tubulin⁷³: growing end is therefore characterized by the GTP-cap, which enhances stability. Microtubules are therefore polar molecules, with a fast-growing plus end and a slow-growing minus end; the plus end is characterized by a switching behavior, called *dynamic instability*, between periods of slow growth and rapid disassembly¹⁸. The polymerization is a complex process and is associated with structural modifications of the tubulin dimers from curved to straight conformation: according to the *allosteric model*, tubulins in GTP state are straighter than those bound to GDP and are more compatible for microtubule integration, while, for the *lattice model*, tubulin dimers adopt curved conformations regardless of the nucleotide state and, after integration in the lattice, dimers are forced to straight conformation due to lateral contacts^{33,34}. The debate between these two models is still open and there are evidences for both, but anyway conformational state of tubulin is strongly related to microtubule polymerization³⁵.

Microtubules are widely employed as targets for pharmacological treatments and drugs which bind MTs are called *microtubule targeting agents* (MTAs). MTAs can be divided into two classes that either stabilize or destabilize microtubules³⁶. Destabilizing drugs are widely employed in cancer chemotherapy and normally are antimetabolic agents, such as colchicine, which interfere with tubulin dynamic and block mitosis. Colchicine blocks cell division by disrupting microtubules⁸¹: after binding in the colchicine binding site at the interface between monomers, colchicine stabilizes the curved conformation of tubulin, preventing the integration in the microtubule lattice. The crucial problem in the colchicine application is its toxicity, that is largely gastrointestinal in customary doses: in the past years, several studies have proposed new colchicine binding site inhibitors (CBSIs) and colchicine derivatives with lower toxicity^{37,40–43}.

Several isotypes of α and β tubulin, that differ for punctual or restricted structural variations, are present in humans and different cells express different tubulin isotypes⁵³. The different expression of the tubulin isotypes is a great opportunity to design novel drugs based on specific isotype differences and to improve the efficacy of the pharmacological treatment. The expression of several β -tubulin isotypes permits also to develop drugs with increased specificity for only those isotypes expressed principally in cancerous cells^{60,61}: isotype $\alpha\beta$ III is considered as an excellent target for anti-tumoral therapies because it is over-expressed in tumoral cells, but it is less widespread than other isotypes, such as $\alpha\beta$ I, $\alpha\beta$ II and $\alpha\beta$ IV, in normal cells and it is probably related to drug resistance^{58,59,82}.

The central role of microtubules in cell life and in the anti-cancerous treatments has increased the interest on the mechanical and physical properties of these cytoskeletal structures. In this context, Computational Molecular Modeling provides tools, as Molecular Dynamics (MD) or Functional Mode Analysis (FMA), for analyzing the physical properties of molecular systems with atomic resolution. In the past years, several computational studies were focused on the characterization of tubulin dimers and their interaction^{73,76,77}, on the conformational changes related to MT stability^{79,83}, and on the action of drugs on tubulin^{78,80,84,85}. In this work, Molecular Dynamics simulations on different human tubulin isotypes underline the action of colchicine on conformational changes of tubulin dimers and highlight the different activity of this drug on each isotype.

4.3 Materials and methods

In this work, human tubulin isotypes $\alpha\beta$ IIa, $\alpha\beta$ III and $\alpha\beta$ IVa were selected since they cover all possible mutations in the colchicine binding site: isotype $\alpha\beta$ III has three mutations, Cys239 to Ser, Ala315 to Thr and Thr351 to Val, isotype $\alpha\beta$ IIa contains only one modification, that is Val316 to Ile, while isotype $\alpha\beta$ IVa has no modifications in this site⁴⁰.

Table 4.1 – Colchicine binding site mutations in tubulin isotypes $\alpha\beta$ IIa, $\alpha\beta$ III and $\alpha\beta$ IVa.

<i>Isotype</i>	<i>Position</i>		
<i>$\alpha\beta$IIa</i>			Val316-Ile
<i>$\alpha\beta$III</i>	Cys239-Ser	Ala315-Thr	Thr351-Val
<i>$\alpha\beta$IVa</i>			

4.3.1 Homology modeling of tubulin isotypes

Human tubulin isotypes $\alpha\beta$ IIa, $\alpha\beta$ III and $\alpha\beta$ IVa were built by homology modelling using the crystal structure 4O2B.pdb¹⁷ as template. This structure was chosen due to the high resolution (2,3 Å) and the low number of missing residues, only six on the beta chain (from 276 to 281)³⁸.

First, the starting template was refined, removing uninterested molecules and selecting only chains A and B, GTP and Mg^{2+} contained in the α subunit, and GDP and colchicine contained in the β subunit. Missing residues of β tubulin (from 276 to 281) were added using MODELLER 9.20⁸⁶ and the best model was selected on the basis of DOPE (Discrete optimized protein energy) score.

The fasta sequences of the tubulin isotypes were downloaded from Uniprot website: for the α chain the sequence Q71U36 was selected, for the β IIa the Q13885, for the β III the Q13509 and for the β IVa the P04350^{80,84}. Only β tubulin isotypes and not the α ones were considered, since the β subunit is the main binding partner for colchicine and this study is indeed focused on the interaction between tubulin and colchicine⁵². The homology modeling of the different isotypes against the above refined template structure 4O2B.pdb was performed using MODELLER 9.20⁸⁶; for each isotype, the best model was chosen on the basis of the DOPE score. All models showed a sequence identity major than 96,5% and the homology modelling was therefore considered a correct method to build the human tubulin models.

The quality and the reliability of generated models were evaluated using PROCHECK⁸⁷, VERIFY3D⁸⁸ and ERRAT⁸⁹, as done in previous literature^{44,52,77,84}.

4.3.2 System set up

At each isotype GDP, GTP and Mg^{2+} ion from the starting template (4O2B) were added. Each structure was considered both bound to colchicine and without drug, obtaining six different systems for Molecular Dynamics (MD) simulations. Visual Molecular Dynamics (VMD) package⁹⁰ was employed for the representations of molecular systems.

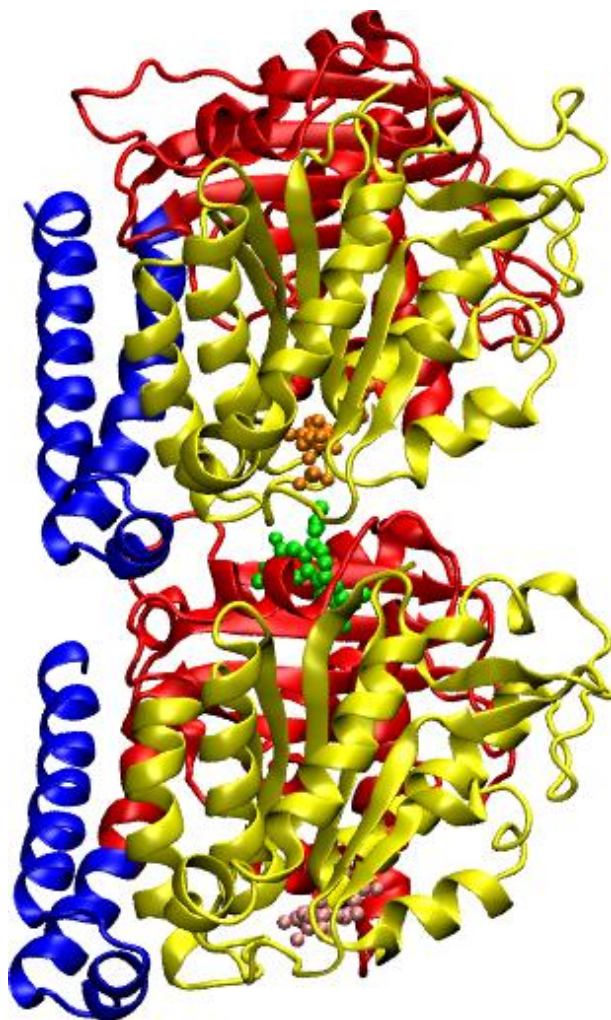


Figure 4.1 – Representation of a simulated structure: tubulin dimer bound to GTP (orange), GDP (pink) and colchicine (green). Tubulin domain are highlighted in different colors: in yellow the Rossman fold (1-205), in red the intermediate domain (206-381) and in blue the C-terminal domain (382-440/427).

MD simulations were performed using GROMACS 5.1.4⁹¹. The AMBER ff99SB-ILDN forcefield⁹² was chosen and the topologies for GTP, GDP and colchicine were built using ANTECHAMBER module^{93,94}, with general amber force field and BCC charge method, and ACPYPE⁹⁵. All systems were solvated using TIP3P explicit water model⁹⁶, a dodecahedron box with a minimum distance between solute and box of 0.45 nm was used and the periodic boundary conditions were always applied. Sodium and chlorine ions were added to the system to neutralize the charge, maintaining an ionic strength of 150 mM. Each system was minimized using the steepest descent algorithm for 1000 steps with a maximum force of 100 kJmol⁻¹nm⁻¹. All systems were equilibrated in NVT and NPT ensemble without position restrains only on water molecules and sodium and chloride ions: the NVT equilibration phase was performed for 100 ps using velocity-rescale thermostat⁹⁷ with the tau constant at 0.1 and the reference temperature at 300 K, while the NPT one for 300 ps using Berendsen barostat⁹⁸ to maintain the pressure at 1 atm. Particle-mesh Ewald (PME) method² was used for electrostatic calculations

with 1.0 nm cutoff, Fourier spacing of 0.2 nm and interpolation order of 4. Finally, each system was simulated for at least 200 ns without any restraint with a time step of 2 fs and coordinates saved at every 2 ps. For each structure two replicas were also simulated to ensure the repeatability of the results.

4.3.3 Functional mode analysis

Functional mode analysis (FMA) was used to highlight collective motion maximally correlated to the fluctuations of an arbitrary function, that is the distance of the center of mass of the M loop from the center of mass of the whole protein. The chosen function was assumed to be a linear function of the Principal Components (PCs), extracted from the first 50 eigenvalues of the PCA analysis. After maximizing the Pearson's coefficients, the FMA underlines the contribution of individual PCA vectors to the variation of the selected arbitrary function and provides a single collective motion, the ensemble weighted Maximally Correlated Motion (ewMCM).

The trajectories of the three replicas for each isotype were concatenated obtaining a single trajectory of 600 ns; first 400 ns were used for the model building set, while last 200 ns were used for the cross validation one. Therefore, the model built on the first two replicas predicts the fluctuations of the quantity of interest for the third replica.

The FMA was performed both on the isotypes with and without colchicine.

4.3.4 Structural analysis

As done in previous literature^{79,83}, conformational changes of tubulin dimer were further investigated since they drastically influenced the microtubule polymerization process. Three indices were therefore calculated to describe the relative movement between the two monomers: the RMSD of the beta subunit from its starting position, the *bending angle variation* (θ) and the *torsion or twisting angle variation* (φ). All these indices were calculated on the trajectories fitted on the internal beta sheets of the alpha subunit, in particular sheets S4 (133-140), S5 (165-172), S6 (200-205), S7 (269-273), S8 (313-321) and S10 (373-381); these structures were selected because they are quasi-static during the simulation and their RMSD is lower than 0,1 nm (see 4.7.4). Considering the trajectories fitted on the internal beta sheets of alpha subunit, the whole motion can be seen as a movement of the beta monomer respect to the fixed alpha tubulin.

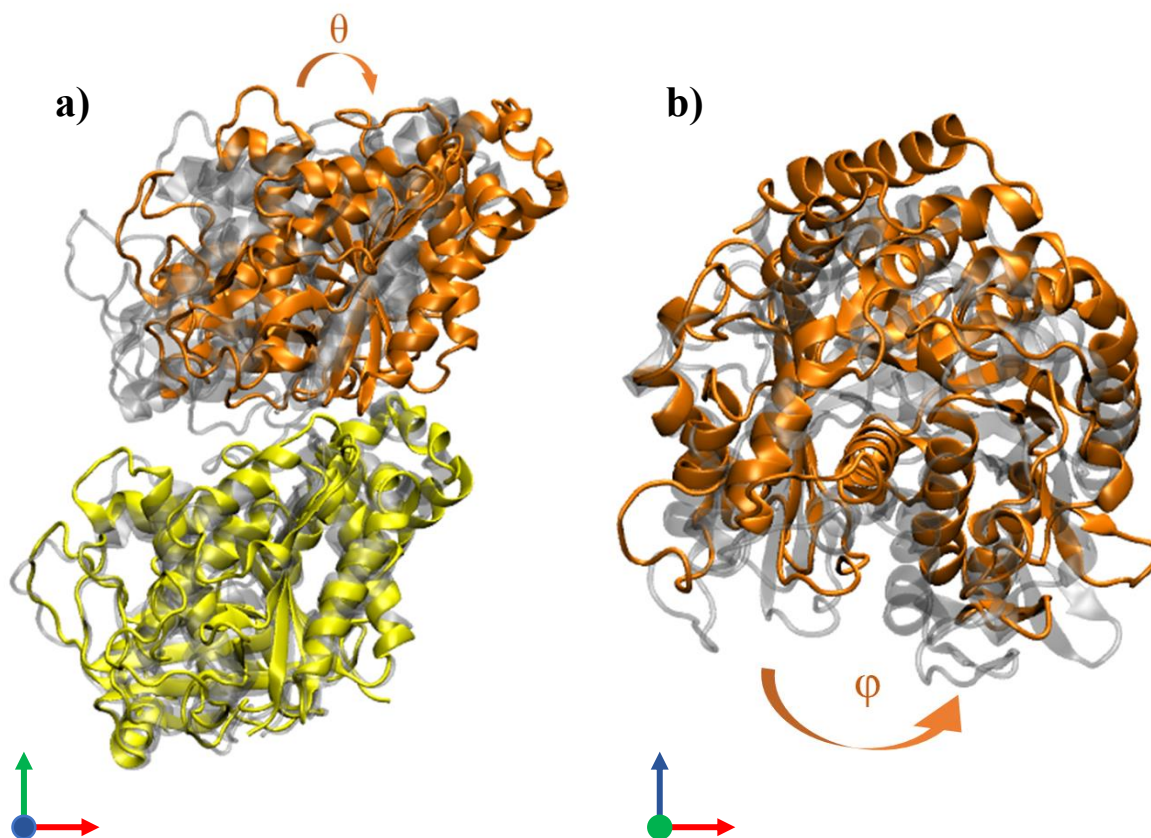


Figure 4.2 – Representation of bending (a) and twisting (b) angles between α (yellow) and β (orange) tubulin; in dimmed gray the starting undeformed structure.

The RMSD of the beta subunit from its starting position is calculated for each frame of the fitted trajectories on the internal beta sheet of alpha tubulin; this quantity is a measure of the whole motion of the beta tubulin from the alpha monomer and includes both the bending and the twisting motions.

The bending angle variation (θ) (Figure 4.3a) was defined by two vectors along monomer axes. The α axis (**A**) was defined by the center of mass (COM) of the internal beta sheets of alpha monomer and the COM of the internal beta sheets of the dimer in the first frame of the simulation. The β axis (**B**), instead, is defined on each frame of the simulation, connecting the COM of internal beta sheets of beta monomer and the COM of the internal beta sheets of the dimer. The angle subtended by the two axes was calculated as:

$$\theta = 180 - \cos^{-1}\left(\frac{\mathbf{A} \cdot \mathbf{B}}{|\mathbf{A}||\mathbf{B}|}\right)$$

The twisting angle variation (ϕ) (Figure 4.3b) was instead calculated as the angle subtended by the axes of the sheets S10 of each monomer minus its starting values.

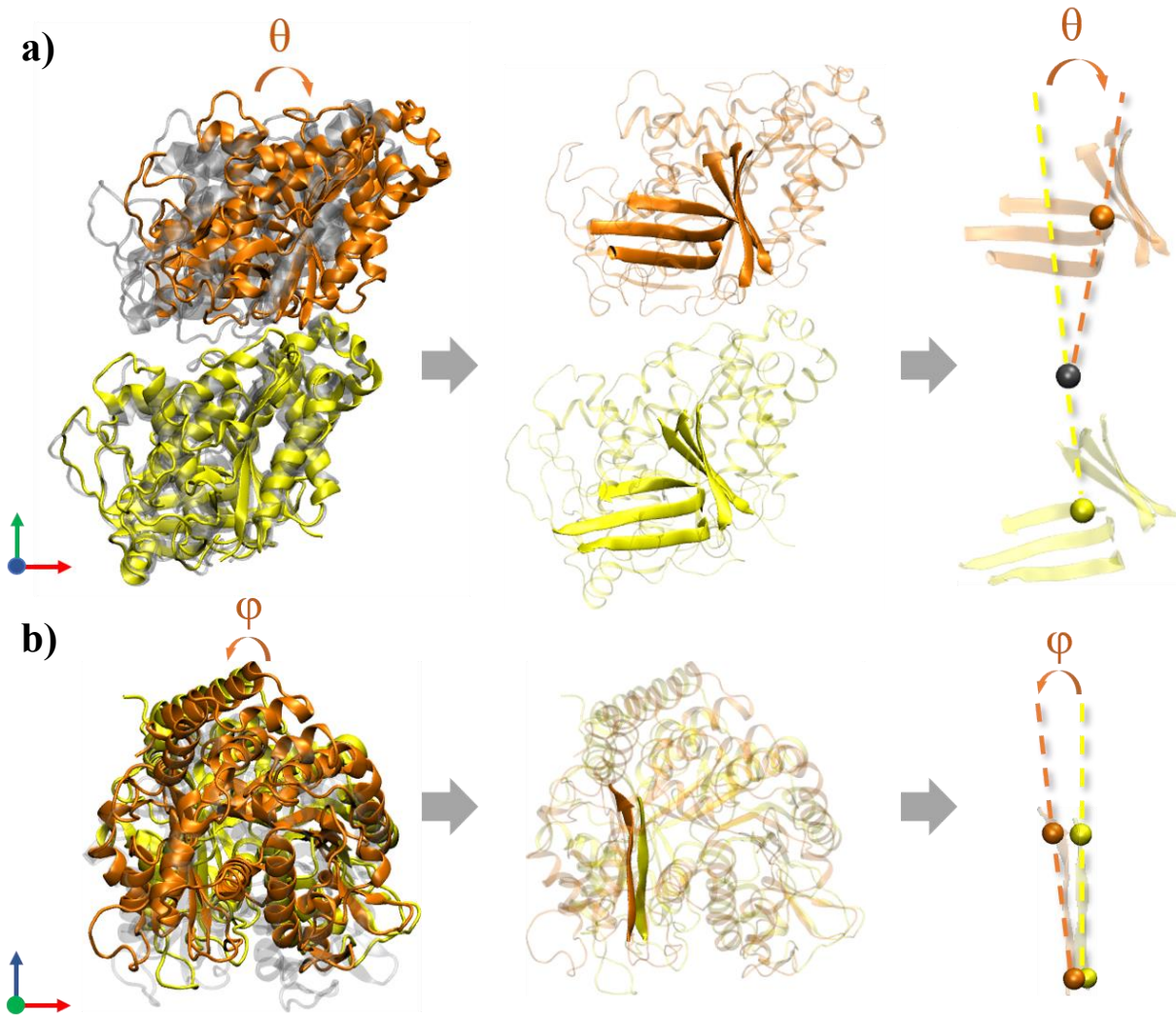


Figure 4.3 - Representation of bending (a) and twisting (b) angles between α (yellow) and β (orange) tubulin; in dimmed gray the starting undeformed structure. In the middle of the figure the sheets used for angle calculation are highlighted and on the right side the considered angles are sharpened.

4.4 Results

4.4.1 Model Validation

The first step was the validation of the structures generated with the homology modeling, based on the DOPE scores and on the analysis with PROCHECK, VERIFY3D and ERRAT.

The DOPE scores for template and isotypes $\alpha\beta$ IIa, $\alpha\beta$ III and $\alpha\beta$ IVa are respectively -112542,7, -110576,4, -110926,6 and -110307,4. The PROCHECK analysis shows that more than the 95,4% of the residues are in most favored regions in the Ramachandran plot for all isotypes and no residues are in the disallowed regions, except for the template structure that exhibit 0,1% of the residues in those regions. Finally, according to the VERIFY3D analysis, more than the

96,77% of the residues exhibit averaged 3D-1D score major or equal than 0,2 and the overall quality factor from ERRAT analysis is higher than 77,26.

These data indicate the good quality of the generated models. More details are provided in the Supporting Information section (4.7.1).

The first analysis of molecular dynamics simulations was performed to check the stability of the structures; the RMSD of the backbone atoms from the starting structure was calculated for the template, 4O2B, and for each isotype with and without colchicine during 200 ns of simulation (see 4.7.2). The RMSD shows that all the structures simulated reach the convergence, with values under 0,4 nm. Moreover, clustering the last 50 ns of simulations with a cutoff of 0,15 nm, only one cluster was identified, confirming that simulations have reached an equilibrated state.

This analysis was repeated also for each replica to ensure the stability for all configurations.

In the following, local effects of the presence of colchicine were firstly analyzed, considering the fluctuations in the colchicine binding site and the variations of the secondary structure; then, global effects were further investigated, focusing on conformational changes of the whole tubulin dimer and their correlations with local rearrangements.

4.4.2 Local effects induced by the presence of colchicine

In the following the colchicine binding site will be considered composed by S9 (349-354) and S8 (310-318) sheets, H7 (223-241) and H8 (250–258) helices, and T7 loop (242-249) of the β -tubulin, and α T5 loop (173-181) of the α -tubulin^{47,99}.

In order to underline different affinities between colchicine and each isotype, the binding energy was calculated using the MM-GBSA methods. For this purpose, the last 40 ns of simulation were considered and 200 frames were extracted. The binding energy calculated with the MM-GBSA method is reported in Table 4.2.

Table 4.2 - Binding energy of tubulin isotypes $\alpha\beta\text{IIa}$, $\alpha\beta\text{III}$, and $\alpha\beta\text{IVa}$ with colchicine calculated using the MM-GBSA approach and expressed in kcal/mol

Protein	ΔE_{vdw}	ΔE_{ele}	ΔE_{gas}	ΔE_{sol}	ΔE_{bind}
$\alpha\beta\text{IIa}$	$-58,93 \pm 2,42$	$-3,98 \pm 1,54$	$-62,93 \pm 2,9$	$8,18 \pm 1,44$	$-54,74 \pm 2,47$
$\alpha\beta\text{III}$	$-68,24 \pm 2,09$	$-2,32 \pm 2,40$	$-70,57 \pm 3,12$	$10,93 \pm 2,30$	$-59,64 \pm 2,45$
$\alpha\beta\text{IVa}$	$-64,79 \pm 2,83$	$-3,15 \pm 4,15$	$-67,94 \pm 4,47$	$10,40 \pm 3,18$	$-57,54 \pm 2,69$

Results from the MM-PBSA calculations are consistent with the previous ones (see 4.7.3).

For both methods, colchicine is a binder for all isotypes because its binding energy for tubulin assumes low negative values. Considering the standard deviations of the mean values of energy and the approximations introduced by these methods, the three isotypes show similar affinity for colchicine and it is not possible to rank the three isotypes based on their affinity.

Moreover, the RMSD of colchicine compared to the starting position of the drug in the template structure in the last 50 ns of simulation is plotted in Figure 4.4a for each simulated structure. Colchicine inside the template structure shows lowest values of RMSD, like those obtained from isotype $\alpha\beta\text{IIa}$: in these structures, colchicine tends to not deviate from the starting position. In isotype $\alpha\beta\text{III}$, instead, the RMSD exhibits the highest values and colchicine shows large deviation from the original position. The snapshot of colchicine position in the last frame of simulation is acquired for each structure and the overlapped snapshots are represented in Figure 4.4b.

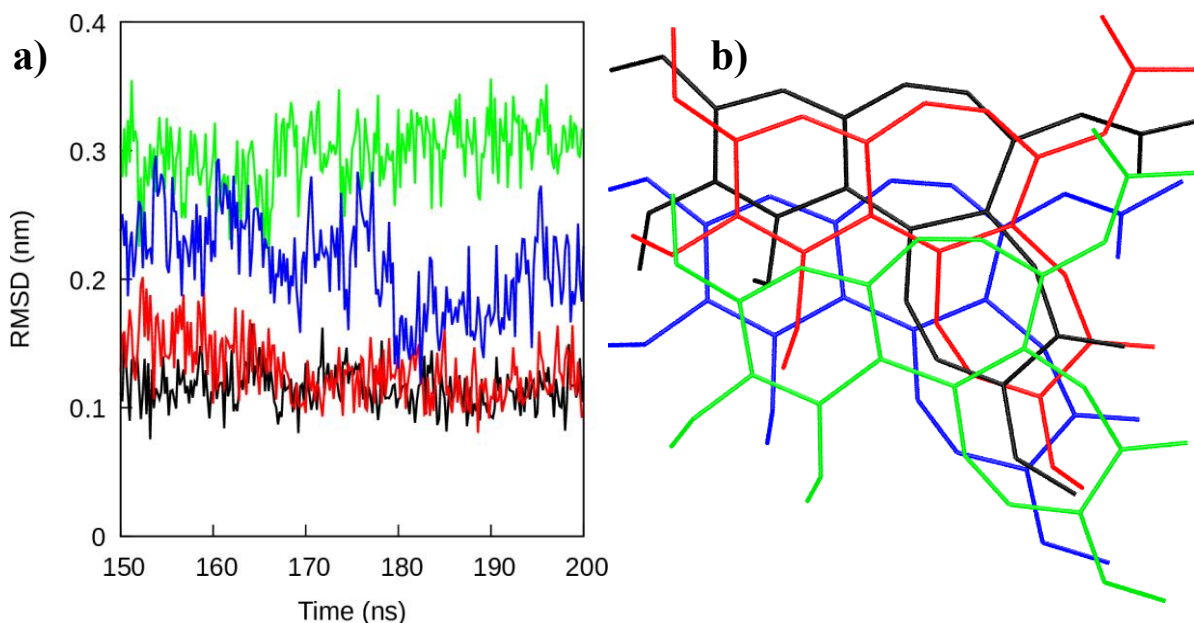


Figure 4.4 – a) RMSD of colchicine from its starting position in the template structure in the last 50 ns of simulation; b) overlap of colchicine molecules from the last frame of simulation. In black colchicine bound to the template structure, in red to isotype $\alpha\beta\text{IIa}$, in green to isotype $\alpha\beta\text{III}$ and in blue to isotype $\alpha\beta\text{IVa}$.

In order to highlight local differences between each isotype in presence of colchicine, the RMSD of the colchicine binding site from the original position in the template structure was calculate during the last 50 ns of simulation (Figure 4.5).

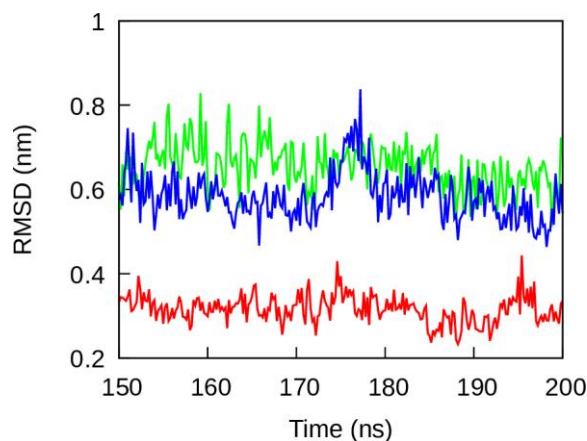


Figure 4.5 – RMSD of the colchicine binding site from its starting position in the template structure in the last 50 ns of simulation for isotypes $\alpha\beta\text{IIa}$ (red), $\alpha\beta\text{III}$ (green) and $\alpha\beta\text{IVa}$ (blue).

The RMSD of the colchicine binding site exhibits lowest values for the isotype $\alpha\beta\text{IIa}$, suggesting that colchicine induces greater local destabilization in isotypes $\alpha\beta\text{III}$ and $\alpha\beta\text{IVa}$.

Secondary structure modifications of the colchicine binding site induced by the presence of colchicine were further investigated. The most relevant structures belonging to the colchicine binding site were analyzed with STRIDE^{100,101} using the last 40 ns from simulation trajectories

and mediating the distributions of the secondary structure over all used frames. The probability of secondary structure is plotted in Figure 4.6 for each isotype.

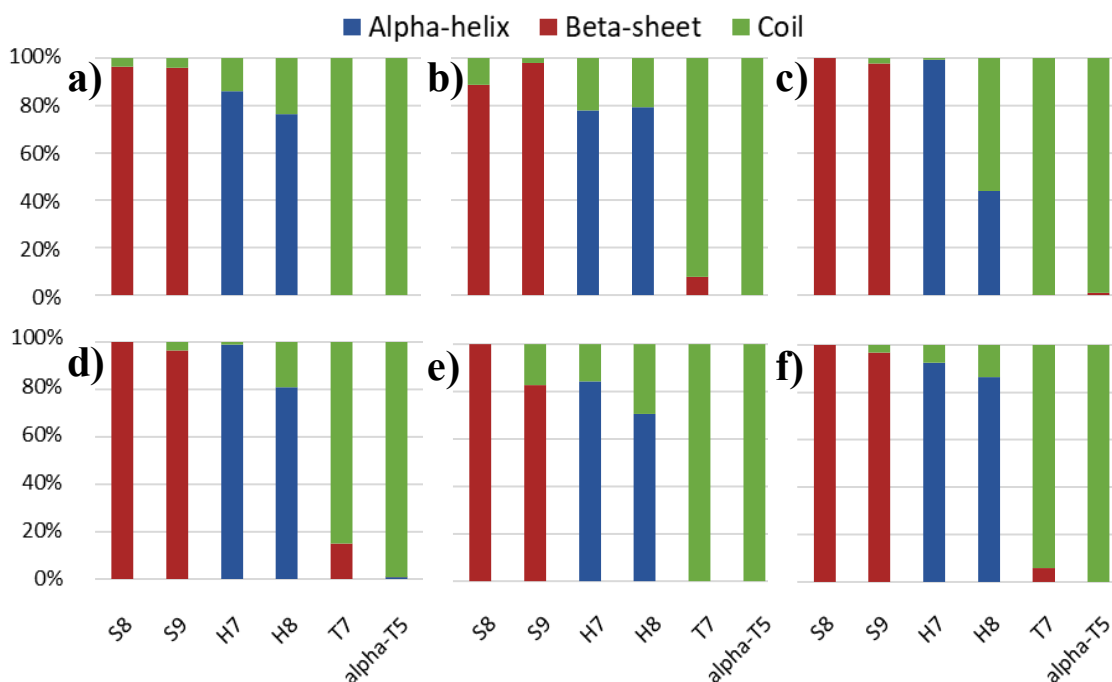


Figure 4.6 – Secondary structure probability in the colchicine binding site during the last 40 ns of simulation for isotypes a) $\alpha\beta\text{IIa}$, b) $\alpha\beta\text{III}$ and c) $\alpha\beta\text{IVa}$ with colchicine and for the same isotypes d), e), f) without colchicine

The presence of colchicine not significantly alters the secondary structure of the colchicine binding site, except for H8 helix in the isotype $\alpha\beta\text{IVa}$; this structure tends to unfold in presence of colchicine.

4.4.3 Global effects induced by the presence of colchicine

In order to underline the most fluctuating regions in the isotype structures, the root mean square fluctuations (RMSF) were analyzed: this index shows the degree of movement of the C-alpha atoms around their average positions for each residue. Therefore, more flexible regions show higher values of RMSF. The following graph represents the average RMSF over the three replicas for the β subunit calculated for each isotype bound to colchicine.

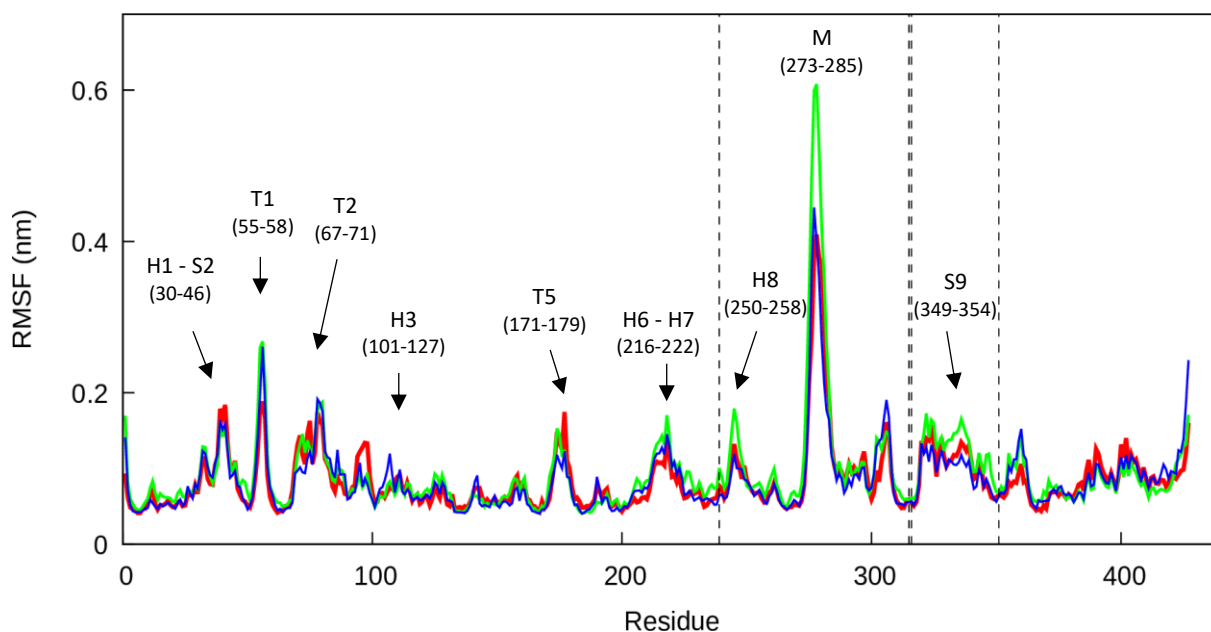


Figure 4.7 – Average RMSF of beta tubulin between the three replicas for isotypes $\alpha\beta$ IIa (red), $\alpha\beta$ III (green) and $\alpha\beta$ IVa (blue) bound to colchicine; dotted lines represent residue modifications in the colchicine binding site.

From the RMSF analysis the most flexible regions are the loops H1-S2, T1, T2, T5, H6-H7 and M, the H8 helix and the S9 sheet. The isotype $\alpha\beta$ IIa shows highest fluctuations in the loop T5 and lowest in the T1 loop, while the M loop of the isotype $\alpha\beta$ III is the most flexible. T5 is crucial for binding nucleotide and for longitudinal contacts⁸⁵; M loop, instead, interacts with H1-S2 loop in adjacent protofilament and it is therefore implicated in lateral interactions⁷⁸. All isotypes show high values of RMSF for the M loop, highlighting the possibility that the fluctuations of this structure could be implicated in important conformational changes.

The RMSF of the α and β subunits were calculated also for the isotypes not bounded to colchicine and for each structure the average RMSF between the three simulated replicas is derived. The average RMSF in correspondence of the M loop (273-285) calculated on the α subunit exhibits very similar values both for isotypes bounded to colchicine and for those without drug and the M loop is not the structure with maximum fluctuations (see 4.7.5). In the β subunit, instead, the fluctuations of the M loop seem higher for isotypes $\alpha\beta$ III and $\alpha\beta$ IVa bounded to colchicine, while for isotype $\alpha\beta$ IIa there is no appreciable differences between the cases with or without colchicine. In the following figure, the RMSF of the beta subunit for isotypes with and without colchicine is represented.

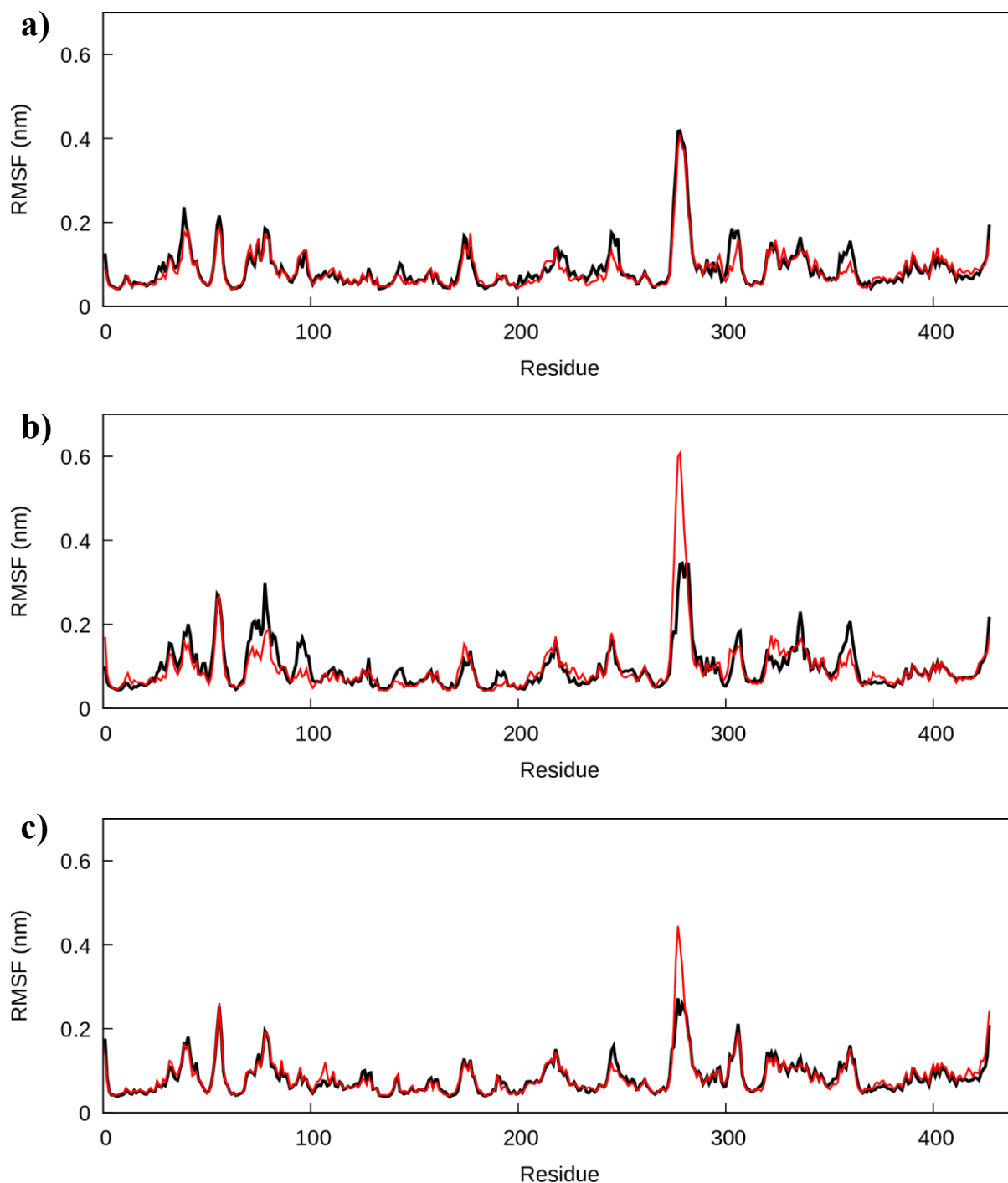


Figure 4.8 – Average RMSF of beta tubulin between three replicas for isotypes a) $\alpha\beta\text{IIa}$, b) $\alpha\beta\text{III}$ and c) $\alpha\beta\text{IVa}$; in black structure without colchicine, in red isotype bound to colchicine.

Since the fluctuations of the M loop are much higher in the beta subunit and the differences between structure with and without colchicine appear evident only in the RMSF of the beta monomer, we decided to focus our attention only on this subunit. This is reasonable also because mutations of isotypes are restricted to the beta monomer and colchicine interacts predominantly with this subunit.

Since colchicine is known as a destabilizing agent, conformational changes of tubulin were studied: the RMSD of the beta subunit from its starting position, the bending angle variation (θ) and the twisting angle variation (φ) were calculated as described in section 4.3.4 for both isotypes with and without colchicine. The averages of these indices between the three replicas were calculated in the last 50 ns of simulation, corresponding to the equilibrium states.

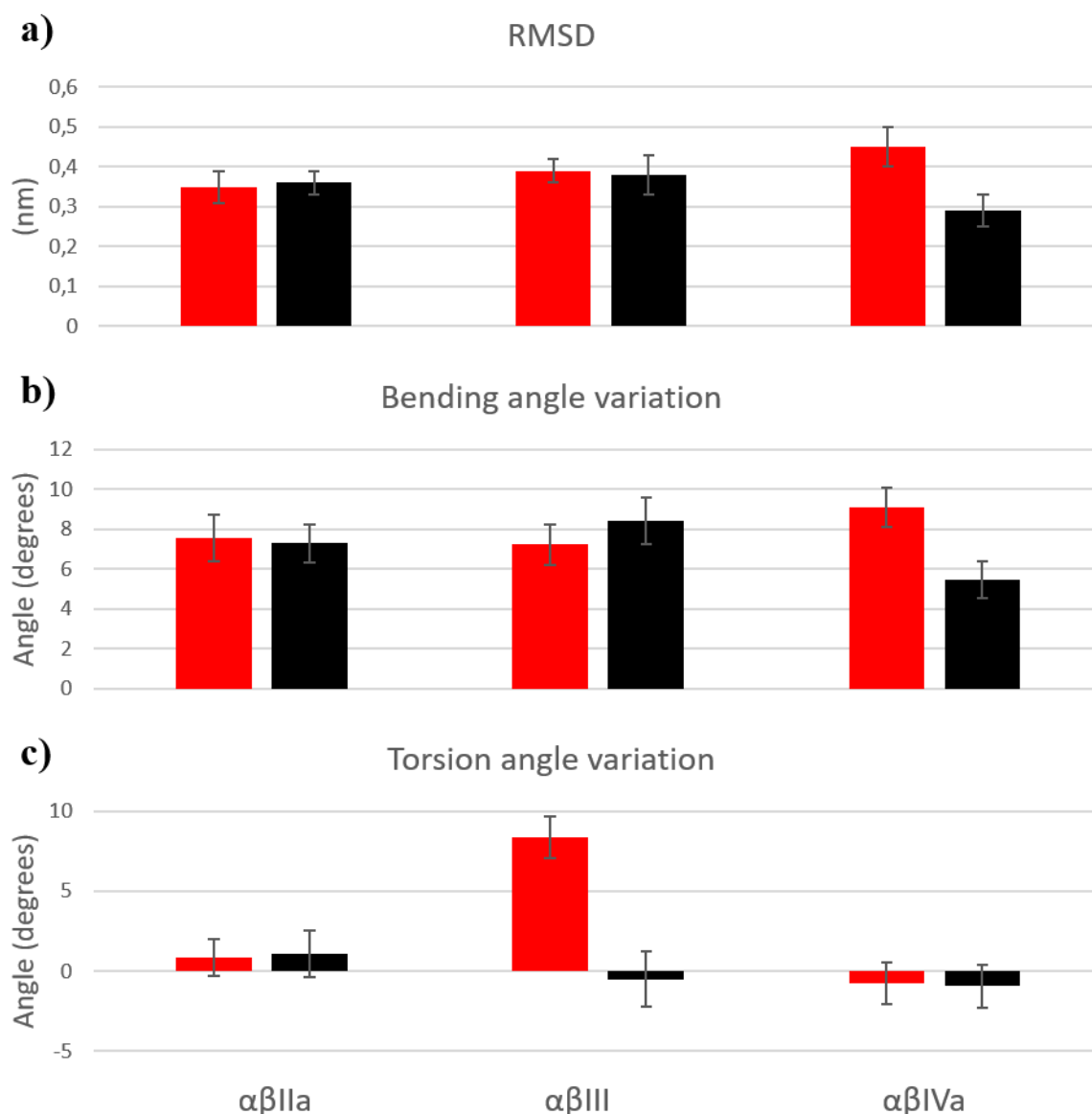


Figure 4.9 - a) Average bending angle variation, b) average twisting angle variation and c) average RMSD of the beta subunit during the last 50 ns of simulation between the three replicas for isotypes $\alpha\beta$ IIa, $\alpha\beta$ III and $\alpha\beta$ IVa with colchicine (in red) and without colchicine (in black).

The three isotypes respond in different ways to the presence of colchicine, modifying preferentially their bending or twisting angle: isotype $\alpha\beta$ IIa exhibits no appreciable differences in presence or absence of colchicine, while isotypes $\alpha\beta$ III and $\alpha\beta$ IVa display an increasing in twisting and bending angles respectively. Isotype $\alpha\beta$ III is characterized by a torsion angle

variation of $8,38 \pm 1,34$ degrees when bounded to colchicine and of $-0,51 \pm 1,72$ degrees without drug; isotype $\alpha\beta IVa$ instead shows a higher bending angle variation when bounded to colchicine ($9,07 \pm 0,98$ degrees) than in absence of the drug ($5,45 \pm 0,93$ degrees). The RMSD considers the complete motion of the beta subunit from its starting position, considering both bending and twisting deformations: only isotype $\alpha\beta IV$ shows an appreciable difference in this value between the colchicine bound and unbound states. This is consistent with the angle variation data because the bending motion is more destabilizing than the torsion one.

The different behavior of the three isotypes is plotted in Figure 4.10 in a scatter chart, in which the x-axis represents the bending angle variation and the y-axis the twisting one: from the last 50 ns of simulation a frame every 200 ps is considered, the bending and the twisting angle variation are calculated for each isotype and the average values between the three replicas are plotted. For each structure we obtain 250 couples of values representing the conformational state of the referred structure at a specific time. The same procedure is repeated both in presence and in absence of colchicine to underline the conformational change due to the action of the drug.

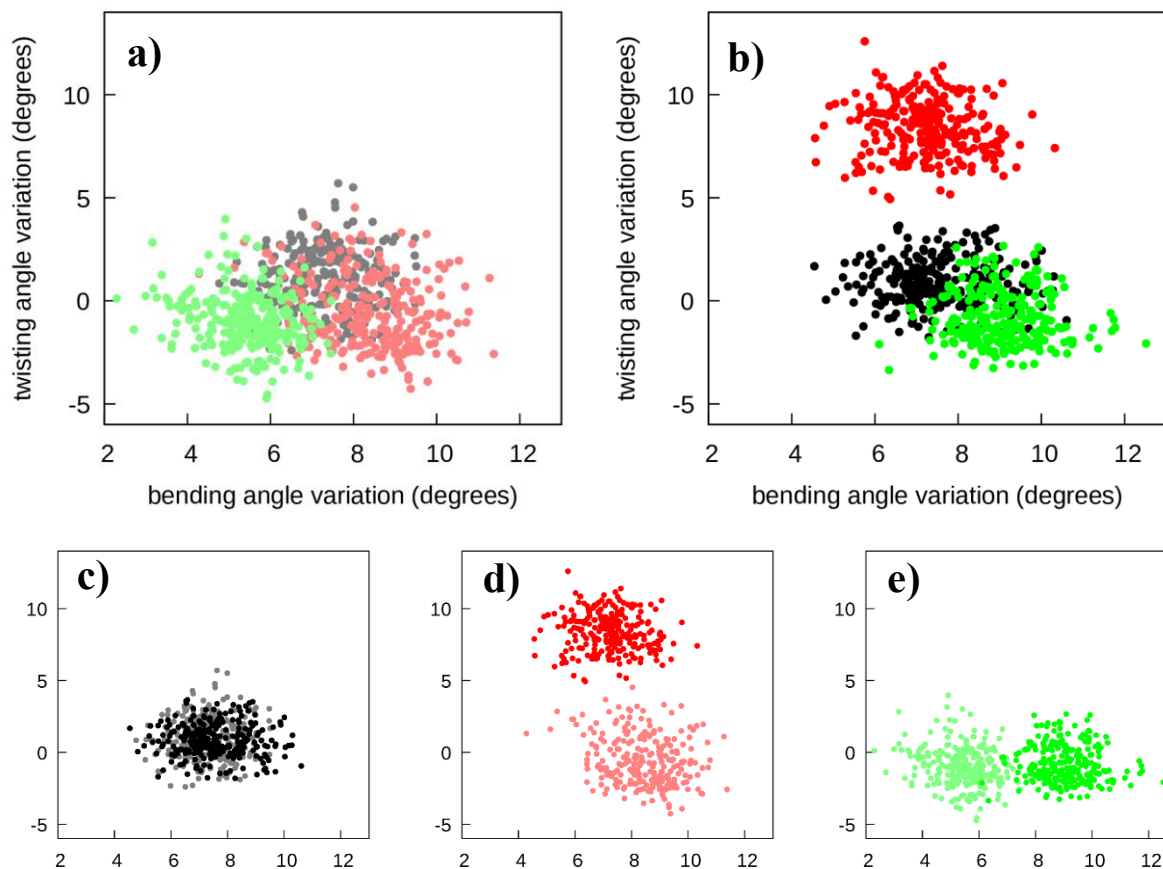


Figure 4.10 – Average bending and twisting angles from the last 50 ns of simulation between the three replicas for isotype $\alpha\beta$ IIIa (black), isotype $\alpha\beta$ III (red) and isotype $\alpha\beta$ IVa (green); a) isotypes without colchicine, b) structures bound to colchicine, c), d) and e) isotype with colchicine in full color and without colchicine in dimmed color.

From the previous figure is evident that the conformational changes of the isotype $\alpha\beta$ IIIa are not relevant, while isotypes $\alpha\beta$ III and $\alpha\beta$ IVa exhibits preferentially twisting and bending variations respectively in presence of colchicine.

4.4.4 Functional mode analysis

Functional mode analysis (FMA) was used to reduce the system dimensionality and to underline the structural modification of tubulin due to the M loop fluctuations. This analysis detects the ensemble weighted Maximally Correlated Motion (ewMCM), that is the collective motion maximally correlated to the selected arbitrary function f , which is, in this case, the distance between the center of mass of the M loop and the center of mass of tubulin.

Table 4.3 summarizes the values of the Pearson's coefficients for the model building set (R_m) and for the cross-validation one (R_c).

Table 4.3 – Pearson's coefficients for the model building set (R_m) and the cross-validation set (R_c).

		Validation of the linear model	
		R_m	R_c
Isotype with colchicine	2A	0,9857	0,8557
	3	0,9797	0,9561
	4A	0,9355	0,8291
Isotype without colchicine	2A	0,9859	0,9429
	3	0,9914	0,8244
	4A	0,9747	0,826

Pearson's coefficients are always higher than 0,8 for both the model building and cross validation sets, confirming the existence of correlation between the fluctuations of the M loop and the motion of the whole dimer. Each isotype without colchicine show higher values of R_m than the corresponding isotype bounded to the drug.

The complex motion of tubulin may be spread over several PCA modes and it is therefore interesting to quantify the influence of different PCA modes on the linear models obtained. The percentual contributions of different PCs to the linear model which approximates the arbitrary function f are represented in Figure 4.11.

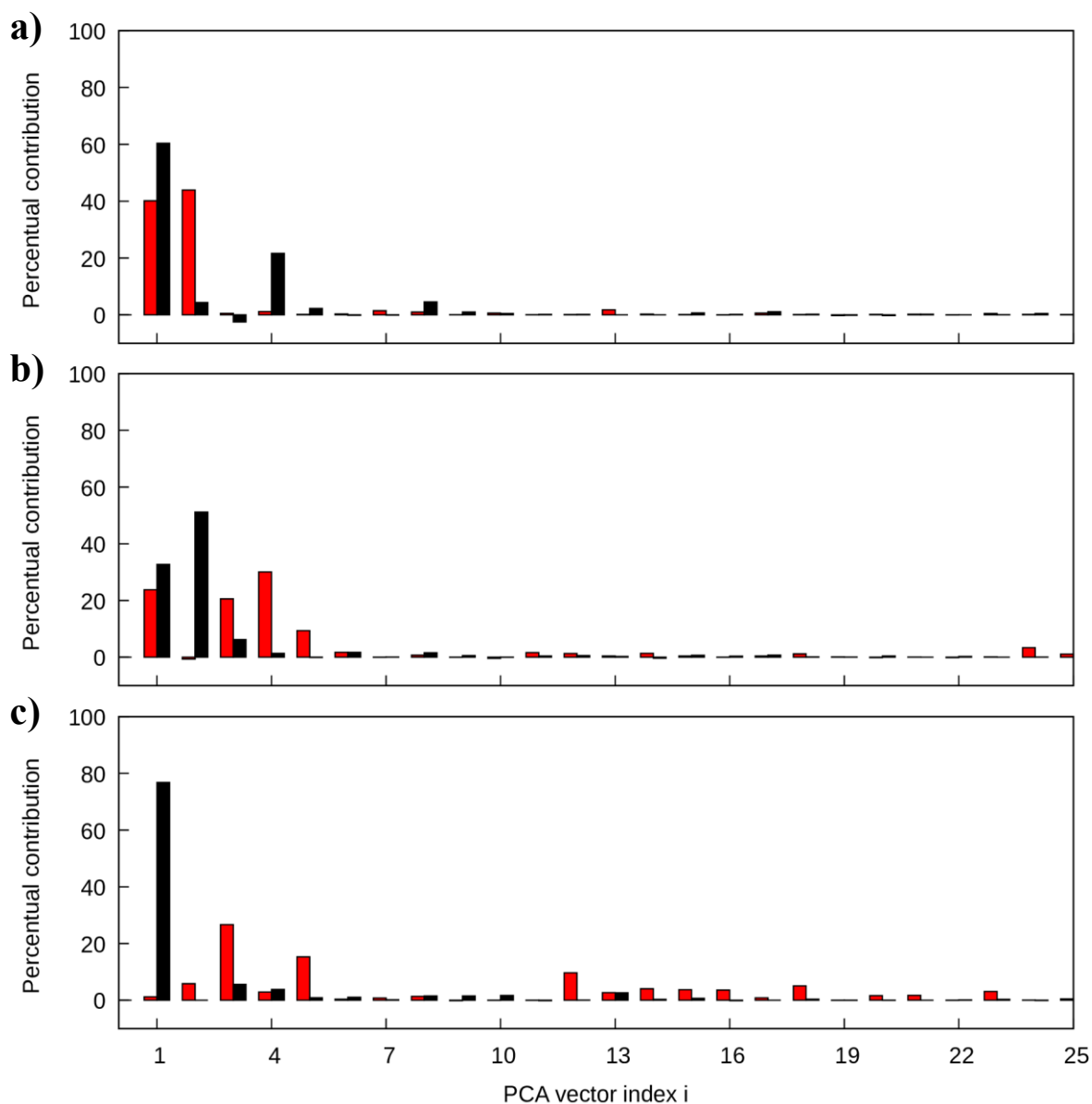


Figure 4.11 - Contribution of the i^{th} PC to the variance of the linear model for isotypes a) $\alpha\beta\text{IIa}$, b) $\alpha\beta\text{III}$ and c) $\alpha\beta\text{IVa}$; in black structure without colchicine, in red isotype bound to colchicine.

The previous figure shows that the first PCs have a great influence for the models relative to isotypes not bound to colchicine, especially for isotype $\alpha\beta\text{IVa}$ where the first PC has a contribution of 77% to the variance of the model. The presence of colchicine modifies the contribution of the PCs: for isotype $\alpha\beta\text{IIa}$ there are no appreciable differences between the presence or absence of colchicine, while for both isotypes $\alpha\beta\text{III}$ and $\alpha\beta\text{IVa}$ also PCs with high indices contribute to the variance of the model.

4.5 Discussion

Results from Molecular Dynamics simulations reveal the effect of colchicine on human tubulin isotypes, $\alpha\beta$ IIa, $\alpha\beta$ III and $\alpha\beta$ IVa. The three isotypes exhibit similar affinities for colchicine and the drug is considered as a good binder, because high negative values of binding energy were obtained with both the MM-PBSA and MM-GBSA methods; the obtained values are similar to those available from previous works⁸⁴. However, due to the high approximations introduced by these methods¹⁰², it is not possible to rank the isotypes based on their affinity for colchicine and therefore correlate affinity data with drug's activity. Both the RMSD of colchicine and colchicine binding site show higher values for isotypes $\alpha\beta$ III and $\alpha\beta$ IVa, suggesting that these isotypes are more sensitive to the presence of the drug and its destabilizing effect is more evident on local rearrangements; anyway, the colchicine does not significantly alter the secondary structures in the colchicine binding site, and its action is therefore analyzed on global conformational changes of the entire tubulin dimer. From the RMSF analysis appears that the M loop (273-285) on the beta tubulin is the most fluctuating structure for all isotypes and the presence of colchicine enhances the fluctuations of this sequence for isotypes $\alpha\beta$ III and $\alpha\beta$ IVa, but not for isotype $\alpha\beta$ IIa. The RMSF analysis for the α tubulin shows that the M loop is not the most fluctuating structure, it exhibits lower values of fluctuations and there are no appreciable differences between the presence or the absence of colchicine; then, only the M loop on β tubulin was considered. It is interesting that M loop is crucial for binding stabilizing drugs, such as taxanes⁸⁵, but also with colchicine its motion is altered; moreover, Mitra and Sept identify a reduction in the M loop fluctuations in presence of taxol and this result is consistent with this study because taxol is a stabilizing drug and induces the opposite effect of colchicine⁷⁸. M loop is known to be crucial for lateral interactions, binding loop H1-B2 on adjacent protofilament, and to act as a hinge allowing the protofilaments to stay closer or further apart into the MT wall²⁴; variation in its flexibility and motility therefore strongly affect the MT stability, as expected by the presence of destabilizing drug, such as colchicine. Variations on M loop fluctuations are correlated to conformational changes of tubulin dimers: isotype $\alpha\beta$ IIa, in fact, shows similar values of bending and twisting angles both in the colchicine bound and in the free state, while isotypes $\alpha\beta$ III and $\alpha\beta$ IVa exhibit greater structure modifications. However, isotype $\alpha\beta$ III preferentially modifies its twisting angle, while isotype $\alpha\beta$ IVa the bending one. Bent structures show bending angles variations of 5-9 degrees and these values are consistent with study by Grafmüller and Voth⁷⁹. The different behavior between the tubulin isotypes suggests a higher activity of colchicine on isotype $\alpha\beta$ IVa, since the bending deformation is

more destabilizing than the twisting one; the torsion mode, in fact, is partially mitigated by steric hindrance of adjacent dimers after the integration in the MT lattice. The similar conformational state of isotype $\alpha\beta\text{IIa}$, instead, is probably due to a very poor activity of colchicine on this isotype, despite its good affinity. The previous results underline also the role of the M loop in conformational changes of tubulin: modifications in its fluctuations lead to a variation in the motion of the entire tubulin. It is also interesting that the motion of the M loop only on β tubulin influences the conformational changes of the whole $\alpha\beta$ -heterodimer. This correlation is further confirmed by the Functional Mode Analysis (FMA): the motion of the M loop, estimated as the distance between its center of mass and the center of mass of the tubulin dimer, exhibit high correlations with the entire motion of the dimer, confirming that the M loop is crucial for the collective motion. From the analysis of the contributions of different PCA vectors to the variance of the linear model of the FMA it is found that for colchicine free isotypes only the first PCs are influential on the model, while in presence of the drug also PCA vectors with higher indices contribute to the variance of the model, but, again, only for isotypes $\alpha\beta\text{III}$ and $\alpha\beta\text{IVa}$. Since only isotypes $\alpha\beta\text{III}$ and $\alpha\beta\text{IVa}$ show important conformational changes, principal modes with lower amplitude and higher frequency may be responsible of structural rearrangements.

4.6 Conclusions

Microtubules are cytoskeletal structures involved in many essential cellular functions, including mitosis. Microtubule functionality is strongly influenced by a complex polymerization process and any factor altering tubulin dynamics may strongly affect the cell homeostasis and leads to mitotic arrest, eventually resulting in cell death. In past years, microtubules became targets in cancer therapy for a wide range of molecules, including taxanes, vinca alkaloids, macrolides and peptides, able to interfere with the microtubule dynamics. In this context, antimitotic drugs, such as colchicine and colchicine derivatives, have been largely studied as chemotherapeutic drugs against cancer.

In this study, molecular dynamics simulations have been performed to highlight the action of colchicine on free tubulin dimers of human isotypes $\alpha\beta\text{IIa}$, $\alpha\beta\text{III}$ and $\alpha\beta\text{IVa}$. The inhibitory action of the drug does not affect local variations in the colchicine binding site, but it is mediated by a variation on the fluctuations of the M loop in the beta tubulin, which has a crucial role in the global conformational changes of tubulin dimer. The different behavior of the three isotypes in presence of colchicine may be related to a different activity of the drug depending on modification on the residue sequence: only isotypes $\alpha\beta\text{III}$ and $\alpha\beta\text{IVa}$ are sensitive to the

presence of colchicine, showing increased fluctuations on the M loop and higher conformational changes. However, isotype $\alpha\beta$ III preferentially modifies its twisting angle, while isotype $\alpha\beta$ IVa the bending one. Since the bending motion is the most destabilizing, the activity of colchicine is therefore highest on isotype $\alpha\beta$ IVa, while it is almost negligible on isotype $\alpha\beta$ IIa, which does not show any appreciable difference in its conformational state between the presence or the absence of the drug. Finally, FMA confirms the correlations between M loop fluctuations and conformational changes, showing that in presence of colchicine also the PCA vectors with higher indices, associated to modes with lower amplitude and higher frequency, are influent on the collective motion, but again only for isotype $\alpha\beta$ III and $\alpha\beta$ IVa.

Future studies may be essential for highlight the action on tubulin dynamic of other colchicine binding site inhibitors with less toxicity, focusing on the effect on the fluctuations of the M loop and dimer conformational changes. Moreover, future developments may provide new drugs with high activity only on isotype $\alpha\beta$ III, which is a great target for anti-tumoral therapies and is known to be related to drug resistance.

4.7 Supporting information

4.7.1 Homology modelling

The best structure built with the homology modelling was chosen based on the lowest values of the DOPE score. The comparison between the dope profiles of the template and the built model are represented in following figures.

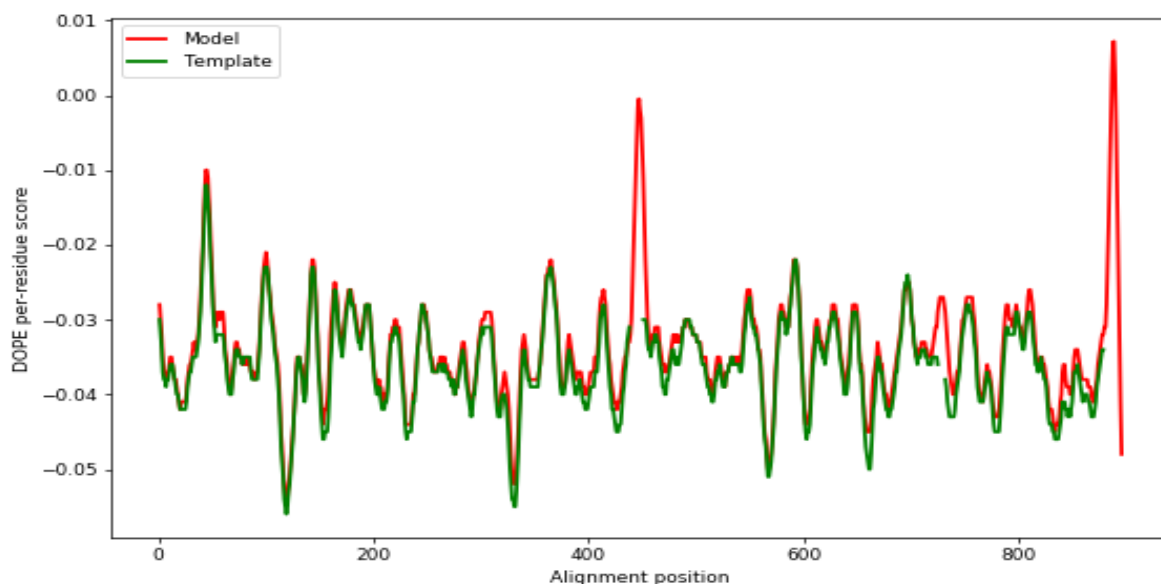


Figure 4.12 - Dope profile comparison between the template structure (green) and the obtained model (red) for the 4O2B structure

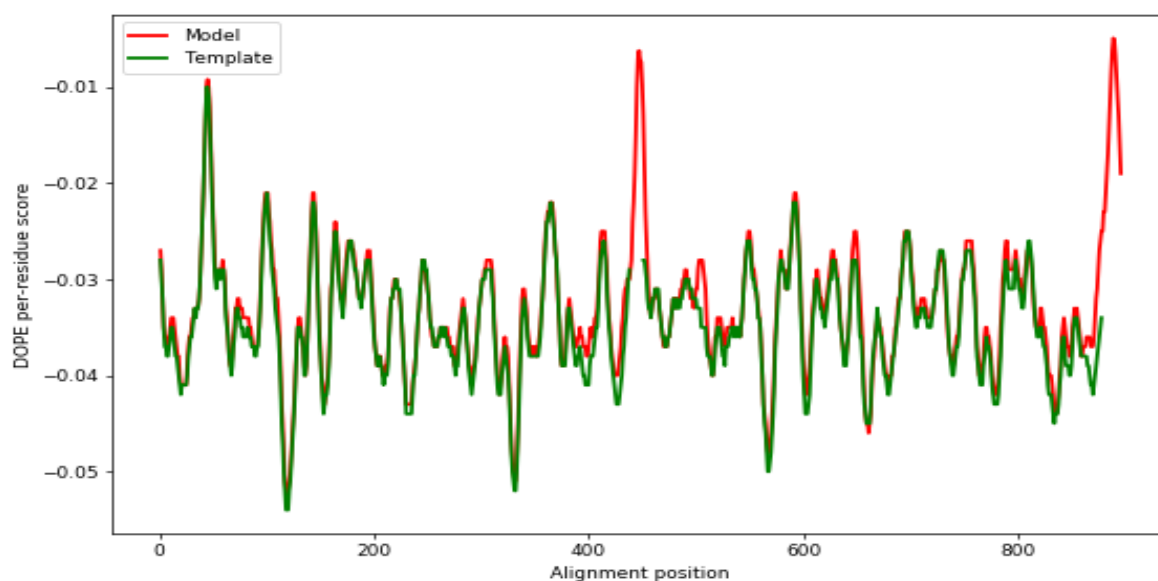


Figure 4.13 - Dope profile comparison between the template structure (green) and the obtained model (red) for the isotype α IIa.

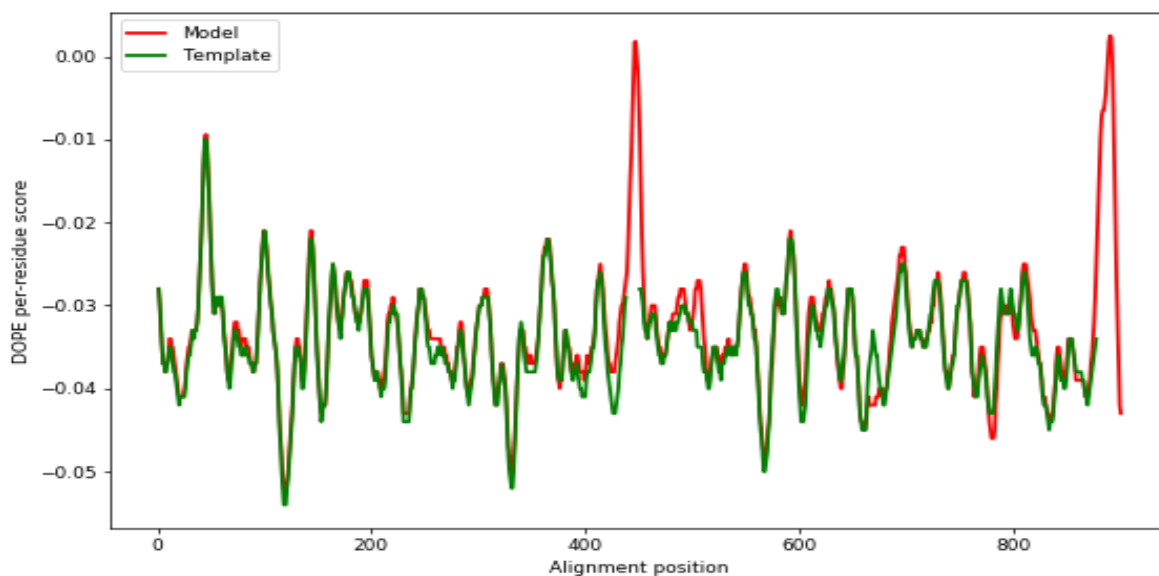


Figure 4.14 - Dope profile comparison between the template structure (green) and the obtained model (red) for the isotype $\alpha\beta III$.

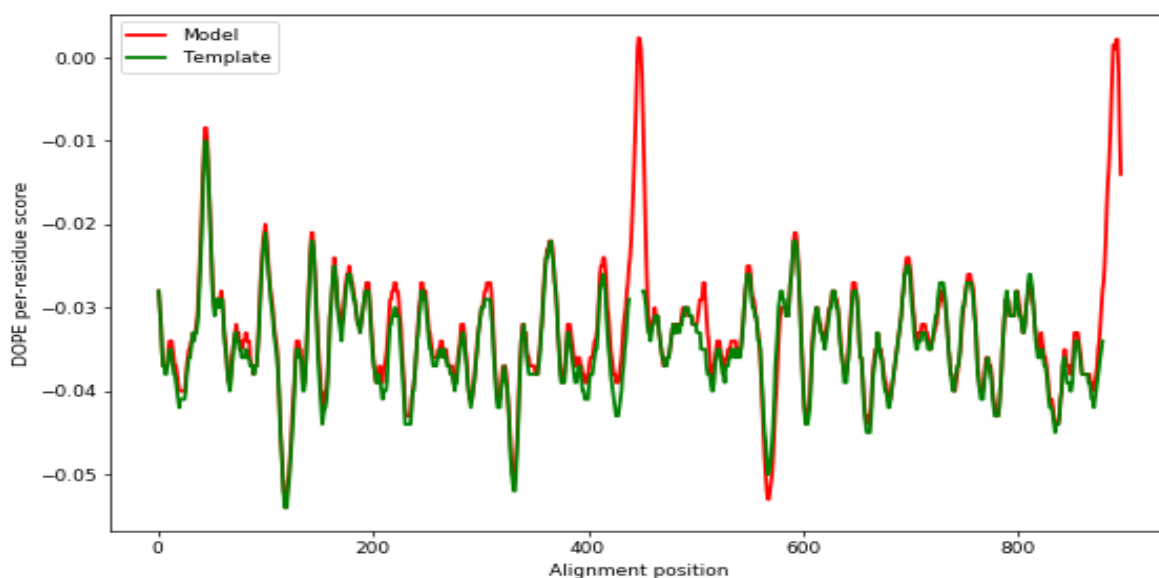


Figure 4.15 - Dope profile comparison between the template structure (green) and the obtained model (red) for the isotype $\alpha\beta IVa$.

Then, the quality of the generated models was evaluated using PROCHECK, VERIFY3D and ERRAT tools.

PROCHECK analysis provides the Ramachandran plot for each generated model: Phi and Psi angles for each residue are plotted, defining most favored, allowed and not allowed regions.

The template model has 95,9% of the residues in the most favored regions, 3,8% in the additional allowed region, 0,1% in the generously allowed regions and 0,1% in the disallowed regions. Percentages for isotype $\alpha\beta IIa$ in the same regions are respectively 95,8%, 4,1%, 0,1%

and no residues in the disallowed regions; for isotype $\alpha\beta$ III 95,6%, 4,2%, 0,1% and 0%; for isotype $\alpha\beta$ IVa 95,4%, 4,5%, 0,1% and 0%. In the Figure 4.16 the Ramachandran plots of each model are represented.

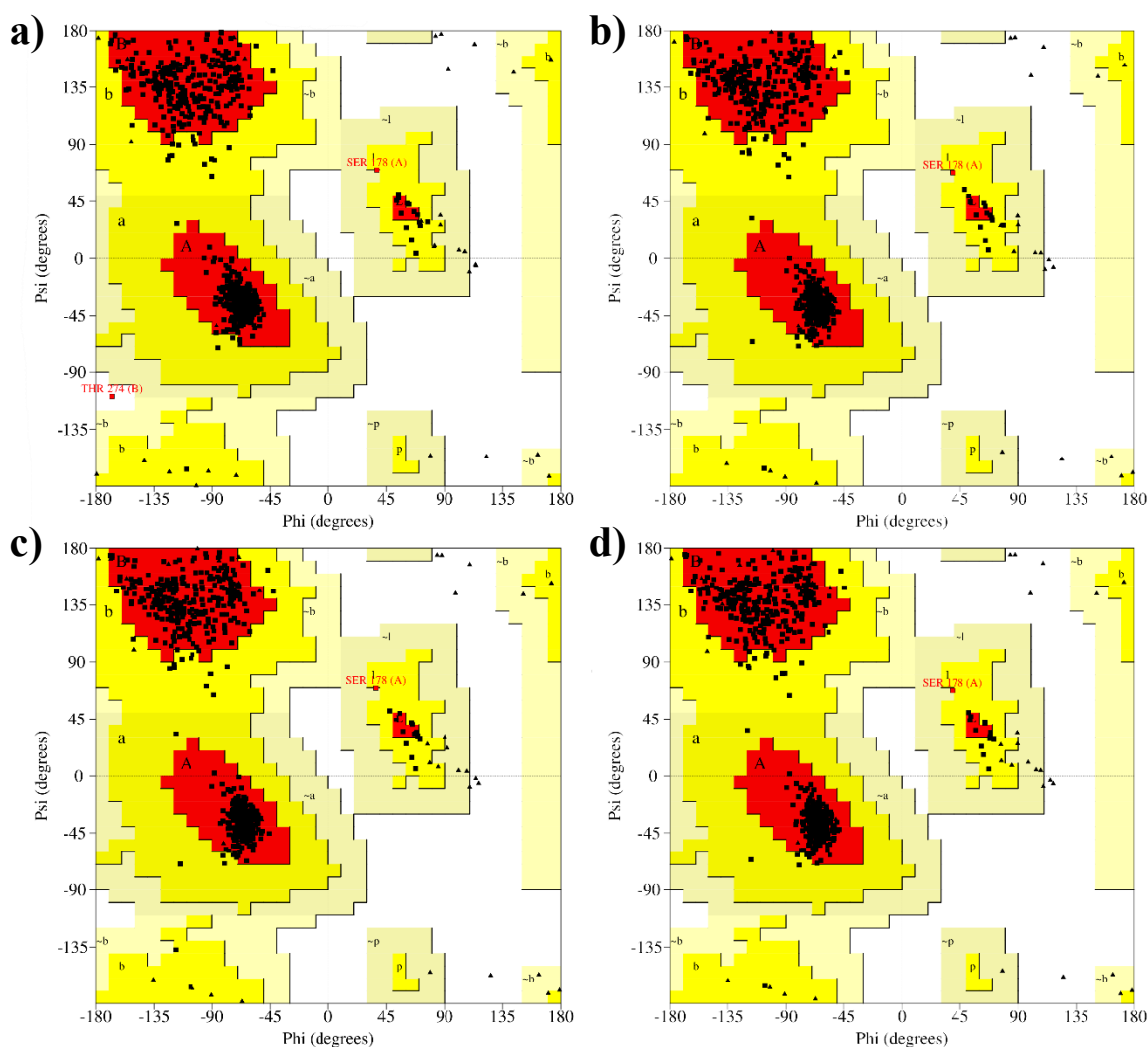


Figure 4.16 – Ramachandran plot for a) the template and for isotypes b) $\alpha\beta$ Ia, c) $\alpha\beta$ III and d) $\alpha\beta$ IVa.

The Overall Quality Factor obtained with the ERRAT tool is 86,68 for chain A and 91,17 for chain B for the template model. For isotype $\alpha\beta$ Ia these values are respectively 79,12 and 88,31; for isotype $\alpha\beta$ III 80,29 and 84,73; for isotype $\alpha\beta$ IVa 77,26 and 84,96.

The VERIFY3D test is considered passed if a high percentage of the residues has an averaged 3D-1D score higher than 0,2. All models pass the VERIFY3D test showing percentages of 96,77% for the template model, 98,85% for isotype $\alpha\beta$ Ia, 98,15% for isotype $\alpha\beta$ III and 97,69% for isotype $\alpha\beta$ IVa.

Results from these tools suggest that the generated models are acceptable.

4.7.2 RMSD of simulated structures

Figure 4.17 shows the RMSD of the simulated structures from their starting point during the 200 ns of simulation.

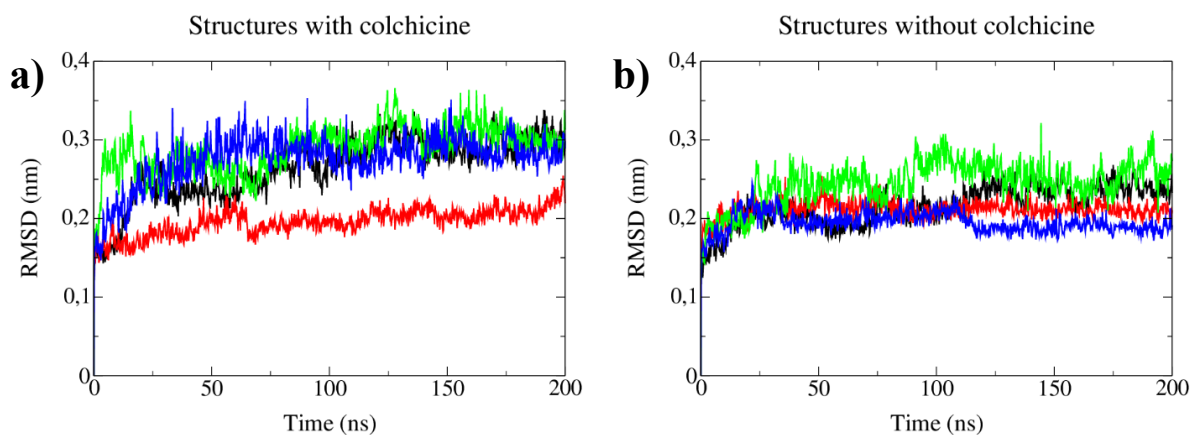


Figure 4.17 – RMSD of tubulin backbone atoms from the starting structure during 200 ns of simulation for structures with colchicine (a) and without colchicine (b). Template structure, 4O2B, is represented in black, isotype $\alpha\beta$ IIa in red, isotype $\alpha\beta$ III in green and isotype $\alpha\beta$ IVa in blue.

Analogous graphs were obtained for each replica to ensure the stability for all configurations.

4.7.3 Binding energy prediction

The binding energy was also calculated using the MM-PBSA methods. For this purpose, the last 40 ns of simulation were considered and 40 frames were extracted.

The binding energy calculated with the MM-PBSA method is reported in Table 4.4.

Table 4.4 - Binding energy of tubulin isotypes $\alpha\beta$ IIa, $\alpha\beta$ III, and $\alpha\beta$ IVa with colchicine calculated with the MM-PBSA approach and expressed in kJ/mol

Isotype	ΔE_{vdw}	ΔE_{ele}	ΔE_{pol}	ΔE_{sasa}	ΔE_{bind}
$\alpha\beta$ IIa	$-58,10 \pm 2,21$	$-2,70 \pm 0,73$	$19,49 \pm 1,20$	$-4,21 \pm 0,20$	$-45,52 \pm 2,28$
$\alpha\beta$ III	$-68,33 \pm 1,71$	$-1,47 \pm 1,02$	$20,93 \pm 1,62$	$-4,45 \pm 0,17$	$-53,32 \pm 2,47$
$\alpha\beta$ IVa	$-64,96 \pm 2,81$	$-1,13 \pm 1,25$	$23,27 \pm 1,93$	$-4,60 \pm 0,18$	$-47,42 \pm 2,92$

4.7.4 RMSD of internal beta sheets

Structural analysis, such as the bending angle variation (θ), the torsion angle variation (φ) and the RMSD of the beta subunit were calculated on trajectories fitted on the internal beta sheets of the alpha subunit; these sheets were assumed as quasi-static structure because their RMSD assumed very low values during simulations (Figure 4.18).

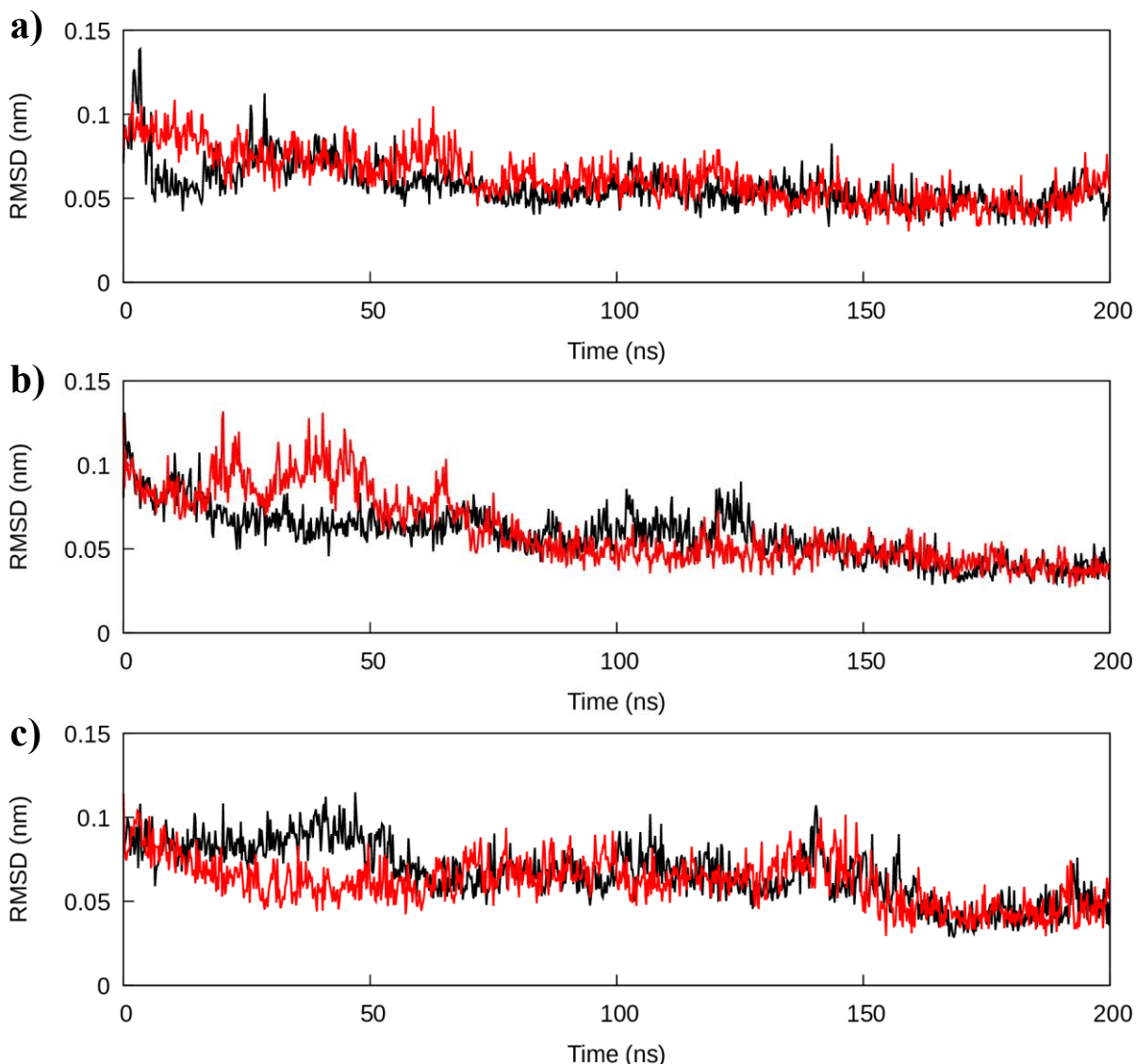


Figure 4.18 – RMSD of the internal beta sheets in the alpha tubulin during 200 ns of simulation for isotypes a) $\alpha\beta$ IIa, b) $\alpha\beta$ III and c) $\alpha\beta$ IVa; in black structure without colchicine, in red isotype bound to colchicine

4.7.5 RMSF of alpha tubulin

The average RMSF of α tubulin between the three replicas during the whole simulations was calculated for each isotype in presence and in absence of colchicine.

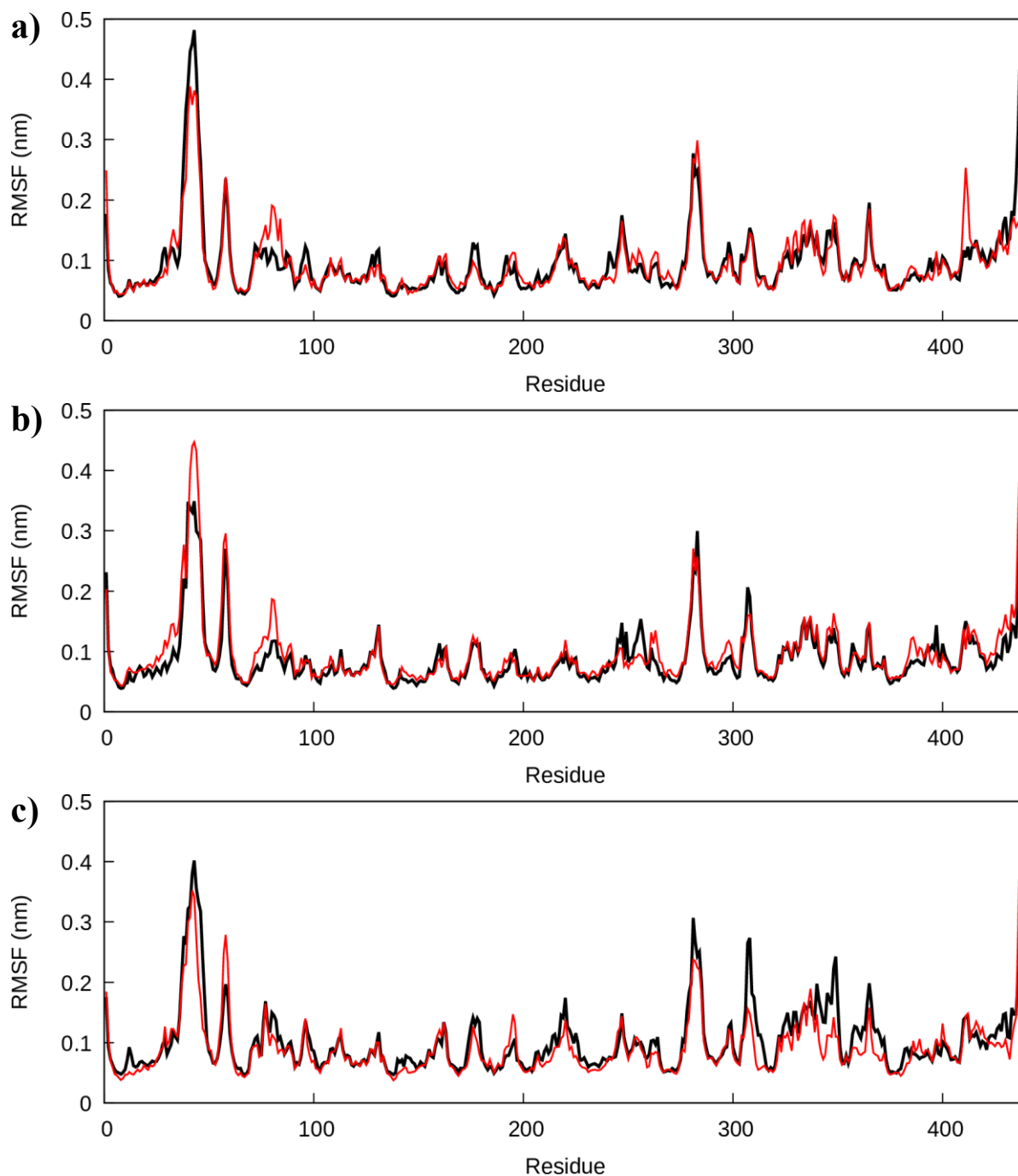


Figure 4.19 - Average RMSF of alpha tubulin between three replicas for isotypes a) $\alpha\beta\text{IIa}$, b) $\alpha\beta\text{III}$ and c) $\alpha\beta\text{IVa}$; in black structure without colchicine, in red isotype bound to colchicine

Contrary to the RMSF values for the β tubulin, the M loop (273-285) is not the most fluctuating structure and there are no appreciable differences in its fluctuations in presence or in absence of colchicine.

4.7.6 Functional Mode Analysis

The FMA assumes that the arbitrary function f , that is in this case the distance between the center of mass of the M loop of the β tubulin and the center of mass of the dimer, is a linear function of the Principal Components (PCs). The validation of the linear model is graphically represented in Figure 4.20, where models derived from the model building and cross validation sets are plotted with the arbitrary function fluctuations.

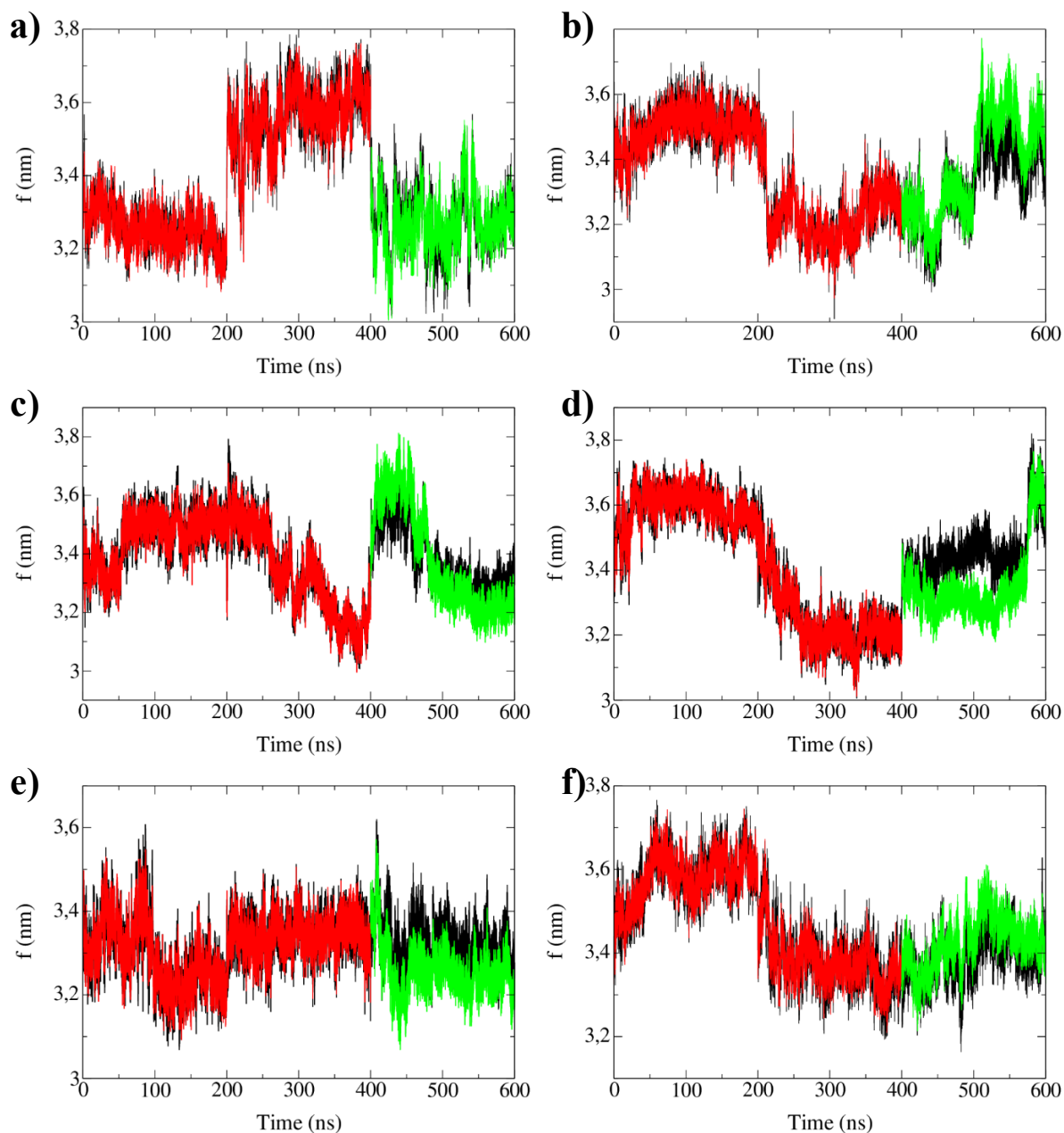


Figure 4.20 – Validation of the linear model obtained with the FMA analysis for isotypes a) $\alpha\beta$ Ia, c) $\alpha\beta$ III and e) $\alpha\beta$ IVa with colchicine and for the same isotypes b), d), f) without colchicine. In black the arbitrary function, that is the distance between the centers of mass of the M loop and the tubulin dimer as a function of time, in red the model building curve and in green the cross-validation curve.

Since the data set was divided into the model building and cross-validation sets, the Pearson's coefficients were obtained for both the series. The following figures represent the scatter plot (data vs model) together with the Pearson's coefficients for both the model building set (Figure 4.21) and the cross-validation set (Figure 4.22).

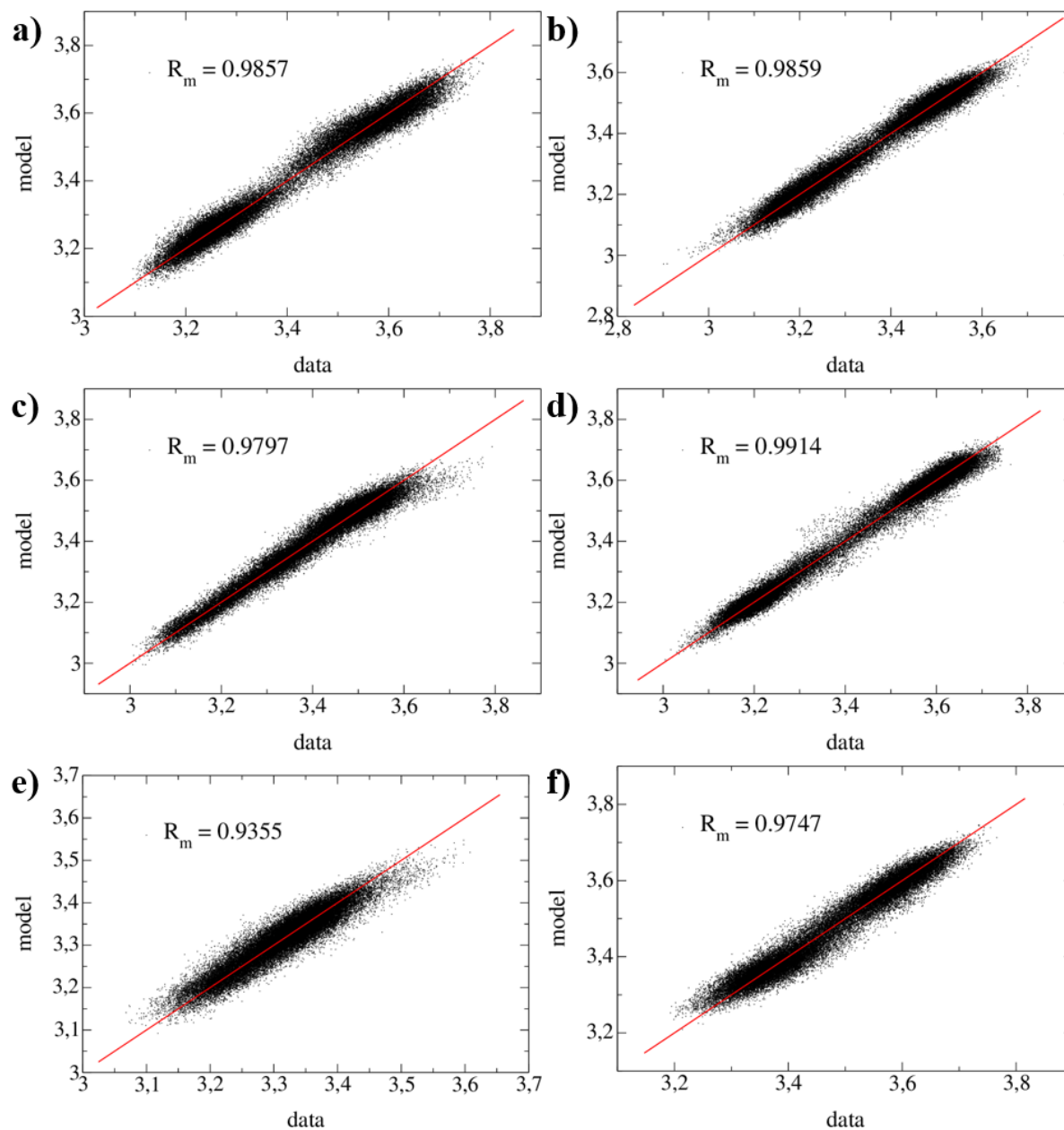


Figure 4.21 – Scatter plot (data vs model) of the model building set with the Pearson's coefficient for isotypes a) $\alpha\beta$ IIa, c) $\alpha\beta$ III and e) $\alpha\beta$ IVa with colchicine and for the same isotypes b), d) and f) without colchicine.

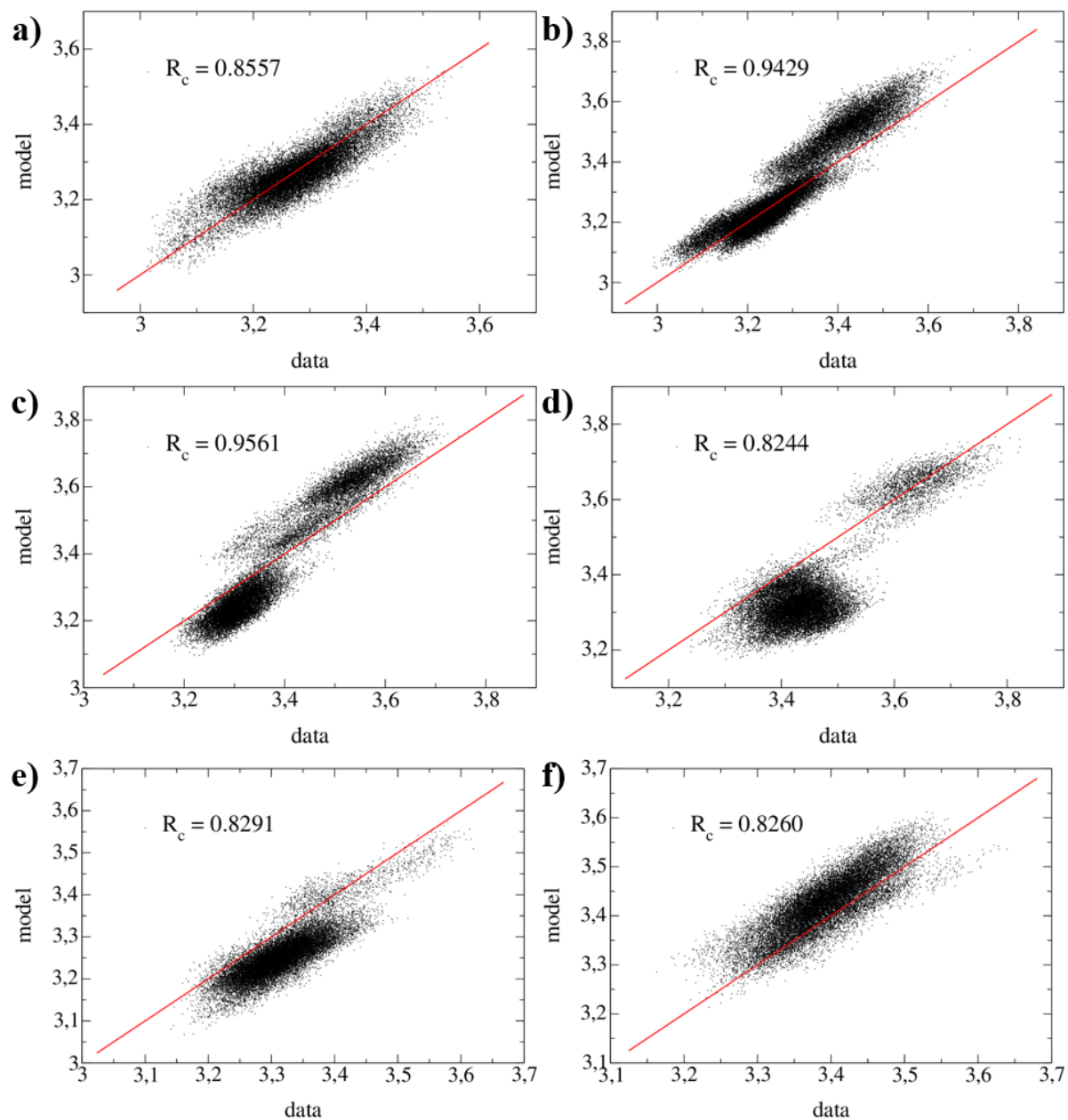


Figure 4.22 – Scatter plot (data vs model) of the model cross-validation set with the Pearson's coefficient for isotypes a) $\alpha\beta$ IIIa, c) $\alpha\beta$ IIIc and e) $\alpha\beta$ IVa with colchicine and for the same isotypes b), d) and f) without colchicine.

Then the RMSF of the ewMCM was estimated for each isotype.

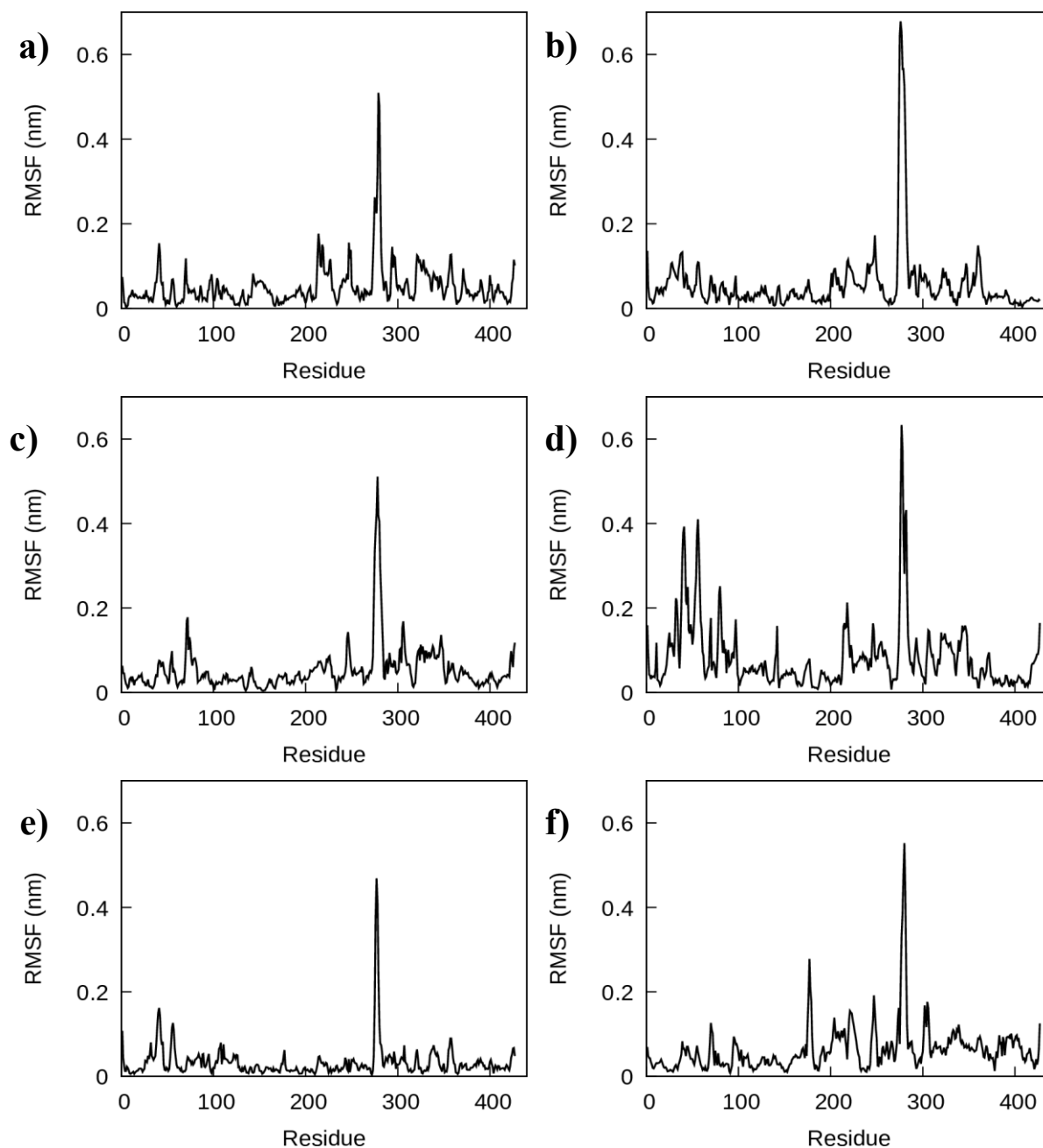


Figure 4.23 - RMSF of beta tubulin of ewMCM for isotypes a) $\alpha\beta$ IIa, c) $\alpha\beta$ III and e) $\alpha\beta$ IVa with colchicine and for the same isotypes b), d) and f) without colchicine.

The RMSF shows high fluctuations of the M loop (273-285): this was expected because the arbitrary function is clearly correlated with the fluctuations of this structure. The RMSF therefore confirms that the FMA has correctly worked, correlating the motions of the M loop with conformational changes of the whole tubulin.

5 Acknowledgments

I would like to thank my supervisor Prof. Marco Agostino Deriu for giving me the opportunity to work on this thesis and for supporting me in every moment; his enthusiasm and professionalism made this research work very exciting and constantly increased my interest in molecular modeling.

I would like to show my gratitude to my co-supervisors Prof. Jacek Adam Tuszynski and Prof. Umberto Morbiducci for the evaluation and critical review of my work.

I would also thank Gianvito Grasso for important hints and explanations, especially about dimensionality reduction techniques.

I am also very thankful to my teammates, Antonio, Stefano, Giacomo, Simone and Chiara, for having built a “*great team*” and for making this last year very fruitful and pleasant. I also thank the other students from the *Aula Tesisti*, especially Martina and Giulia, for enjoying together the working days.

I finally thank my family for supporting my course of study and for constantly encouraging me and all my friends for always being there.

Lorenzo Pallante

6 References

- (1) Leach, A. R. *Molecular Modelling: Principles and Applications* Second Edition. *Pearson Educ. EMA* **2001**. [https://doi.org/10.1016/S0097-8485\(96\)00029-0](https://doi.org/10.1016/S0097-8485(96)00029-0).
- (2) Darden, T.; York, D.; Pedersen, L. Particle Mesh Ewald: An $N \cdot \log(N)$ Method for Ewald Sums in Large Systems. *J. Chem. Phys.* **1993**, *98* (12), 10089–10092. <https://doi.org/10.1063/1.464397>.
- (3) Ding, H. Q.; Karasawa, N.; Goddard, W. A. Atomic Level Simulations on a Million Particles: The Cell Multipole Method for Coulomb and London Nonbond Interactions. *J. Chem. Phys.* **1992**. <https://doi.org/10.1063/1.463935>.
- (4) Kitao, A.; Hayward, S.; Go, N. Energy Landscape of a Native Protein: Jumping-among-Minima Model. *Proteins Struct. Funct. Genet.* **1998**, *33* (4), 496–517. [https://doi.org/10.1002/\(SICI\)1097-0134\(19981201\)33:4<496::AID-PROT4>3.0.CO;2-1](https://doi.org/10.1002/(SICI)1097-0134(19981201)33:4<496::AID-PROT4>3.0.CO;2-1).
- (5) Balsera, M. A.; Wriggers, W.; Oono, Y.; Schulten, K. Principal Component Analysis and Long Time Protein Dynamics. *J. Phys. Chem.* **1996**, *100* (7), 2567–2572. <https://doi.org/10.1021/jp9536920>.
- (6) Hayward, S.; Go, N. Collective Variable Description of Native Protein Dynamics. *Annu. Rev. Phys. Chem.* **2003**, *46* (1), 223–250. <https://doi.org/10.1146/annurev.pc.46.100195.001255>.
- (7) Kitao, A.; Hirata, F.; Go, N. The Effects of Solvent on the Conformation and the Collective Motions of Protein: Normal Mode Analysis and Molecular Dynamics Simulations of Melittin in Water and in Vacuum. *Chem. Phys.* **1991**, *158*(2–3), 447–472. [https://doi.org/10.1016/0301-0104\(91\)87082-7](https://doi.org/10.1016/0301-0104(91)87082-7).
- (8) Hub, J. S.; de Groot, B. L. Detection of Functional Modes in Protein Dynamics. *PLoS Comput. Biol.* **2009**, *5* (8), e1000480. <https://doi.org/10.1371/journal.pcbi.1000480>.
- (9) Krivobokova, T.; Briones, R.; Hub, J. S.; Munk, A.; de Groot, B. L. Partial Least-Squares Functional Mode Analysis: Application to the Membrane Proteins AQP1, Aqy1, and

- CLC-Ec1. *Biophys. J.* **2012**, *103* (4), 786–796.
<https://doi.org/10.1016/j.bpj.2012.07.022>.
- (10) Gohlke, H.; Klebe, G. Approaches to the Description and Prediction of the Binding Affinity of Small-Molecule Ligands to Macromolecular Receptors. *Angewandte Chemie - International Edition*. John Wiley & Sons, Ltd August 2, 2002, pp 2644–2676. [https://doi.org/10.1002/1521-3773\(20020802\)41:15<2644::AID-ANIE2644>3.0.CO;2-O](https://doi.org/10.1002/1521-3773(20020802)41:15<2644::AID-ANIE2644>3.0.CO;2-O).
- (11) Genheden, S.; Ryde, U. The MM/PBSA and MM/GBSA Methods to Estimate Ligand-Binding Affinities. *Expert Opin. Drug Discov.* **2015**, *10* (5), 449–461. <https://doi.org/10.1517/17460441.2015.1032936>.
- (12) Luo, R.; Qi, R.; Xiao, L.; Wang, C.; Greene, D. Recent Developments and Applications of the MMPBSA Method. *Front. Mol. Biosci.* **2018**, *4*, 87. <https://doi.org/10.3389/fmolb.2017.00087>.
- (13) Clark Still, W.; Tempczyk, A.; Hawley, R. C.; Hendrickson, T. Semianalytical Treatment of Solvation for Molecular Mechanics and Dynamics. *J. Am. Chem. Soc.* **1990**. <https://doi.org/10.1021/ja00172a038>.
- (14) Case, D. A. Normal Mode Analysis of Protein Dynamics. *Curr. Opin. Struct. Biol.* **1994**, *4* (2), 285–290. [https://doi.org/10.1016/S0959-440X\(94\)90321-2](https://doi.org/10.1016/S0959-440X(94)90321-2).
- (15) Karplus, M.; Kushick, J. N. Method for Estimating the Configurational Entropy of Macromolecules. *Macromolecules* **1981**, *14* (2), 325–332. <https://doi.org/10.1021/ma50003a019>.
- (16) Shirts, M. R.; Mobley, D. L.; Brown, S. P. Free-Energy Calculations in Structure-Based Drug Design. In *Drug Design*; Merz, K. M., Ringe, D., Reynolds, C. H., Eds.; Cambridge University Press: Cambridge, 2010; pp 61–86. <https://doi.org/10.1017/CBO9780511730412.007>.
- (17) Prota, A. E.; Danel, F.; Bachmann, F.; Bargsten, K.; Buey, R. M.; Pohlmann, J.; Reinelt, S.; Lane, H.; Steinmetz, M. O. The Novel Microtubule-Destabilizing Drug BAL27862 Binds to the Colchicine Site of Tubulin with Distinct Effects on Microtubule

- Organization. *J. Mol. Biol.* **2014**, *426* (8), 1848–1860. <https://doi.org/10.1016/j.jmb.2014.02.005>.
- (18) Mitchison, T.; Kirschner, M. Dynamic Instability of Microtubule Growth. *Nature* **1984**, *312* (5991), 237–242. <https://doi.org/10.1038/312237a0>.
- (19) Jordan, M. A.; Wilson, L. Microtubules as a Target for Anticancer Drugs. *Nat. Rev. Cancer* **2004**, *4* (4), 253–265. <https://doi.org/10.1038/nr1317>.
- (20) Siegrist, S. E.; Doe, C. Q. Microtubule-Induced Cortical Cell Polarity. *Genes Dev.* **2007**, *21* (5), 483–496. <https://doi.org/10.1101/gad.1511207>.
- (21) Gadde, S.; Heald, R. Mechanisms and Molecules of the Mitotic Spindle. *Current Biology*. September 2004, pp R797–R805. <https://doi.org/10.1016/j.cub.2004.09.021>.
- (22) Amos, L. A. Microtubule Structure and Its Stabilisation. *Organic and Biomolecular Chemistry*. The Royal Society of Chemistry July 27, 2004, pp 2153–2160. <https://doi.org/10.1039/b403634d>.
- (23) Nettles, J. H.; Snyder, J. P.; Nogales, E.; Cornett, B.; Downing, K. H. The Binding Conformation of Taxol in α -Tubulin: A Model Based on Electron Crystallographic Density. *Proc. Natl. Acad. Sci.* **2002**, *98* (9), 5312–5316. <https://doi.org/10.1073/pnas.051309398>.
- (24) Downing, K. H.; Nogales, E. Tubulin Structure: Insights into Microtubule Properties and Functions. *Curr. Opin. Struct. Biol.* **1998**, *8* (6), 785–791.
- (25) Nogales, E.; Wolf, S. G.; Downing, K. H. Structure of the $\alpha\beta$ Tubulin Dimer by Electron Crystallography. *Nature* **1998**, *391* (6663), 199–203. <https://doi.org/10.1038/34465>.
- (26) Löwe, J.; Li, H.; Downing, K. .; Nogales, E. Refined Structure of $\alpha\beta$ -Tubulin at 3.5 Å Resolution 1 Edited by I. A. Wilson. *J. Mol. Biol.* **2001**, *313* (5), 1045–1057. <https://doi.org/10.1006/jmbi.2001.5077>.
- (27) Jimenez, M. A.; Evangelio, J. A.; Aranda, C.; Lopez-Brauet, A.; Andreu, D.; Rico, M.;

- Lagos, R.; Andreu, J. M.; Monasterio, O. Helicity of α (404-451) and β (394-445) Tubulin C-Terminal Recombinant Peptides. *Protein Sci.* **2008**, *8* (4), 788–799. <https://doi.org/10.1110/ps.8.4.788>.
- (28) Okada, Y.; Hirokawa, N. Mechanism of the Single-Headed Processivity: Diffusional Anchoring between the K-Loop of Kinesin and the C Terminus of Tubulin. *Proc. Natl. Acad. Sci.* **2000**, *97*(2), 640–645. <https://doi.org/10.1073/pnas.97.2.640>.
- (29) Chrétien, D.; Wade, R. H. New Data on the Microtubule Surface Lattice. *Biol. Cell* **1991**, *71* (1–2), 161–174. [https://doi.org/10.1016/0248-4900\(91\)90062-R](https://doi.org/10.1016/0248-4900(91)90062-R).
- (30) Savage, C.; Hamelin, M.; Culotti, J. G.; Coulson, A.; Albertson, D. G.; Chalfie, M. Mec-7 Is a Beta-Tubulin Gene Required for the Production of 15-Protofilament Microtubules in *Caenorhabditis Elegans*. *Genes Dev.* **1989**, *3* (6), 870–881.
- (31) Grafmüller, A.; Noya, E. G.; Voth, G. A. Nucleotide-Dependent Lateral and Longitudinal Interactions in Microtubules. *J. Mol. Biol.* **2013**, *425* (12), 2232–2246. <https://doi.org/10.1016/j.jmb.2013.03.029>.
- (32) Desai, A.; Mitchison, T. J. MICROTUBULE POLYMERIZATION DYNAMICS. *Annu. Rev. Cell Dev. Biol.* **1997**, *13* (1), 83–117. <https://doi.org/10.1146/annurev.cellbio.13.1.83>.
- (33) Rice, L. M.; Montabana, E. A.; Agard, D. A. The Lattice as Allosteric Effector: Structural Studies of α - and β -Tubulin Clarify the Role of GTP in Microtubule Assembly. *Proc. Natl. Acad. Sci.* **2008**, *105* (14), 5378–5383. <https://doi.org/10.1073/pnas.0801155105>.
- (34) Buey, R. M.; Fernando Díaz, J.; Andreu, J. M. The Nucleotide Switch of Tubulin and Microtubule Assembly: A Polymerization-Driven Structural Change. *Biochemistry* **2006**, *45* (19), 5933–5938. <https://doi.org/10.1021/bi060334m>.
- (35) Bennett, M. J.; Chik, J. K.; Slysz, G. W.; Luchko, T.; Tuszyński, J.; Sackett, D. L.; Schriemer, D. C. Structural Mass Spectrometry of the $\alpha\beta$ -Tubulin Dimer Supports a Revised Model of Microtubule Assembly. *Biochemistry* **2009**, *48* (22), 4858–4870. <https://doi.org/10.1021/bi900200q>.

- (36) Tangutur, A. D.; Kumar, D.; Krishna, K. V.; Kantevari, S. Microtubule Targeting Agents as Cancer Chemotherapeutics: An Overview of Molecular Hybrids as Stabilizing and Destabilizing Agents. *Curr. Top. Med. Chem.* **2017**, *17* (22), 2523–2537. <https://doi.org/10.2174/1568026617666170104145640>.
- (37) Lu, Y.; Chen, J.; Xiao, M.; Li, W.; Miller, D. D. An Overview of Tubulin Inhibitors That Interact with the Colchicine Binding Site. *Pharm. Res.* **2012**, *29* (11), 2943–2971. <https://doi.org/10.1007/s11095-012-0828-z>.
- (38) Aryapour, H.; Dehdab, M.; Sohraby, F.; Bargahi, A. Prediction of New Chromene-Based Inhibitors of Tubulin Using Structure-Based Virtual Screening and Molecular Dynamics Simulation Methods. *Comput. Biol. Chem.* **2017**, *71*, 89–97. <https://doi.org/10.1016/j.compbiolchem.2017.09.007>.
- (39) Wallace, S. L. Colchicine. *Semin. Arthritis Rheum.* **1974**, *3* (4), 369–381. [https://doi.org/10.1016/0049-0172\(74\)90006-7](https://doi.org/10.1016/0049-0172(74)90006-7).
- (40) Johnson, L.; Goping, I. S.; Rieger, A.; Mane, J. Y.; Huzil, T.; Banerjee, A.; Luduena, R.; Hassani, B.; Winter, P.; Tuszynski, J. A. Novel Colchicine Derivatives and Their Anti-Cancer Activity. *Curr. Top. Med. Chem.* **2017**, *17* (22). <https://doi.org/10.2174/1568026617666170104143618>.
- (41) Majcher, U.; Urbaniak, A.; Maj, E.; Moshari, M.; Delgado, M.; Wietrzyk, J.; Bartl, F.; Chambers, T. C.; Tuszynski, J. A.; Huczyński, A. Synthesis, Antiproliferative Activity and Molecular Docking of Thiocolchicine Urethanes. *Bioorg. Chem.* **2018**, *81*, 553–566. <https://doi.org/10.1016/j.bioorg.2018.09.004>.
- (42) Wang, Y.; Zhang, H.; Gigant, B.; Yu, Y.; Wu, Y.; Chen, X.; Lai, Q.; Yang, Z.; Chen, Q.; Yang, J. Structures of a Diverse Set of Colchicine Binding Site Inhibitors in Complex with Tubulin Provide a Rationale for Drug Discovery. *FEBS J.* **2016**, *283* (1), 102–111. <https://doi.org/10.1111/febs.13555>.
- (43) Majcher, U.; Klejborowska, G.; Moshari, M.; Maj, E.; Wietrzyk, J.; Bartl, F.; Tuszynski, J. A.; Huczyński, A. Antiproliferative Activity and Molecular Docking of Novel Double-Modified Colchicine Derivatives. *Cells* **2018**, *7* (11), 192. <https://doi.org/10.3390/cells7110192>.

- (44) Mane, J. Y.; Klobukowski, M.; Huzil, J. T.; Tuszynski, J. Free Energy Calculations on the Binding of Colchicine and Its Derivatives with the α/β -Tubulin Isoforms. *J. Chem. Inf. Model.* **2008**, *48* (9), 1824–1832. <https://doi.org/10.1021/ci800054n>.
- (45) Gigant, B.; Curmi, P. A.; Martin-Barbey, C.; Charbaut, E.; Lachkar, S.; Lebeau, L.; Siavoshian, S.; Sobel, A.; Knossow, M. The 4 Å X-Ray Structure of a Tubulin:Stathmin-like Domain Complex. *Cell* **2000**, *102* (6), 809–816. [https://doi.org/10.1016/S0092-8674\(00\)00069-6](https://doi.org/10.1016/S0092-8674(00)00069-6).
- (46) Nettles, J. H. The Binding Mode of Etoposide on β -Tubulin by Electron Crystallography. *Science* (80-.). **2004**, *305* (5685), 866–869. <https://doi.org/10.1126/science.1099190>.
- (47) Ravelli, R. B. G.; Gigant, B.; Curmi, P. A.; Jourdain, I.; Lachkar, S.; Sobel, A.; Knossow, M. Insight into Tubulin Regulation from a Complex with Colchicine and a Stathmin-like Domain. *Nature* **2004**, *428* (6979), 198–202. <https://doi.org/10.1038/nature02393>.
- (48) Gigant, B.; Wang, C.; Ravelli, R. B. G.; Roussi, F.; Steinmetz, M. O.; Curmi, P. A.; Sobel, A.; Knossow, M. Structural Basis for the Regulation of Tubulin by Vinblastine. *Nature* **2005**, *435* (7041), 519–522. <https://doi.org/10.1038/nature03566>.
- (49) Huzil, J. T.; Chen, K.; Kurgan, L.; Tuszynski, J. A. The Roles of Beta-Tubulin Mutations and Isoform Expression in Acquired Drug Resistance. *Cancer Inform.* **2007**, *3*, 159–181.
- (50) Alushin, G. M.; Lander, G. C.; Kellogg, E. H.; Zhang, R.; Baker, D.; Nogales, E. High-Resolution Microtubule Structures Reveal the Structural Transitions in $\alpha\beta$ -Tubulin upon GTP Hydrolysis. *Cell* **2014**, *157* (5), 1117–1129. <https://doi.org/10.1016/j.cell.2014.03.053>.
- (51) Panda, D.; Miller, H. P.; Banerjee, A.; Ludueña, R. F.; Wilson, L. Microtubule Dynamics in Vitro Are Regulated by the Tubulin Isoform Composition. *Proc. Natl. Acad. Sci. U. S. A.* **1994**, *91* (24), 11358–11362. <https://doi.org/10.1073/PNAS.91.24.11358>.
- (52) Huzil, J. T.; Ludueña, R. F.; Tuszynski, J. Comparative Modelling of Human β Tubulin

- Isotypes and Implications for Drug Binding. *Nanotechnology* **2006**, *17* (4), S90–S100. <https://doi.org/10.1088/0957-4484/17/4/014>.
- (53) Leandro-García, L. J.; Leskelä, S.; Landa, I.; Montero-Conde, C.; López-Jiménez, E.; Letón, R.; Cascón, A.; Robledo, M.; Rodríguez-Antona, C. Tumoral and Tissue-Specific Expression of the Major Human β -Tubulin Isotypes. *Cytoskeleton* **2010**, *67* (4), 214–223. <https://doi.org/10.1002/cm.20436>.
- (54) Sullivan, K. F.; Cleveland, D. W. Identification of Conserved Isotype-Defining Variable Region Sequences for Four Vertebrate Beta Tubulin Polypeptide Classes. *Proc. Natl. Acad. Sci.* **1986**, *83* (12), 4327–4331. <https://doi.org/10.1073/pnas.83.12.4327>.
- (55) Ludueña, R. F. Multiple Forms of Tubulin: Different Gene Products and Covalent Modifications. *Int. Rev. Cytol.* **1998**, *178*, 207–275.
- (56) Katsetos, C. D.; Legido, A.; Perentes, E.; Mörk, S. J. Class III β -Tubulin Isotype: A Key Cytoskeletal Protein at the Crossroads of Developmental Neurobiology and Tumor Neuropathology. *J. Child Neurol.* **2003**, *18* (12), 851–866. <https://doi.org/10.1177/088307380301801205>.
- (57) Burgoyne, R. D.; Cambray-Deakin, M. A.; Lewis, S. A.; Sarkar, S.; Cowan, N. J. Differential Distribution of Beta-Tubulin Isotypes in Cerebellum. *EMBO J.* **1988**, *7* (8), 2311–2319.
- (58) Ferlini, C.; Raspaglio, G.; Cicchillitti, L.; Mozzetti, S.; Prislei, S.; Bartollino, S.; Scambia, G. Looking at Drug Resistance Mechanisms for Microtubule Interacting Drugs: Does TUBB3 Work? *Curr. Cancer Drug Targets* **2007**, *7* (8), 704–712. <https://doi.org/10.2174/156800907783220453>.
- (59) Tseng, C.-Y.; Mane, J. Y.; Winter, P.; Johnson, L.; Huzil, T.; Izbicka, E.; Luduena, R. F.; Tuszynski, J. A. Quantitative Analysis of the Effect of Tubulin Isotype Expression on Sensitivity of Cancer Cell Lines to a Set of Novel Colchicine Derivatives. *Mol. Cancer* **2010**, *9*(1), 131. <https://doi.org/10.1186/1476-4598-9-131>.
- (60) Luduena, R. F.; Roach, M. C.; Prasad, V.; Chaudhuri, A. R.; Tomita, I.; Mizuhashi, F.;

- Murata, K. Interaction of Bovine Brain Tubulin with the 4(1H)-Pyridazinone Derivative IKP104, an Antimitotic Drug with a Complex Set of Effects on the Conformational Stability of the Tubulin Molecule. *Biochemistry* **1995**, *34* (48), 15751–15759. <https://doi.org/10.1021/bi00048a020>.
- (61) Lu, Q.; Luduena, R. F. In Vitro Analysis of Microtubule Assembly of Isotypically Pure Tubulin Dimers: Intrinsic Differences in the Assembly Properties of β II, β III, and β IV Tubulin Dimers in the Absence of Microtubule-Associated Proteins. *J. Biol. Chem.* **1994**, *269* (3), 2041–2047.
- (62) Huzil, J. T.; Mane, J.; Tuszynski, J. A. Computer Assisted Design of Second-Generation Colchicine Derivatives. *Interdiscip. Sci. Comput. Life Sci.* **2010**, *2* (2), 169–174. <https://doi.org/10.1007/s12539-010-0076-z>.
- (63) Verdier-Pinard, P.; Wang, F.; Burd, B.; Angeletti, R. H.; Horwitz, S. B.; Orr, G. A. Direct Analysis of Tubulin Expression in Cancer Cell Lines by Electrospray Ionization Mass Spectrometry †. *Biochemistry* **2003**, *42* (41), 12019–12027. <https://doi.org/10.1021/bi0350147>.
- (64) Banerjee, A.; Roach, M. C.; Trcka, P.; Luduena, R. F. Increased Microtubule Assembly in Bovine Brain Tubulin Lacking the Type III Isoform of β -Tubulin. *J. Biol. Chem.* **1990**, *265* (3), 1794–1799.
- (65) Banerjee, A.; Luduena, R. F. Kinetics of Colchicine Binding to Purified β -Tubulin Isoforms from Bovine Brain. *J. Biol. Chem.* **1992**, *267* (19), 13335–13339.
- (66) Banerjee, A.; Kasmala, L. T. Differential Assembly Kinetics of α -Tubulin Isoforms in the Presence of Paclitaxel. *Biochem. Biophys. Res. Commun.* **1998**, *245* (2), 349–351. <https://doi.org/10.1006/bbrc.1998.8426>.
- (67) Kamath, K.; Wilson, L.; Cabral, F.; Jordan, M. A. β III-Tubulin Induces Paclitaxel Resistance in Association with Reduced Effects on Microtubule Dynamic Instability. *J. Biol. Chem.* **2005**, *280* (13), 12902–12907. <https://doi.org/10.1074/jbc.M414477200>.
- (68) Derry, W. B.; Wilson, L.; Khan, I. A.; Ludueña, R. F.; Jordan, M. A. Taxol Differentially

- Modulates the Dynamics of Microtubules Assembled from Unfractionated and Purified β -Tubulin Isotypes. *Biochemistry* **1997**, *36* (12), 3554–3562. <https://doi.org/10.1021/bi962724m>.
- (69) Kasas, S.; Cibert, C.; Kis, A.; Rios, P. L.; Riederer, B. M.; Forró, L.; Dietler, G.; Catsicas, S. Oscillation Modes of Microtubules. *Biol. Cell* **2004**, *96* (9), 697–700. <https://doi.org/10.1016/j.biolcel.2004.09.002>.
- (70) VanBuren, V.; Cassimeris, L.; Odde, D. J. Mechanochemical Model of Microtubule Structure and Self-Assembly Kinetics. *Biophys. J.* **2005**, *89* (5), 2911–2926. <https://doi.org/10.1529/biophysj.105.060913>.
- (71) Tuszyński, J. A.; Brown, J. A.; Crawford, E.; Carpenter, E. J.; Nip, M. L. A.; Dixon, J. M.; Satarić, M. V. Molecular Dynamics Simulations of Tubulin Structure and Calculations of Electrostatic Properties of Microtubules. *Math. Comput. Model.* **2005**, *41* (10), 1055–1070. <https://doi.org/10.1016/j.mcm.2005.05.002>.
- (72) Amadei, A.; Linssen, A. B. M.; Berendsen, H. J. C. Essential Dynamics of Proteins. *Proteins Struct. Funct. Genet.* **1993**, *17* (4), 412–425. <https://doi.org/10.1002/prot.340170408>.
- (73) Gebremichael, Y.; Chu, J.-W.; Voth, G. A. Intrinsic Bending and Structural Rearrangement of Tubulin Dimer: Molecular Dynamics Simulations and Coarse-Grained Analysis. *Biophys. J.* **2008**, *95* (5), 2487–2499. <https://doi.org/10.1529/biophysj.108.129072>.
- (74) Keskin, O.; Durell, S. R.; Bahar, I.; Jernigan, R. L.; Covell, D. G. Relating Molecular Flexibility to Function: A Case Study of Tubulin. *Biophys. J.* **2002**, *83* (2), 663–680. [https://doi.org/10.1016/S0006-3495\(02\)75199-0](https://doi.org/10.1016/S0006-3495(02)75199-0).
- (75) Enemark, S.; Deriu, M. A.; Soncini, M.; Redaelli, A. Mechanical Model of the Tubulin Dimer Based on Molecular Dynamics Simulations. *J. Biomech. Eng.* **2008**, *130* (4), 041008. <https://doi.org/10.1115/1.2913330>.
- (76) Deriu, M. A.; Soncini, M.; Orsi, M.; Patel, M.; Essex, J. W.; Montecchi, F. M.; Redaelli, A. Anisotropic Elastic Network Modeling of Entire Microtubules. *Biophys. J.* **2010**,

- 99(7), 2190–2199. <https://doi.org/10.1016/j.bpj.2010.06.070>.
- (77) Deriu, M. A.; Enemark, S.; Soncini, M.; Montecchi, F. M.; Redaelli, A. Tubulin: From Atomistic Structure to Supramolecular Mechanical Properties. *J. Mater. Sci.* **2007**, *42* (21), 8864–8872. <https://doi.org/10.1007/s10853-007-1784-6>.
- (78) Mitra, A.; Sept, D. Taxol Allosterically Alters the Dynamics of the Tubulin Dimer and Increases the Flexibility of Microtubules. *Biophys. J.* **2008**, *95* (7), 3252–3258. <https://doi.org/10.1529/biophysj.108.133884>.
- (79) Grafmüller, A.; Voth, G. A. Intrinsic Bending of Microtubule Protofilaments. *Structure* **2011**, *19* (3), 409–417. <https://doi.org/10.1016/j.str.2010.12.020>.
- (80) Gajewski, M. M.; Tuszynski, J. A.; Barakat, K.; Huzil, J. T.; Klobukowski, M. Interactions of Laulimalide, Peloruside, and Their Derivatives with the Isoforms of β -Tubulin. *Can. J. Chem.* **2013**, *91* (7), 511–517. <https://doi.org/10.1139/cjc-2012-0360>.
- (81) Bhattacharyya, B.; Panda, D.; Gupta, S.; Banerjee, M. Anti-Mitotic Activity of Colchicine and the Structural Basis for Its Interaction with Tubulin. *Med. Res. Rev.* **2008**, *28* (1), 155–183. <https://doi.org/10.1002/med.20097>.
- (82) Ludueña, R. F. Multiple Forms of Tubulin: Different Gene Products and Covalent Modifications. *Int. Rev. Cytol.* **1998**.
- (83) Natarajan, K.; Mohan, J.; Senapati, S. Relating Nucleotide-Dependent Conformational Changes in Free Tubulin Dimers to Tubulin Assembly. *Biopolymers* **2013**, *99* (5), 282–291. <https://doi.org/10.1002/bip.22153>.
- (84) Kumbhar, B. V.; Borogaon, A.; Panda, D.; Kunwar, A. Exploring the Origin of Differential Binding Affinities of Human Tubulin Isoforms $\alpha\beta$ II, $\alpha\beta$ III and $\alpha\beta$ IV for DAMA-Colchicine Using Homology Modelling, Molecular Docking and Molecular Dynamics Simulations. *PLoS One* **2016**, *11* (5), e0156048. <https://doi.org/10.1371/journal.pone.0156048>.
- (85) Natarajan, K.; Senapati, S. Understanding the Basis of Drug Resistance of the Mutants of $\alpha\beta$ -Tubulin Dimer via Molecular Dynamics Simulations. *PLoS One* **2012**,

- 7(8), e42351. <https://doi.org/10.1371/journal.pone.0042351>.
- (86) Šali, A.; Blundell, T. L. Comparative Protein Modelling by Satisfaction of Spatial Restraints. *J. Mol. Biol.* **1993**, *234* (3), 779–815. <https://doi.org/10.1006/jmbi.1993.1626>.
- (87) Laskowski, R. A.; MacArthur, M. W.; Moss, D. S.; Thornton, J. M.; IUCr. PROCHECK: A Program to Check the Stereochemical Quality of Protein Structures. *J. Appl. Crystallogr.* **1993**, *26* (2), 283–291. <https://doi.org/10.1107/S0021889892009944>.
- (88) Colovos, C.; Yeates, T. O. Verification of Protein Structures: Patterns of Nonbonded Atomic Interactions. *Protein Sci.* **1993**, *2* (9), 1511–1519. <https://doi.org/10.1002/pro.5560020916>.
- (89) Bowie, J.; Luthy, R.; Eisenberg, D. A Method to Identify Protein Sequences That Fold into a Known Three-Dimensional Structure. *Science (80-.)*. **1991**, *253*(5016), 164–170. <https://doi.org/10.1126/science.1853201>.
- (90) Humphrey, W.; Dalke, A.; Schulten, K. VMD: Visual Molecular Dynamics. *J. Mol. Graph.* **1996**, *14*(1), 33–38. [https://doi.org/10.1016/0263-7855\(96\)00018-5](https://doi.org/10.1016/0263-7855(96)00018-5).
- (91) Abraham, M. J.; Murtola, T.; Schulz, R.; Páll, S.; Smith, J. C.; Hess, B.; Lindahl, E. GROMACS: High Performance Molecular Simulations through Multi-Level Parallelism from Laptops to Supercomputers. *SoftwareX* **2015**, *1–2*, 19–25. <https://doi.org/10.1016/J.SOFTX.2015.06.001>.
- (92) Lindorff-Larsen, K.; Piana, S.; Palmo, K.; Maragakis, P.; Klepeis, J. L.; Dror, R. O.; Shaw, D. E. Improved Side-Chain Torsion Potentials for the Amber Ff99SB Protein Force Field. *Proteins Struct. Funct. Bioinforma.* **2010**, NA-NA. <https://doi.org/10.1002/prot.22711>.
- (93) Wang, J.; Wang, W.; Kollman, P. A.; Case, D. A. Automatic Atom Type and Bond Type Perception in Molecular Mechanical Calculations. *J. Mol. Graph. Model.* **2006**, *25*(2), 247–260. <https://doi.org/10.1016/j.jmgm.2005.12.005>.
- (94) Wang, J.; Wolf, R. M.; Caldwell, J. W.; Kollman, P. A.; Case, D. A. Development and

- Testing of a General Amber Force Field. *J. Comput. Chem.* **2004**, *25* (9), 1157–1174. <https://doi.org/10.1002/jcc.20035>.
- (95) Sousa Da Silva, A. W.; Vranken, W. F. ACPYPE - AnteChamber PYthon Parser Interface. *BMC Res. Notes* **2012**, *5* (1), 367. <https://doi.org/10.1186/1756-0500-5-367>.
- (96) Mark, P.; Nilsson, L. Structure and Dynamics of the TIP3P, SPC, and SPC/E Water Models at 298 K. *J. Phys. Chem. A* **2001**, *105* (43), 9954–9960. <https://doi.org/10.1021/jp003020w>.
- (97) Bussi, G.; Donadio, D.; Parrinello, M. Canonical Sampling through Velocity Rescaling. *J. Chem. Phys.* **2007**, *126* (1), 014101. <https://doi.org/10.1063/1.2408420>.
- (98) Berendsen, H. J. C.; Postma, J. P. M.; van Gunsteren, W. F.; DiNola, A.; Haak, J. R. Molecular Dynamics with Coupling to an External Bath. *J. Chem. Phys.* **1984**, *81* (8), 3684–3690. <https://doi.org/10.1063/1.448118>.
- (99) Tripathi, S.; Srivastava, G.; Singh, A.; Prakasham, A. P.; Negi, A. S.; Sharma, A. Insight into Microtubule Destabilization Mechanism of 3,4,5-Trimethoxyphenyl Indanone Derivatives Using Molecular Dynamics Simulation and Conformational Modes Analysis. *J. Comput. Aided. Mol. Des.* **2018**, *32* (4), 559–572. <https://doi.org/10.1007/s10822-018-0109-y>.
- (100) Frishman, D.; Argos, P. Knowledge-based Protein Secondary Structure Assignment. *Proteins Struct. Funct. Bioinforma.* **1995**, *23* (4), 566–579. <https://doi.org/10.1002/prot.340230412>.
- (101) Heinig, M.; Frishman, D. STRIDE: A Web Server for Secondary Structure Assignment from Known Atomic Coordinates of Proteins. *Nucleic Acids Res.* **2004**, *32* (WEB SERVER ISS.), W500–W502. <https://doi.org/10.1093/nar/gkh429>.
- (102) Genheden, S.; Ryde, U. How to Obtain Statistically Converged MM/GBSA Results. *J. Comput. Chem.* **2009**, *31* (4), NA-NA. <https://doi.org/10.1002/jcc.21366>.